THE USE OF RUTHENIUM Y ZEOLITE CATALYSTS FOR THE SELECTIVE METHANATION OF CARBON MONOXIDE

DISSERTATION

IN FULFILLMENT OF THE REQUIREMENT FOR THE DEGREE OF

MASTER OF SCIENCE IN CHEMICAL ENGINEERING

Prepared By:

Zaheera Ahmed

Prepared For:

Professor Jack Fletcher

Dr Roald Brosius

UNIVERSITY OF CAPE TOWN

September 2015

Synopsis

Fuel processing is the conversion of hydrocarbons to produce a mixture of H_2 and CO, whereby the H_2 will be used in a PEMFC. CO needs to be removed as the tolerance level of the Pt based electro catalyst is only 10 ppm of CO. In order to lower the concentration from 1% post-WGS, to 10 ppm, CO can be converted to CH_4 via selective methanation. A selective catalyst primarily methanates CO and inhibits the methanation of CO_2 which results in the over consumption of H_2. Common catalysts for SMET include Ru/Al_2O_3 and Ru/Y zeolites.

This study involved the use of Ru/Y zeolite catalysts with loadings between 1 wt.%-5.4 wt.% Ru prepared via ion exchange, and a commercial 5 wt.% Ru/Al_2O_3. These catalysts were tested in a fixed bed reactor at temperatures between 160°C and 210°C at various space velocities with a feed composition of 1% CO, 20% CO_2, 10% H_2O, 59% H_2 and 10% Ar.

The effects of loading, space velocity and reaction temperature on the CO conversion and CO selectivity were investigated. The 2.2 wt.% was found to be the optimum loading by displaying the highest selectivity of 72%, and 100% CO conversion at 170°C. The higher loadings produced large amounts of CH_4 displaying lower selectivity, coupled with a high undesirable consumption of H_2. The 1 wt.% Ru/Y zeolite showed low activity for SMET but was active for the WGS reaction. The 5 wt.% Ru/Al_2O_3 displayed the highest selectivity of 60%, and 100% CO conversion at 180°C.

The water vapour content was found to have a significant impact on the CO selectivity when increased from 10% to 20%. The CO selectivity increased from 43% to 66% where the CO conversion decreased by 5%. The effect of CO concentration on CO selectivity was determined in experiments with only 0.5% rather than 1%. Similar CO selectivities to the ones observed at 1% CO were obtained at lower temperatures and the same space velocity when the concentration was halved. Overall the 2.2 wt.% Ru/Y zeolite was capable of removing CO at lower temperatures compared to the 5 wt.% Ru/Al_2O_3, while displaying higher selectivities toward CO.

Acknowledgements

I would like to take this opportunity to thank everyone that played a role whether big or small in helping me complete my MSc Degree. Firstly I would like to thank my supervisor, Professor Jack Fletcher, for giving me the opportunity to be a part of the Chemical Engineering Department and for the guidance throughout my research. I would also like to thank my co-supervisor, Dr Roald Brosius for all his help and supervision, as well as Niels Luchters and the rest of the HySA/Catalysis Fuel Processing team.

I would also like to thank the following people:

The NRF and HySA/Catalysis for co-funding my research.

My fellow students who were always willing to help and support me in the lab.

The lab manager, Dirk Reyskons, for making sure the lab was always in a workable condition and for his kindness and wise words.

The administrative and technical staff at the Centre for Catalysis Research, Ms Eloise Williams, Ms Lee-Anne Kallum, Mr Marc Wüst and Mr Gideon Kaufmann.

A special thank you to Yi Zhou and Waldo Koorts, who never refused to help out and whom without I would not have been able to get through the last two years.

A special thank you to Sibongile Muziki, who made long hours in the lab bearable and for her constant motivation and support.

Most importantly my Creator and my family and friends who supported me throughout my studies and for giving me the strength to accomplish it.

Declaration

I know the meaning of plagiarism and declare that all the work in the document, save for that which is properly acknowledged, is my own

Signed by candidate ……..

Date ……30 November 2015……..

Zaheera Ahmed

Table of Contents

List of Tables

List of Figures

List of Graphs

Nomenclature

CEC	Cationic Exchange Capacity
CH_4	Methane
CO	Carbon Monoxide
CO_2	Carbon Dioxide
FCEV	Fuel Cell Electric Vehicle
GC	Gas Chromatograph
H_2	Hydrogen
HOR	Hydrogen Oxidation Reaction
HTS	High Temperature Shift
HySA	Hydrogen South Africa
ICP-OES	Inductively Couple Plasma Optical Emission Spectroscopy
kJ/mol	Kilojoules per mole
LTS	Low Temperature Shift
O_2	Oxygen
ORR	Oxidation Reduction Reaction
PEMFC	Polymer Electrolyte Membrane Fuel Cell
PROX	Preferential Oxidation
Ru	Ruthenium
RWGS	Reverse Water Gas Shift
SMET	Selective Methanation
SV	Space Velocity
TCD	Thermal Conductivity Detector
TEM	Transmission Electron Microscopy
TPR	Temperature Programmed Reduction
WGS	Water Gas Shift
wt.%	Weight Percentage
XRD	X-ray Diffraction
ΔH	Heat of Reaction

1. Introduction

The demand for energy is rapidly increasing as the world's population continues to grow. An increase in carbon dioxide (CO_2) emissions will follow an increase in energy usage which negatively impacts the environment. There is a drive to lower CO_2 emissions by finding alternative forms of energy. The need for clean energy has sparked interest in fuel cell technology that uses Hydrogen (H_2), derived from hydrocarbons or the electrolysis of H_2O, as a fuel. It is a form of renewable energy where the CO_2 emissions can be lowered or completely eliminated (Kolb, G 2008).

Fuel cells can be used in stationary power units or replace the regular combustion engine which releases large amounts of CO_2. In order for this to occur, the transition from the electric economy to the H_2 economy needs to take place. Fuel cells that use H_2 as fuel are the most common types of fuel cells. Polymer Electrolyte Membrane Fuel Cells (PEMFC) operate at low temperatures and can be used in fuel cell electric vehicles. Many challenges face fuel cell technologies which include its efficiency and lack of infrastructure, which make the transition from regular combustion engines a difficult one.

Another challenge facing PEMFC's is the exposure limit of the platinum catalyst to carbon monoxide (CO). CO is derived from the reforming of hydrocarbons to produce H_2 gas. This project aims to lower the CO concentration to less than 10 ppm as this is the tolerance level of the fuel cell catalyst. This study involves the use of Ru/Y zeolites to catalyse the selective methanation of CO in order to produce a clean H_2 rich fuel.

2. Background and Literature Review

2.1 The Hydrogen Economy

The transition to a H_2 Economy is adopting H_2 as a fuel in order to replace regular fossil fuels which will produce sustainable and environmentally friendly energy. Some of the main issues that face the H_2 economy is efficiency and the lack of infrastructure which exists to meet public demands, as well as the storage and transportation of H_2. The answer to our energy crisis could be a balance between the electric and H_2 economy. Electrical energy produced via renewable resources such a sunlight, wind or hydropower is a sustainable way to produce energy (Marchenko,O.V. and Solomin,S.V 2015 ; Ren, J *et al*. 2015).

Currently our main use of fossil fuels is to produce electricity and used as fuel in the transport sector. The use of non-renewable resources is unsustainable and they produce greenhouse gasses (GHG) which affect the global climate.

H_2 is commonly produced from hydrocarbons but can be produced by renewable means. Regular liquid fuels from fossil fuels is still preferred and dominantly used as the infrastructure already exists and the fuel is easy to store, handle and distribute (Ball, M and Weeda, M 2015)

2.2 Fuel Cells

The need for off grid power generation in areas where direct electricity is not accessible comprises one of the main drivers for fuel cell technology. A fuel cell uses a fuel, such as H_2, and converts chemical energy into electrical energy. They can be used in cars, or stand by power units such as telecommunication towers in remote areas (Kalmula,B and Kondapuran, V.R 2015; Icardi,U.A. *et al*. 2008). They are essentially batteries that constantly produce power using a continuous supply of fuel (Devrim, Y *et al*. 2015).

There is a variety of fuel cells that utilise different types of fuels, each having their advantages and disadvantages. They are based on their operating temperature, charge carrier and electrolyte present. Focussing on the low temperature PEMFC, one of the major problems that need to be dealt with is the CO tolerance level. The CO present is a by-product of the reforming process used to produce the H_2 gas from fossil fuels (Kalmula, B and Kondapuram, V.R 2015).

The fuel cell is integrated with a fuel processor to directly produce the H_2 that is needed. The fuel processor also has its own specifications that are required to be met in order for it to function at high efficiencies when producing H_2. It consists of 3 major steps namely; reforming, water gas shift (WGS) reaction and a CO clean-up step which is either preferential oxidation (PROX) or selective methanation (SMET) (Kolb, G 2008). The steps will be described in further detail in section 2.4.

2.2.1 Different Types of Fuel Cells

There are various types of fuel cells where each type operates under certain conditions. Some fuel cells have the ability to operate at temperatures as low as 40°C while other fuel cells can operate at temperatures as high as 1000°C. Their cell types are named after the specific electrolyte used, for example the PEMFC is named after the polymer electrolyte used whereas the MCFC is named after the molten carbonate electrolyte. Their power outputs also differ making each fuel cell suitable for specific applications which vary from remote storage to commercial and residential use. The main downside to all of these fuel cells are their tolerance levels to different impurities. Some of the main impurities which affect the range of fuel cells is CO and sulphur (Kalmula, B and Kondapuram, V.R 2015). This is detailed in table 1.

Table 1 : Classification of different fuel cell types (Kalmula, B and Kondapuram, V.R 2015).

Classification		Low Temperature	Medium Temperature		High Temperature	
Cell type		PEMFC	AFC	PAFC	MCFC	SOFC
1	Characteristic features					
1.1	Temperature range (°C)	40–80	65–220	205	650	600–1000
1.2	Charge carrier	H^+	OH^-	H^+	CO^{-3}	O^-
1.3	Electrolyte	PE membrane/perfluoro sulphonic acid	KOH	Phosphoric acid	Molten carbonate in $LiAlO_2$	Yttria stabilized zirconia
1.4	Catalyst	Pt	Pt	Pt	Ni	Inorganic or Steel
1.5	Cell components	Carbon	Carbon	Graphite	Stainless steel	Ceramics
1.6	Energy efficiency (%)					
	Electrical	45+	60	40+	45+	38+
	Heat and power	70–90	>80	>85	>80	90
1.7	Power packs (kW)	1–250	10–100	50–1000	1–1000	1–3000
1.8	Preferred applications	Backup power, automotive and small stationary platforms	Remote stationery power systems	Distributed power systems	Electrical, industrial and strategic areas	Residential and commercial

2	Impurity tolerance levels					
2.1	CO	Poison (<0.5%)	Fuel	Poison	Poison (<10 ppm)	Fuel
2.2	CO_2	Diluent	Recirculated	Poison	Diluent	Diluent
2.3	H_2O	Diluent	Diluent	Poison	Diluent	Diluent
10	S	Poison	Poison	Poison	No studies to date (a)	Poison <1 ppm (H_2S)
		<20 ppm (H_2S)	<10 ppm			
		<50 ppm (COS)	<0.5ppm (H_2S)			
11	NH_3	<0.2 mol%	<1 vol%			<5000 ppm
12	Halogens	<4 ppm	<1 ppm			<1 ppm

2.3 Proton Exchange Membrane Fuel Cells

The membrane in the PEMFC fuel cell has the ability to transport protons from the anode to the cathode. The H_2 from the feed is split at the anode via the Hydrogen Oxidation Reaction (HOR) to form electrons and protons where the protons are able to move through the membrane. Once the protons move through the membrane, they react with the oxygen (O_2) via the Oxygen Reduction Reaction (ORR) at the cathode to form water. The electrons are then used to generate a current (Kolb, G 2008). A schematic of the PEMFC can be seen in figure 1.

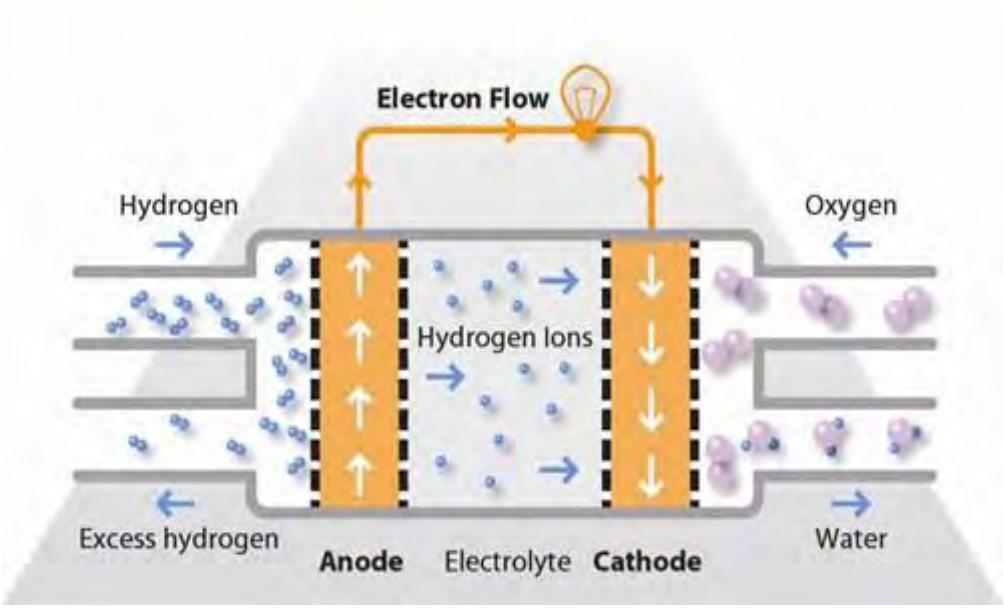

Figure 1: Schematic of a PEMFC (Fuel Cell Basics, 2012).

HOR	**$H_2 \rightarrow 2H^+ + 2\bar{e}$**	**Reaction 1**
ORR	**$\frac{1}{2} O_2 + 2H^+ + 2\bar{e} \rightarrow H_2O$**	**Reaction 2**

The catalyst used in this type of fuel cell is platinum (Pt) which is sensitive to CO poisoning at low temperatures. The CO present in the feed will preferentially adsorb and the active sites will no longer be available for the desired reactions to proceed (Kolb, G 2008). This will decrease the performance and efficiency of the fuel cell due to the tolerance level of CO being as low as 10 ppm.

2.4 Fuel Processing

The fuel processor is an essential part of the fuel cell system as its purpose is to produce the H_2 fuel via the reforming of hydrocarbons to yield a mixture containing H_2 and CO. There are a number of sequential reactions that take place in a fuel processor before the final feed for the fuel cell is produced.

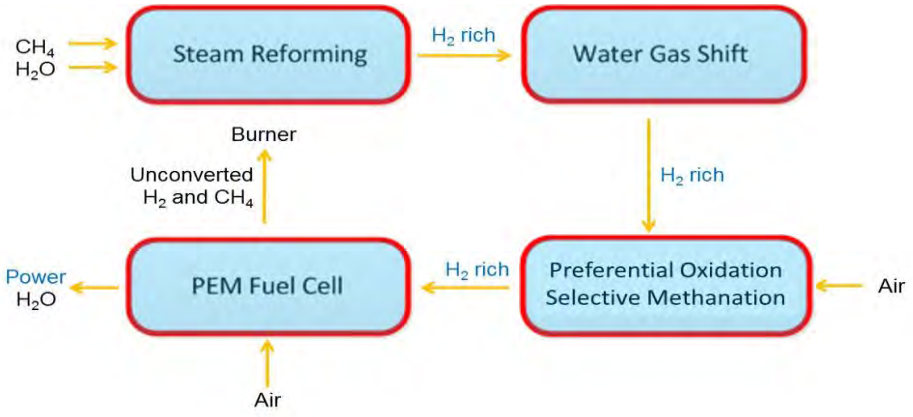

Figure 2 : The steps involved in fuel processing.

2.4.1 Steam Reforming

The first reaction is steam reforming (SR) which is the conversion of hydrocarbons with steam to produce the reformate gas mixture of H_2 and CO. There are various fuels that can be used for reforming such as methane (CH_4), gasoline, propane and butane. Other types of reforming include the partial oxidation (POX) of hydrocarbons and auto thermal reforming (ATR) (Shekhawat, D *et al*. 2011).

Steam reforming is a strongly endothermic reaction so obtaining sufficient heat for the reaction to take place is challenging. The high temperatures near 800°C is required to ensure complete conversion is obtained, therefore the choice of catalyst is important in order to withstand these conditions. The catalyst must be stable, resistant to possible poisons, and must be selective for the reaction in order to achieve high conversions. Typical catalysts for these reactions are nickel based (Shekhawat, D *et al*. 2011).

Steam reforming	**$C_xH_y + n\ H_2O \leftrightarrow (x + y/2)\ H_2 + xCO$**	**Reaction 3**
Auto thermal	**$C_xH_yO_z + n(O_2 + 3.76N_2) + (x-2n-z)H_2O \rightarrow$**	**Reaction 4**
Reforming	**$xCO + (x-2n-z+y/2)H_2 + 3.76nN_2$**	
Partial Oxidation	**$C_xH_y + 1/2O_2 \rightarrow xCO + (y/2)\ H_2$**	**Reaction 5**

The reformate then undergoes further reactions in order to increase the H_2 concentration and to remove the CO. Equations 3-5 show the various types of reforming that can be used to produce H_2 rich gas.

2.4.2 CO Clean-up

In order to lower the CO concentration to acceptable levels for the fuel cell, the following clean-up stages take place.

2.4.2.1 The Water Gas Shift Reaction

The first clean-up step is the WGS reaction and its main purpose is to increase the H_2 content by converting CO and H_2O to form CO_2 and H_2 as seen in reaction 6 below (Kolb, G 2008). It removes the bulk of CO from the feed but essentially 1% CO remains.

$CO + H_2O \rightarrow CO_2 + H_2$	**ΔH_{298K} = -41.16KJ/mol**	**Reaction 6**
$CO_2 + H_2 \rightarrow CO + H_2O$	**ΔH_{298K} = +41.16KJ/mol**	**Reaction 7**

In figure 3, the effect of steam to carbon ratio, R, on the equilibrium conversion of CO can be seen over a range of temperatures. As the R value increases, the equilibrium conversion of CO is seen to move to higher temperatures (Smirniotis, P and Gunugunuri, K 2015).

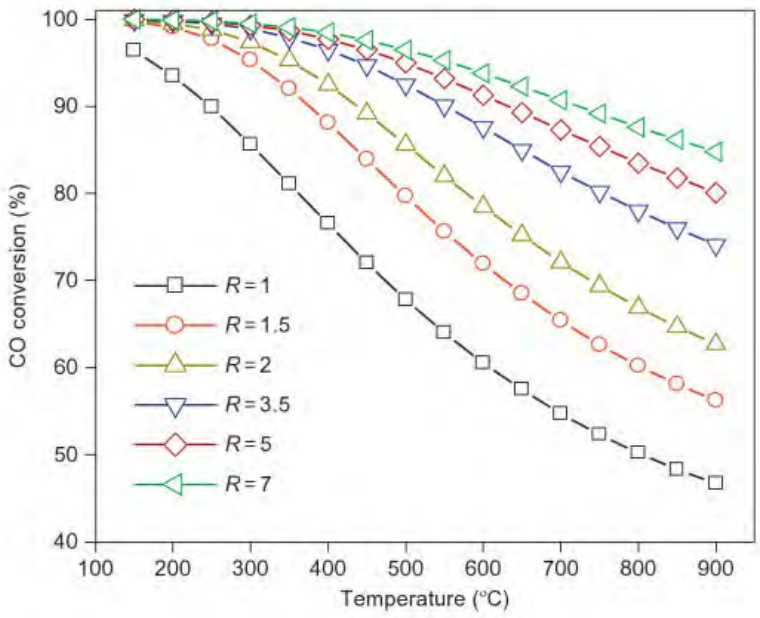

Figure 3 : The effect of S/C ratio on the equlibrium conversion of CO between 100°C and 900°C (Smirniotis,P and Gunugunuri ,K. 2015).

The WGS reaction can be classified into a high and low temperature shift. The high temperature shift (HTS) takes place between 310°C and 450°C whereas the low temperature shifts (LTS) takes place between 190°C and 250°C. A two stage process is put into place as the HTS converts 95% to 97% of CO and the concentration of CO that remains is still too high to be fed into the fuel cell. The LTS is therefore used to remove the remaining CO although this reaction is kinetically controlled.

Different catalysts are used in each step. For the HTS, common catalyts include Fe-Cr whereas in the LTS, Cu-ZnO catalytsts are used. Although these are the common catalysts used, supported noble metals are known to be active for the LTS. These include ruthenium (Ru), platinum , rhodium (Rh) and gold (Au) suppported on ZrO_2, CeO_2 and TiO_2. (Smirniotis,P and Gunugunuri ,K 2015). A final clean-up step is needed to lower the CO concentration to below 10 ppm to prevent the fuel cell catalyst from undergoing deactivation.

2.4.2.2 Preferential Oxidation and Selective Methanation

Preferential oxidation and selective methanation are both viable routes used to remove CO post WGS. Table 2 below summarises some of the differences between PROX and SMET in terms of H_2 loss, selectivity and ease of reactor usage. It is clear that PROX uses less valuable H_2 if the selectivity of the catalyst is high. Whereas 100% selectivity in terms of SMET, will result in a 3% H_2 loss, obtaining high selectivities is challenging in the presence of CO_2 where a greater loss in H_2 can occur due to CO_2 methanation.

Table 2: Comparison of PROX and SMET reactions (Ashraf, M A. *et al*. 2014).

CO-PROX reactor characteristics	CO-SMET reactor characteristics
Theoretically no H_2 loss, if a very active catalyst with selectivity = 1 is available	Theoretically only CO methanation, if a very active catalyst with selectivity = 1 is available
Practically selectivity is <1 and to obtain a complete removal of CO some H_2 is consumed by parallel oxidation	Practically selectivity is <1 and some CO_2 is transformed in CH_4 increasing the H_2loss, which is higher than that in CO-PROX reactor
Strong exothermic nature: the heat associated with the consumed H_2 is practically recovered from the reactor together with that from CO oxidation	CO and CO_2 methanation reactions are less exothermic than CO and H_2 oxidations; the developed heat is practically recovered from the reactor
	The heat associated to the formed CH_4 is practically equal to the one associated to the consumed H_2
Mixing the oxygen into the gas could be problematical in terms of safety	The reactor inherently easier to be controlled

Preferential Oxidation

PROX is the oxidation of CO to form CO_2 as shown in reaction 8 below. Reaction 9, which is a side reaction with H_2, will lower the concentration of H_2 in the feed. A common catalyst used for this reaction is Ru/Al_2O_3 and operates around 150°C. Although SMET uses H_2 to remove CO, it is to some extent preferred as the addition of O_2 during PROX causes safety concerns and there is a need for the reformer to be modified (Kolb, G 2008).

$$2CO + O_2 \rightarrow 2CO_2 \qquad \Delta H_{298}^{\circ} = -283\ kJ/mol \qquad \textbf{Reaction 8}$$

$$2H_2 + O_2 \rightarrow 2H_20 \qquad \Delta H_{298}^{\circ} = -242\ kJ/mol \qquad \textbf{Reaction 9}$$

Selective Methanation

SMET converts CO to CH_4 (reaction 10), but in the presence of CO_2, the reaction will no longer be favourable if the catalyst is not highly selective as seen in equation 11. This will cause more valuable H_2 to be consumed via the methanation of CO_2. The CH_4 produced only acts as a diluent and does not affect nor react in the fuel cell (Dagle, R.A. *et al*. 2007).

$CO + 3H_2 \rightarrow CH_4 + H_2O$	**$\Delta H_{298}° = -253$ kJ/mol**	**Reaction 10**
$CO_2 + 4H_2 \rightarrow CH_4 + 2H_2O$	**$\Delta H_{298}° = -165$ kJ/mol**	**Reaction 11**

The most commonly used catalysts for this reaction in fuel processing are Ru or Rh supported on alumina or zeolites operating between 180°-210°C (Galleti, C *et al*. 2011).There is also the risk of the reverse water gas shift (RWGS) reaction taking place if high temperatures higher than 230°C are reached. The RWGS reaction can be seen in reaction 7 whereby CO_2 is converted to CO which will cause more valuable H_2 to be consumed during methanation. One of the advantages of SMET is that the reactants required are already present (Dagle, R.A. *et al*. 2007).

2.4.3 The Need for CO Clean-up

The need for CO clean-up arises from the fact that the WGS reaction is moderately exothermic and is unable to convert all the CO at low temperatures. Figure 4 shown below, illustrates the effect of temperature on the exit concentration of CO for the WGS reaction at different H_2O/ CO ratios. It is clear that the exit CO concentration is seen to increase with increasing temperature for a given H_2O/CO ratio.

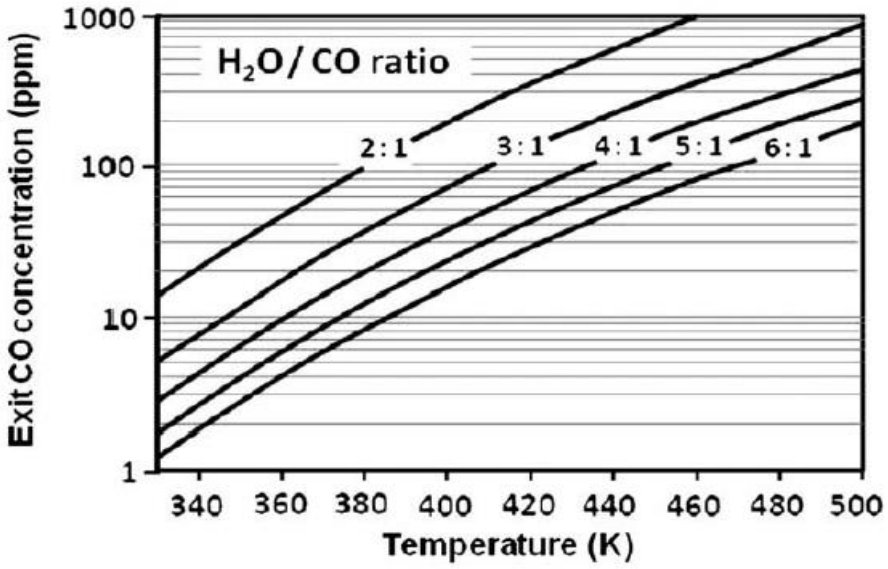

Figure 4: The effect of H_2O/CO ratio on the exit concentration of CO between 340K and 500K (Shekhawat, D *et al.* 2011).

As the H_2O/CO ratio is increased, lower CO concentrations in the exit stream can be achieved at low temperatures. In order to operate at low temperatures, the catalyst needs to be highly active and selective for the WGS reaction.

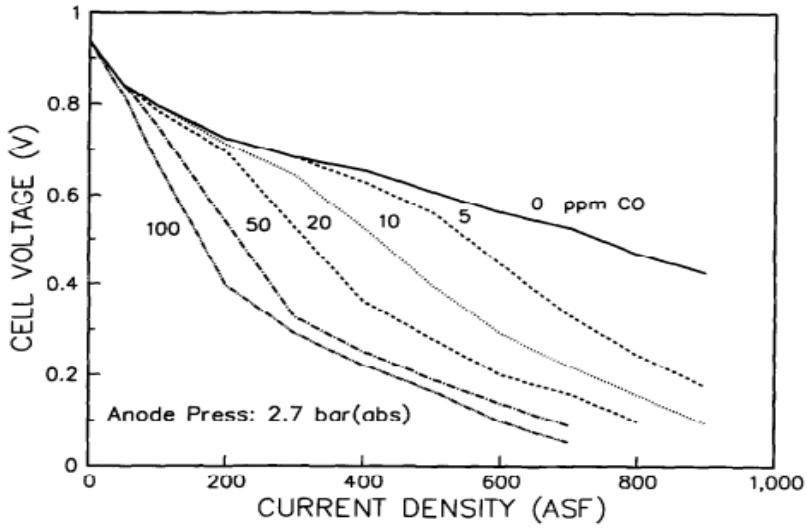

Figure 5 : The effect of CO concentration on the current density of the fuel cell (Amphlett,J.C *et al*. 1996).

Figure 5 demonstrates that the current density of the fuel cell decreases dramatically with increasing CO concentrations from 0 ppm to 100 ppm. The concentration of CO must be kept below 10 ppm in order to prevent this from occurring.

2.5 Zeolites

Zeolites are porous crystalline materials and are essentially aluminosilicates whose structural framework comprises a network of SiO_4 and AlO_4 tetrahedra (Smith,J.V 1984). The 3-D network form the cavities and channels by shared vertices of adjacent tetrahedra (Meier, W.M 1986). The general formula for zeolites is shown below (Smith,J.V 1984).

$$\mathbf{M_{n/2}O.Al_2O_3.x.SiO_2.yH_2O}$$

Reactions in heterogeneous catalysis proceed via the diffusion of reactants to an active site where they are adsorbed. The zeolites active sites are located in the pores and the channels of the structure. The product is formed and desorbs before diffusion occurs (Naccache,C and Taarit,Y.B 1980).

Zeolites are important in heterogeneous catalysis as they are able to undergo cation exchange which allows cations to be replaced in the zeolite structure giving rise to various catalytic properties (Csicsery, S.M 1986). The cations present are isolated and the structure still has coordination ability (Naccache,C 1980). The uniform pores only allow certain molecules to pass through giving rise to sieving properties. If the reactant molecule is too large to diffuse through, the reaction will not proceed. The same applies to the products that are formed that are too large to diffuse out of the pore. Zeolites can be made using crystallisation methods involving a supersaturated solution under hydrothermal conditions. A template is required in order to direct the crystallisation process to form the structure that is desired. There are many naturally occurring and synthetic zeolites available, each with their own morphology and unique set of properties (Csicsery,S.M 1986).

2.5.1 The Y Zeolite

The Y zeolite has a faujasite (FAU) morphology and is composed of cavities where there are 12 tetrahedra in the ring structure and this gives rise to a pore diameter of 0.8nm. The largest cavity is called the supercage (Baerlocher, C and McCusker,L.B 2014). In the Y zeolite, the pore size is also dependent on the type of cation present in the structure (Csicsery, S.M 1986).

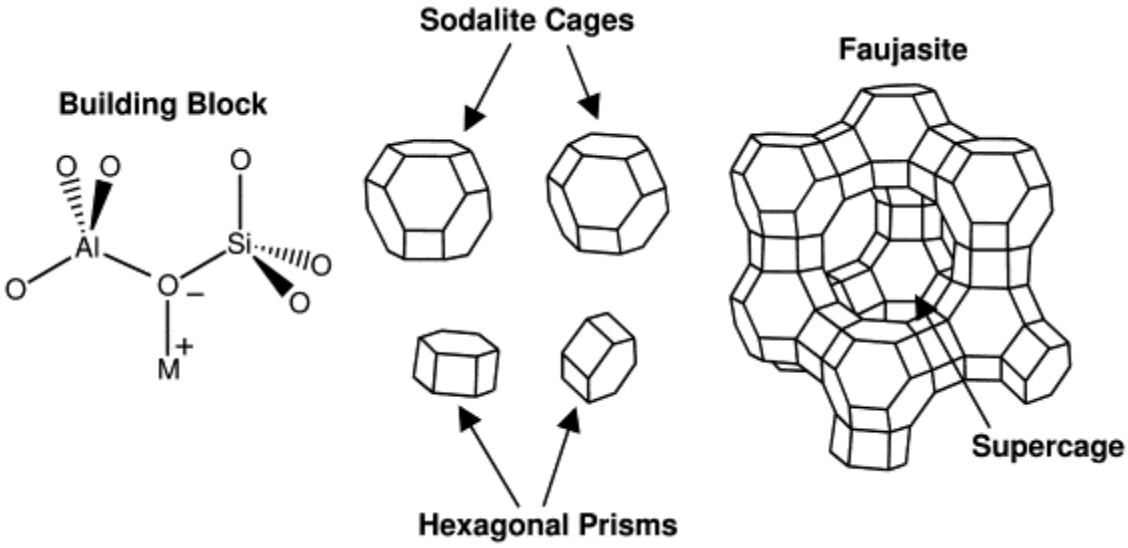

Figure 6: A representation of the building block that make up the faujasite structure (Davis, R.J 2003).

The Y zeolites pores are too large to be considered being shape selective. The structure of the Y type zeolite can be seen in figure 6. Another zeolite of faujasite morphology exists, zeolite X, where the difference between them being their Si/Al ratios. Zeolite Y has Si/Al ratio of 3, whilst when Si/Al ratios greater than 3 are present, the zeolite relevant is considered to be zeolite X (Csicsery,S.M 1986).

2.5.2 Ruthenium Y Zeolite

In 1980 it was already clear that Ru was a highly active catalyst for the steam reforming of CH_4, Fischer-Tropsch synthesis and the methanation of CO. It was also known that Ru could be exchanged into a Y zeolite by means of a $Ru(NH_3)_6Cl_3$ precursor (Chen, Y.W *et al*. 1984; Jacobs, P.A *et al.* 1979). To use the zeolite as a support, the metal is introduced as a metal complex in aqueous solution by performing an ion exchange. Amine complexes such as $[Ru(NH_3)_6]^{3+}$ in solution are generally stable over a range of pH values which make it suitable for ion exchange. The dispersion of the metal in the zeolite complex is dependent on the pre-treatment performed before the complex is reduced in H_2. When the complex thermally decomposes, the Ru^{3+} is reduced to the metal state (Naccache, C 1980).

The effects of oxidation and reduction were investigated using a 5.79 wt.% Ru/Y zeolite catalyst. Verdonck *et al*., 1980 found that in order to obtain finely dispersed Ru within the zeolite framework, the catalyst had to be carefully decomposed and reduced. This procedure involved the slow heating of the catalyst at 0.08 K/sec under vacuum to 350°C and holding the catalyst at this temperature for one hour. The catalyst was then reduced in H_2 for one hour and cooled naturally to the desired reaction temperature (Verdonck,J.J *et al*. 1980). Although the heating rate is equivalent to 4.8°C/min, this relatively high heating rate could be used as it was performed under vacuum. Under flowing helium, a heating rate of 0.5°C/min can be used to produce finely dispersed Ru particles (Oukaci, R *et al*. 1987). This was also described by Pearce *et al*., 1979 who reported on a slow heating rate needed to produce finely dispersed Ru, and that auto thermal reduction occurred when $Ru(NH_3)_6Cl_3$ was used, as nitrogen was observed during the decomposition (Pearce, J.R *et al.* 1979).

Temperature programed reduction (TPR) was performed on the catalyst and the graph below was obtained. Figure 7 displays three distinct peaks which correspond to the change in the Ru complex valency from Ru^{3+} to Ru^{0}.

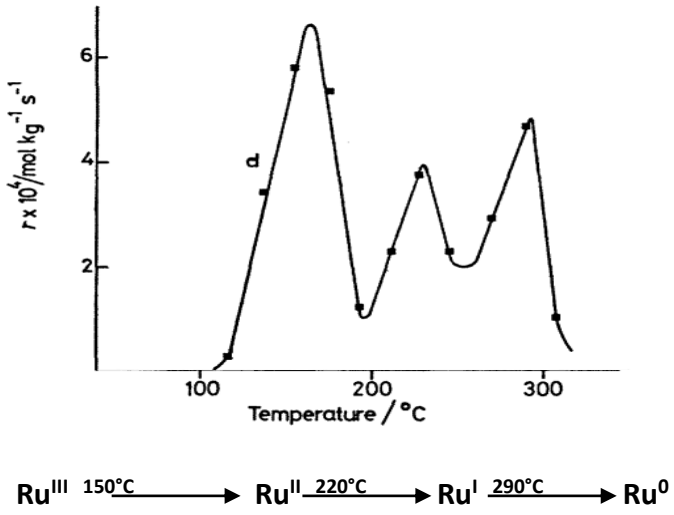

Figure 7: TPR obtained for the Ru/Y zeolite indicating valency changes (Verdonck, J.J *et al*. 1979).

Temperature programmed oxidation was used to determine whether the Ru particles were situated inside the zeolite cages, within holes created by the presence of water, or outside the zeolite framework. The results showed that if the metal oxidises:

- At ambient temperature, this is indicative of finely dispersed metal particles inside the zeolite cages.
- Above 500°C, this indicates the Ru is present outside the zeolite.
- Around 277°C, the metal is present in Ru clusters which are probably located in the holes formed by the presence of water (Verdonck,J.J *et al*. 1980).

2.5.2.1 Factors that influence this dispersion of Ru in zeolite Y

1. The effect of reduction temperature

The effect of reduction temperature was investigated whereby the catalyst was degassed at 300°C and then reduced at increasing temperatures between 300°C and 700°C shown in figure 8a. The amount of metal that remained in the zeolite cages after the reduction treatment was then calculated. It was found that at increasing reduction temperatures, the

amount of Ru contained in the zeolite cages did not change nor did this method show an increase in particle size as metal re-oxidised at room temperature which indicates the metal is present in the form of finely dispersed particles (Verdonck,J.J *et al*. 1980).

H_2 and CO chemisorption were also performed in order to investigate this further. It was found that the chemisorption of H_2 did not show changes in the particle sizes of the catalyst reduced at increasing temperatures. When chemisorption was performed using CO, the ratio of CO/Ru did change with the change in reduction temperature, as sintering of the metal occurred causing Ru particles to agglomerate inside the supercages (Verdonck,J.J *et al*. 1980).

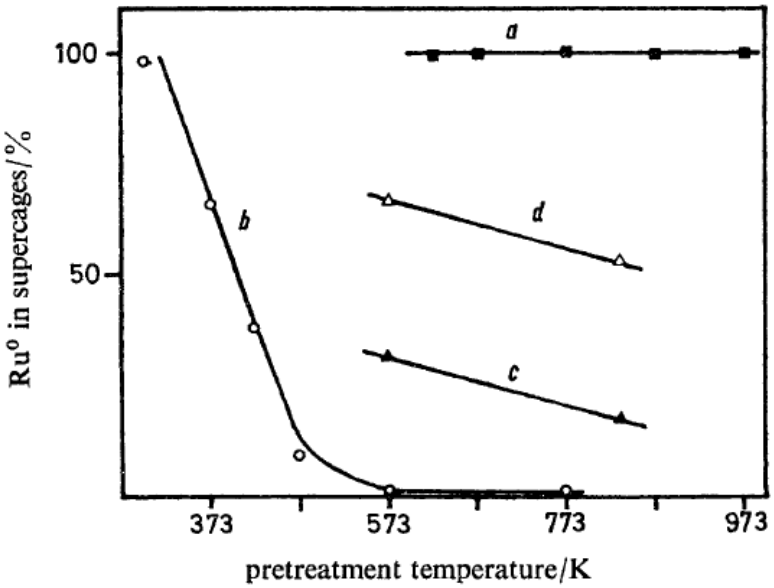

Figure 8: The percentage of Ru that remained inside the zeolite cages after different pre-treatments and reductions (Verdonck,J.J *et al*. 1980).

2. The presence of water

The distribution and size of Ru particles is affected by the H_2O present during the reduction. It is important to remove the H_2O present during decomposition to ensure that minimal amounts remain during the reduction treatment (Verdonck,J.J *et al*. 1980).

In order to investigate the effect of H_2O present, the sample was degassed at room temperature (figure 8(c)) and at 100°C (figure 8(d)) prior to undergoing a TPR. The

temperature at which the samples were degassed, clearly affected the amount of metal that remained in the zeolite cages. More metal was found to remain in the supercage when a higher degassing temperature was used as less H_2O remained prior to reduction.

This could be due to the H_2O hydrolysing parts of the zeolite lattice which results in the formation of holes. The size of these holes will determine to what extent the particles sinter and grow. Therefore it is possible to control the growth of these particles as well as the migration from the supercage by monitoring the temperature at which reduction takes place (Naccache,C 1980 ; Verdonck,J.J *et al*. 1980).

3. The treatment in oxygen

To investigate the effect of treatment in oxygen, the catalyst was degassed, reduced at 350°C, and then presented with oxygen at increasing temperatures. The catalyst was then re-reduced and a TPO was performed. The results in figure 8(b) clearly show that an increase in the amount of sintering is caused by an increase in the temperature at which the catalyst was exposed to oxygen (Verdonck,J.J *et al*. 1980).

From figure 8(b), it can be seen that below 300°C, contact with oxygen gives rise to bi-dispersed particle sizes. Above this temperature, sintering had occurred to such an extent that no Ru remains present in the zeolite cages (Verdonck,J.J *et al*. 1980).

2.5.3 Ion Exchange

One possibility to alter the properties of zeolites is by means of ion exchange which changes chemical composition of the zeolite. When the zeolite crystals are immersed in an aqueous electrolyte, the zeolitic ions communicate with the zeolite-external solution, resulting in an exchange of ions between the solid phase and the solution (Keuhl, G.H 1999). In figure 9 below, a pictorial interpretation of ion exchange can be seen where sodium ions are replaced by calcium ions.

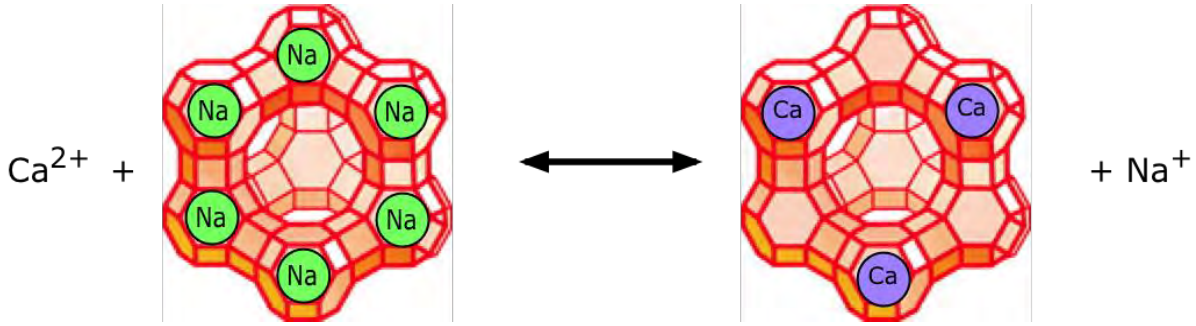

Figure 9 : A schematic of the ion exchange process observed in a zeolite Y (Lower, S 2013).

The Si/Al ratio affects the cationic exchange capacity (CEC) of the zeolite. Zeolites with high Si/Al have low CEC as an inverse relationship exists between them. The exchange capacity of zeolite Y is ≈40%. This method allows for the introduction of Ru in a controlled manner. Once the exchange is complete, the solution is filtered and washed in order to remove excess metal salt and recover the zeolite powder (Schwarz, J *et al*. 1995).

2.6 Selective Methanation Over Noble Metal Catalysts

Selective methanation can be performed using noble metal catalysts supported on alumina (Al_2O_3) where high CO conversion and selectivities can be obtained. A large amount of work has been done in order to determine which noble metal and which loading performs best at temperatures where CO_2 methanation and the RWGS are insignificant.

Various noble metals were supported on γ-Alumina in order to investigate the effect of the metal loading on SMET of CO under various conditions. All catalyst prepared contained 0.5 wt.% metal and were tested under realistic feed compositions and temperatures from 190°C to 470°C (Panagiotopoulou, P *et al.* 2008).

Table 3: The various catalysts used along with the particle sizes obtained (Panagiotopoulou,P *et al*. 2008).

Catalyst 0.5% M/Al_2O_3	Metal dispersion (%)	Metal crystallite size (nm)
Ru	70	1.3
Rh	79	1.4
Pt	100	1
Pd	100	1.1

The different catalysts prepared, as summarised in table 3, were tested under normal SMET feed conditions where it was found that Rh/Al_2O_3 was the most active catalyst for SMET and 98% CO conversion was achieved at 350°C. As the temperature was increased, the conversion was seen to drop due to RWGS. For Ru/Al_2O_3, the conversion of CO observed did not exceed 50% at 320°C and starts to decrease thereafter when RWGS sets in. In both catalysts, the CO_2 methanation is only initiated once the CO reaches its peak conversion. The two remaining catalysts prepared using Pt and Pd were essentially inactive for this reaction (Panagiotopoulou,P *et al.* 2008). The inability for Ru/Al_2O_3 to reach higher conversions could be due to the low loading of Ru present.

2.7 The Ruthenium/Alumina Catalyst

In order to find the optimum loading of Ru needed to completely remove CO, while still maintaining high selectivities, different metal loadings have been investigated for this reaction in various gas compositions and over a range of different temperatures.

2.7.1 The Effect of Loading on SMET

The effect of loading was investigated by several authors in the loading range between 1 wt.% and 5 wt.% where emphasis has been placed on 1 wt.%, 3 wt.% and 5 wt.%. In work done by Dagle *et al*., 2007, Ru/Al_2O_3 was investigated whereby catalysts with different Ru loadings were prepared as seen in table 4. A realistic feed composition containing 0.9% CO, 24.5% CO_2, 68.9% H_2 and 5.7% H_2O was used when testing these catalysts.

Table 4 : Summary of the catalysts used in the study by Dagle *et al*.,2007.

Ru (wt.%)	Support material	Reduction temperature (°C)	Ru^0 crystallite size (nm)
1	Al_2O_3	350	7.5
3	Al_2O_3	350	10.9
5	Al_2O_3	350	17.8
7	Al_2O_3	350	20

Table 4 summarises the catalysts prepared as well as the reduction temperature and particle size of Ru obtained. It is clear that as the loading increased from 1 wt.% to 7 wt.%, the particle size increased from 7.5nm to 20nm, respectively. Some of the results obtained from these tests are shown in figure 10 which illustrates the effect of Ru loading on the exit CO concentration and H_2 consumption. If the catalysts are selectively methanating CO, the H_2 consumption should remain below 3% given that only 0.9% of CO is being added to the feed. Therefore an increase in H_2 consumption is an indication that CO_2 is being methanated as well (Dagle,R.A *et al.* 2007).

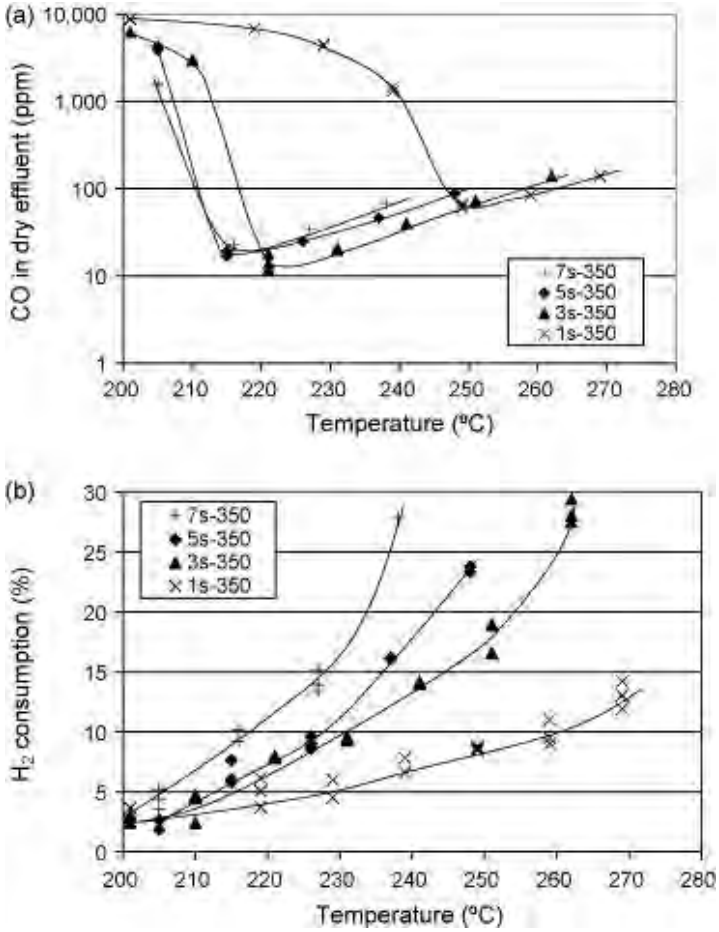

Figure 10: The exit CO concentration (a) and the H_2 consumption (b) for the 4 different Ru loadings tested (Dagle, R.A *et al*. 2007).

It is clear from figure 10a that RWGS is taking place above 230°C as the concentration of CO in the exit stream increases. This highlights the importance of maintaining the temperature below this range. It is also clear that an acceptable level of CO in the exit stream can only be achieved over a small temperature window before the onset of RWGS and an increase in H_2 consumption takes place. Increasing the metal loading is seen to decrease the exit CO

concentration but increase the H_2 consumption. The most promising catalyst based on loading is the 5 wt.% as it displays low CO exit concentrations between 10 ppm and 20 ppm combined with low H_2 consumption of ≈6% which indicates high selectivity towards CO (Dagle, R.A *et al*. 2007).

SMET was also investigated by Djinovic *et al*., 2011 using Ru/Al_2O_3 with a 1 wt.%, 3 wt.% and 5 wt.% Ru. The reaction temperatures ranged from 150°C to 450°C. This work also reported that the conversion of CO was affected by metal loading and that complete conversion can be obtained over a wide temperature range. The 5 wt.% Ru/Al_2O_3 was found to have the largest temperature window of 62°C over which complete conversion was achieved. This temperature window is between 210°C and 272°C which is similar to the temperature reported by Dagle *et al*., 2007 for the same catalyst. Beyond this temperature, RWGS starts to take place (Djinović,Petar 2011).

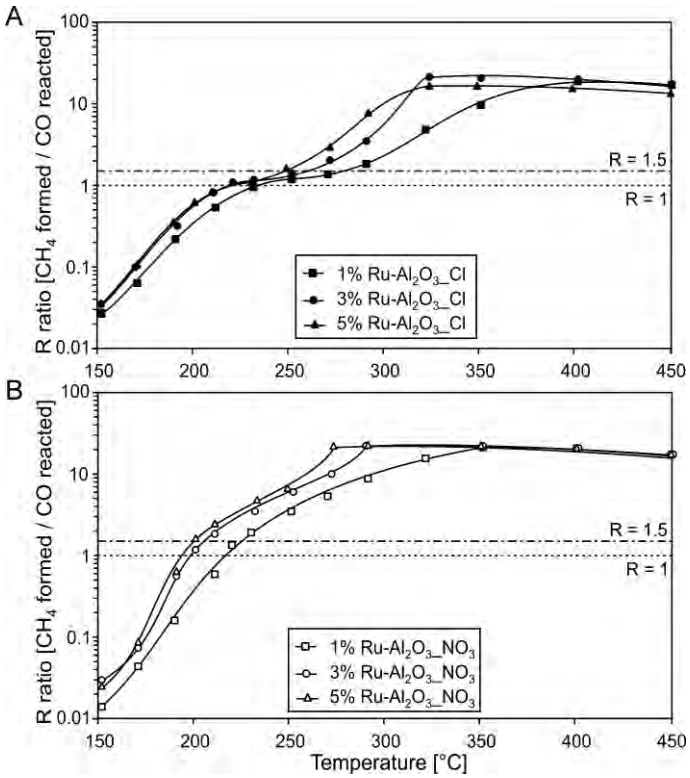

Figure 11: The R values for the catalyst prepared with different precursors where R= CH_4 formed/CO converted (Djinović,P *et al*. 2011).

Figure 11 above shows the R value, CH_4 formed/CO converted, for the catalysts prepared with different precursors as a function of temperature. Catalysts prepared by $RuCl_3$ were found to be more selective as its R value exceeded 1 at higher temperatures, as there exists a larger temperature window before selectivity drops below 100%. Catalysts prepared with $Ru(NO_3)_3(NO)$ display R values that exceed 1 at lower temperatures which indicates the presence of CO_2 methanation (Djinović, P *et al*. 2011).

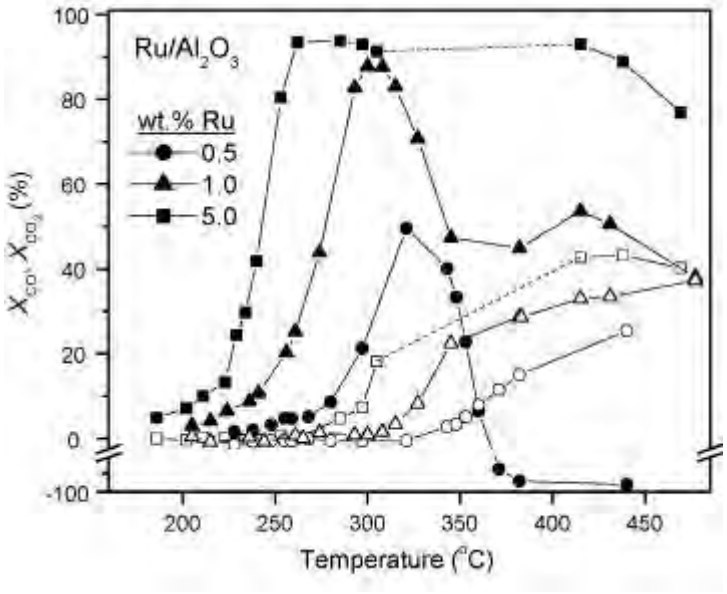

Figure 12 : Conversion curves of CO (Closed) and CO_2 (Open) for the different Ru loadings (Panagiotopoulou,P *et al*. 2009).

Table 5 : The particle size and metal dispersion of the different Ru catalyts.

Loading	Metal dispersion (%)	Metal crystallite size (nm)
0.5	70	1.3
1	68	1.4
2	63	1.5
5	43	2.2

Figure 12 above shows the conversion of CO and CO_2 for different Ru loadings from a study by Panagiotopoulou *et al*., 2009. It is clear that as the loading is increased, the conversion curves are shifted to lower temperatures and that the 5 wt.% Ru/Al_2O_3 has the highest conversion at the lowest temperature. The particle size, seen in table 5, increases with loading causing a decrease in dispersion. Larger particles in Ru/Al_2O_3 are favoured for the

methanation reaction (Panagiotopoulou, P *et al.* 2009). Looking at the various studies on the effect of loading, it is clear that a loading of 5 wt.% Ru performs best for the complete conversion of CO while still displaying high selectivities and this can be achieved at lower temperatures where the risk of RWGS is less significant.

2.7.2 The Effect of Water Vapour

The effect of water vapour on SMET was investigated by measuring the conversion of CO and CO_2 in the absence and presence of 30% water vapour in the feed. The results obtained are seen in figure 13 below.

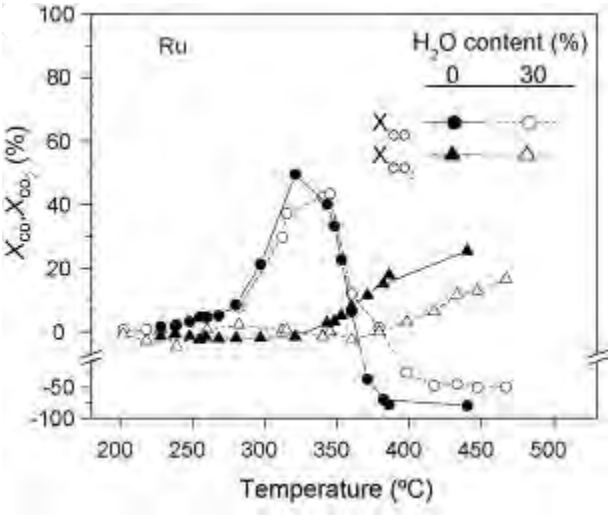

Figure 13 : Conversion curves for both CO and CO_2 for 0.5% Ru/Al_2O_3 in the presence and absence of H_2O (Panagiotopoulou, P *et al.* 2008)

It is clear that the addition of water vapour does not affect the conversion of CO significantly but seems to shift the conversion of CO_2 to higher temperatures. The effects of the addition of water vapour are important as they increase the temperature window between CO conversion and CO_2 conversion (Panagiotopoulou,P *et al.* 2008). The increase in the temperature between CO and CO_2 conversion will have positive effects on the selectivity of the catalyst as CO_2 methanation will only become significant at higher temperatures.

2.8 The Ruthenium/Zeolite Catalyst

In a study by Jacobs *et al*., 1979, it was shown that the methanation of CO can be performed using a Ru/Y zeolite catalyst. The results were compared to Ru/Al_2O_3 which is the more common catalyst used for this reaction. The results suggested that Ru/Y zeolite and Ru/Al_2O_3 display high initial activity with CO conversion of 100% and 80%, respectively. The difference between these two catalysts observed in figure 14 was that the Ru/zeolite catalyst maintained 100% conversion of CO after 15 hours on stream at 300°C whereas the Ru/Al_2O_3 CO conversion declined rapidly with time on stream (Jacobs,P.A *et al*. 1979).

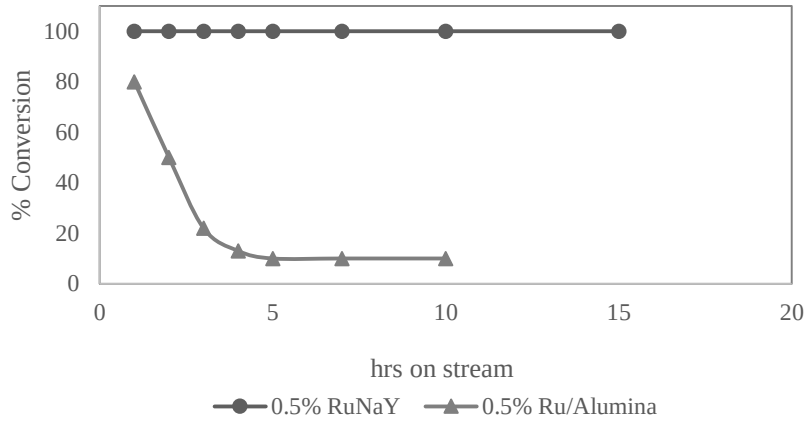

Figure 14 : The conversion of CO for 0.5% RuNaY and 0.5% Ru/Alumina at 300°C; GHSV= 3600 h^{-1}; H_2/CO=4/1 (Jacobs,P.A *et al*. 1979).

2.8.1 The Effect of Metal Loading on SMET

Eckle *et al*., 2012 investigated the effect of Ru loading on SMET by testing a range of catalysts prepared by Sud Chemie AG. The weight percent of Ru ranged from 1 wt.% to 5.6 wt.%. It is not clear however which zeolite framework group the catalyst belongs to. After characterisation using different methods such as XPS, XRD and in situ EXAFS measurements, mean particle size values for the catalysts were established. No information regarding the pre-treatment of the catalyst was given.

Table 6 : Particle size and selectivities in SR-ref 6000 and SR-ref 100 for the different catalysts.

Catalyst	Selectivity %	Mean Ru particle size/nm
1 wt.% Ru/zeolite	100/–	/
2.2 wt.% Ru/zeolite	100/100	0.9
3.6 wt.% Ru/zeolite	100/90	1.6
5.6 wt.% Ru/zeolite	100/80	1.9

Table 6 above shows the particle size and corresponding selectivity for the catalysts with different loadings. The selectivity was calculated based on the ratio of CO converted to the amount of CH_4 produced. As the loading of Ru increased from 2.2 wt.% to 5.6 wt.%, the mean particle size increased from 0.9nm to 1.9nm.

In the lower loaded catalysts, 1 wt.% and 2.2 wt.%, the small Ru nano-particles dominate and are less active for the formation of CO from the dissociation of CO_2. This is due to the higher barrier for CO_2 dissociation. At high concentrations of CO in the SR-ref 6000, adsorbed CO forms a layer on the surface blocking CO_2 adsorption and methanation which also plays a role in the high selectivities observed for these catalyst. Compositions of all mixtures are given in table 7. At low CO concentrations in SR-ref 100, the catalysts are still able to maintain 100% selectivity.

Table 7: Summary of all feed compositions used where feeds contained 2.8% N_2 and H_2 Balance (Eckle,S *et al*. 2011)

Reaction gas		
	CO content	**CO_2 content**
ID-ref 100: low-CO idealized reformate (100 ppm CO)	100 ppm	0%
ID-ref 1000: idealized reformate (1000 ppm CO):	1000 ppm	0%
SR-ref 100: low-CO semi-realistic reformate (100 ppm CO)	100 ppm	15.50%
SR-ref 1000: semi-realistic reformate (1000 ppm CO)	1000 ppm	15.50%
SR-ref 3000: semi-realistic reformate (3000 ppm CO)	3000 ppm	15.50%
SR-ref 6000: semi-realistic reformate (6000 ppm CO):	6000 ppm	15.50%
CO_2-ref: CO_2 reformate (CO-free)	0 ppm	15.50%

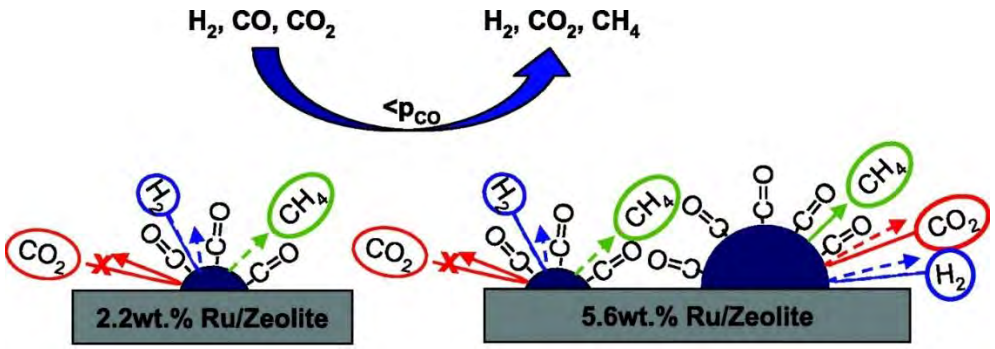

Figure 15: The effect of metal loading on CO selectivity (Eckle,S *et al*. 2012).

Figure 15 above depicts the effect of loading and particle size on the conversion of CO and CO_2 to form CH_4. Larger particles convert both CO and CO_2 whereas smaller particles inhibit the dissociation of CO_2 to CO to form CH_4. For catalysts with higher loadings of 3.6 wt.% and 5.6 wt.%, both small and large particles are present and are more active for methanation. The selectivity of these catalysts are affected by the concentration of CO in the feed. It was observed that at high concentrations (SR ref 6000), high selectivities were achieved due to the ad-layer of adsorbed CO blocking the surface for CO_2 adsorption. As the concentration of CO decreases (SR ref 100), the selectivity drops below 100% as CO_2 methanation is initiated.

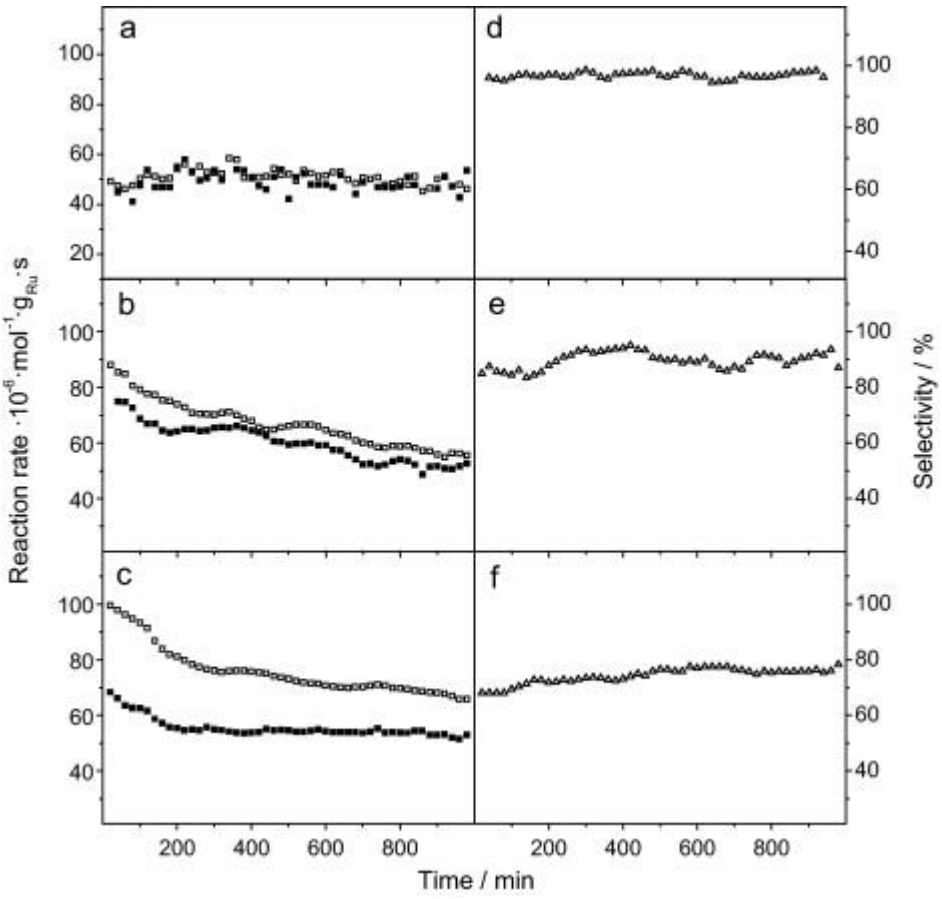

Figure 16: Reaction rates (left panels) and selectivities (right panels) obtained for reaction over the 2.2 (a, d), 3.6 (b, e), and 5.6 wt.% (c, f) Ru/zeolite catalysts (diluted with SiO_2) under differential reaction conditions in SR-ref 100. (■) CO reaction rate, (□) CH_4 formation rate, (▵) selectivity (Eckle,S *et al*. 2012).

The rate of CO consumption and the rate at which CH_4 forms in a SR-ref 100 feed was measured for the different loadings and the selectivity of each catalyst was calculated. At a loading of 2.2 wt.%, the rate of CO consumption is similar to the rate at which CH_4 is produced with an observed selectivity of 100% in figure 16 a, d. As the loading is increased, the rate at which CH_4 forms increases and surpasses that of CO consumption. Therefore, if CH_4 is formed faster than CO is being consumed, CO_2 is essentially being methanated which results in the loss of CO selectivity as seen in figure 16 c, f (Eckle,S *et al*. 2012).

The low activity of lower loaded catalysts to form CO_{ads} was investigated by Diffuse Reflectance Infrared Fourier Transform Spectroscopy (DRIFTS). Measurements were taken of CO_{ads} in a CO-free feed composition where the band intensity for CO_{ads} increased as the loading increased. This suggested that larger particles are more active for CO_2 dissociation and methanation compared to smaller particles.

The selectivity obtained using this catalyst is governed by different mechanisms depending on particle size and the partial pressure of CO. When the concentration of CO is high, all catalysts display 100% selectivity due to CO forming a layer of adsorbed CO which blocks the sites for CO_2 adsorption but when CO concentration levels drop, the size of the particle determines the selectivity. Only the 2.2 wt.% catalyst exhibits 100% selectivity regardless of the partial pressure of CO by the difference in the activity for CO_2 dissociation to CO_{ads} (Eckle, S *et al*. 2012).

The effect of the support cannot be ruled out as the 5.6 wt.% Ru/zeolite was compared to a 5 wt.% Ru/Al_2O_3 with similar particle sizes. The higher activity of the Ru/zeolite could be attributed to chemical and physical properties of the support which include the BET surface area, pore structure and acidity.

2.9 Selectivity in Ru/Zeolite and Ru/Al_2O_3

The conversion curves in figure 17 for CO and CO_2 methanation are shown for both 5 wt.% Ru/Al_2O_3 (left) and a 2.2 wt.% Ru/zeolite (right) catalysts over a temperature range between 150°C and 400°C. The maximum CO conversion is achieved at different temperatures for the two catalysts where the Ru/zeolite catalyst is able to achieve 100% conversion at 190°C whereas Ru/Al_2O_3 reaches 100% conversion at 230°C. The conversion of CO_2, shown using the open symbols, seems to be significant at temperatures close to CO conversion for Ru/Al_2O_3. The same curve for Ru/zeolite is only significant at temperatures around 230°C. Within this temperature window, the selectivity starts to drop from 100% to 85% selectivity.

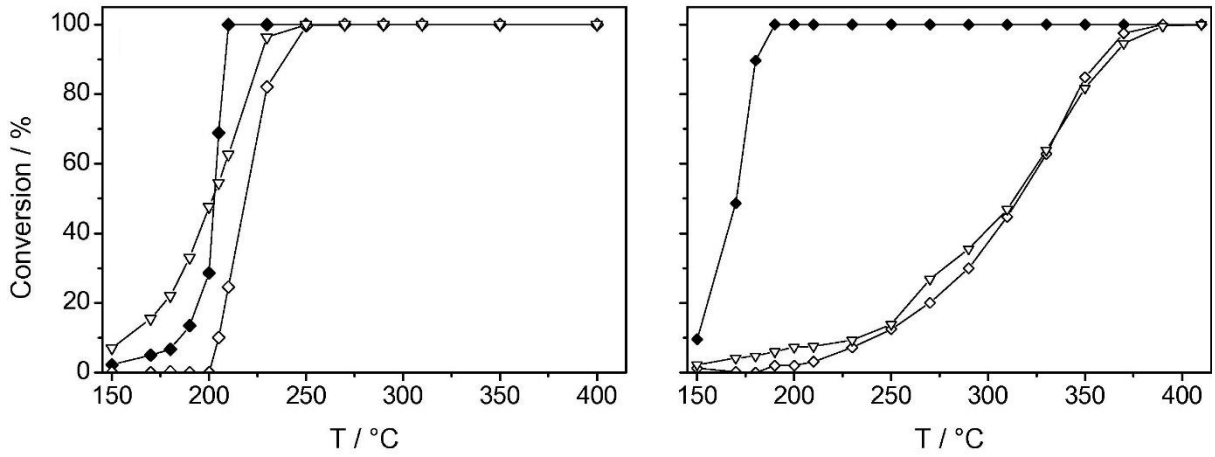

Figure 17: Curves of Ru/Al_2O_3 (left) and Ru/zeolite (right) for CO (closed) and CO_2 (open) conversion in different reaction mixtures. ◊= CO_2-rich idealised reformate (0.6 kPa CO, 2.8 kPa N_2, 1.2 kPa CO_2, rest H_2); Δ= CO_2/H_2 mixture (1.2kPa CO_2, 2.8kPa N_2, rest H_2), (Eckle, S *et al.* 2010).

Eckle *et al.,* 2011 investigated the difference in selectivities observed in the Ru/zeolite and Ru/Al_2O_3. In order to understand this difference, they tested a 2.2 wt.% Ru/zeolite and a 5 wt.% Ru/Al_2O_3 where both catalysts were prepared by Sud Chemie AG. All reactions were performed at 190°C under various feed compositions as seen in table 7. The concentration of CO was varied in order to determine whether the partial pressure of CO affected selectivity in both catalysts. Particle sizes were determined in the same manner as discussed in section 2.7. The resulting particles of Ru in the zeolite and on alumina were 1nm and 3nm, respectively. XPS also revealed that most of the Ru was situated inside the pores of the zeolite (Eckle, S *et al*. 2011).

When Ru/Al_2O_3 was exposed to both CO_2-ref and SR-ref 100, the presence of CO_2 increased the band intensity of adsorbed CO after comparing the results to the ID-ref 100. The Ru/zeolite was exposed to these feeds where the presence of CO_2 had no effect on CO_{ads}. These results indicate that CO_{ads} from CO_2 dissociation is facile on the Ru/Al_2O_3. The formation of CO_{ads} on the Ru/zeolite is therefore slow and the high selectivities are not entirely due to the build-up of CO_{ads} on the surface preventing CO_2 adsorption.

Figure 18: Proposed mechanism of selectivity in the Ru/zeolite and Ru/Al_2O_3 (Eckle, S *et al*. 2011).

Figure 18 shows the proposed mechanism of selectivity in the Ru/zeolite and Ru/Al_2O_3. Ru/zeolite is unaffected by the concentration of CO where high selectivities in Ru/Al_2O_3 can only be achieved when CO_{ads} forms a layer on the surface.

At 190°C, the Ru/zeolite was found to be more selective under all compositions tested compared to Ru/Al_2O_3. The selectivity of Ru/Al_2O_3 is dependent on the concentration of CO similar to that observed in the higher loaded Ru/zeolites. As the concentration of CO decreased from 6000 ppm to 3000 ppm, the selectivity decreased from 100% to 86%. A further decrease in CO concentration to 100 ppm resulted in a selectivity of 42% (Eckle,S *et al*. 2011). The results can be seen in table 8 below.

Table 8 : Reaction gas mixtures with varying CO and CO_2 concentrations(Eckle,S *et al*. 2011).

Reaction gas		
	Ru/zeolite	**Ru/Al_2O_3**
	Selectivity (%)	Selectivity (%)
Low-CO semi-realistic reformate (100 ppm CO)	100	42
Semi-realistic reformate (1000 ppm CO)	100	86
Semi-realistic reformate (3000 ppm CO)	100	100
Semi-realistic reformate (6000 ppm CO)	100	100

The Ru/zeolite catalyst displays 100% selectivity over all concentration of CO. Therefore high selectivity is not due to the ad-layer of CO_{ads} which prevents CO_2 dissociation. The bond between the substrate and the catalyst is weaker on this catalyst according to the Bronstedt-Evans-Polanyi relation which corresponds to the higher barrier for CO_2 dissociation. Complete removal of CO is therefore not possible without CO_2 methanation occurring on the Ru/Al_2O_3 at low concentrations. However, this can be achieved with the Ru/zeolite as CO_2 methanation is inhibited by the small nano-particles present.

2.10 Catalyst Selection

To select a suitable catalyst for this study, research into Ru/zeolites was conducted. It was suggested by Verdonck *et al.*, 1980 that Ru/Y zeolites were capable of performing methanation of CO at high temperatures. The catalyst used was a 5.6 wt.% Ru/Y zeolite with a CEC of 40%. In several studies performed by Eckle *et al.*, 2010-2012, a commercial Ru/zeolite was used to perform SMET under fuel processing conditions that would precede the PEMFC. Calculations were performed in order to determine whether Ru/Y was used in these studies.

The CEC was calculated by determining the number of acid sites in 1g of zeolite containing 5.6 wt.% of Ru. The Ru exists as Ru^{3+} and there are 5.54 $x10^{-4}$ mols of Ru^{3+} in 0.056g of Ru metal. The zeolite Y has a mass of 11532g/mol, therefore 1g contains $8.67x10^{-5}$ mols of zeolite. The number of acid sites is equivalent to the amount of aluminium present. Since Ru is present in the Ru^{3+} state, three aluminium sites would be needed to coordinate one Ru^{3+} ion. This gives the Y zeolite the capacity to exchange 40% of its cations for Ru^{3+}. If the Si/Al ratio is increased, the CEC values increases close to 100% which is not possible, since all aluminium sites are not in close proximity for the Ru^{3+} to coordinate. The sodium ions cannot all be replaced as some are trapped inside cages. Therefore it is proposed that the Y zeolite with a low Si/Al ratio is used in current literature for the methanation reaction of CO. The full calculation can be found in Appendix A.

3. Objectives of Study

The aim of this study is to investigate the Ru/Y zeolite catalyst for selective methanation in order to lower the CO concentration to 10 ppm. This is required for the gas to be used in the PEMFC. More specifically, the following objectives have been identified:

- To determine whether the Ru/Y zeolite is used in literature for SMET
- To prepare Ru/ Y Zeolite catalyst with different loadings in order to investigate its effect on the activity of selective methanation of CO.
- To test commercial Ru/Al_2O_3 catalyst to be used as a standard for comparison.
- To determine the effect of water vapour content on conversion and selectivity in Ru/Y zeolite
- To find the optimum loading and reaction conditions to obtain the lowest concentration of CO while maintaining high selectivities toward CO under fuel processing conditions.

4. Hypotheses

During the selective methanation reaction of CO in fuel processors, the smaller nano-particles of Ru found in the Y zeolite are more active and selective toward CO methanation than larger Ru particles.

Higher conversions of CO to CH_4 can be obtained due to the lower activity of these Ru nano-particles in the Y zeolite for CO_2 methanation.

5. Experimental Procedure

The experimental procedure followed throughout this study is given in detail in this section.

5.1 Catalyst Synthesis and Characterisation

5.1.1 Catalyst Synthesis

Material

The catalysts used in this study were prepared using the precursors $Ru(NO)(NO_3)_3$ (Alfa Aesar) and $[Ru(NH_3)_6]Cl_3$ and zeolite powder supplied by Linde (Zeolite LZ-52).

Preparation

The catalysts were prepared by conventional ion exchange and were stirred for 36 hours to allow the solution to reach equilibrium. Catalysts with different loadings, seen in table 9, were prepared by varying the amount of Ru precursor used. The solution was filtered and the catalyst was dried overnight at 60°C.

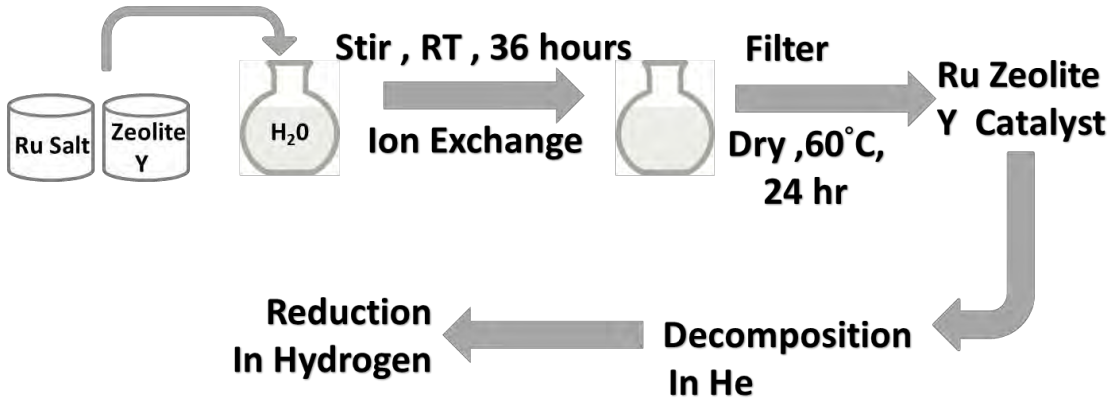

Figure 19 : Catalyst preparation procedure.

Table 9: Various catalysts prepared by $Ru(NO)(NO_3)_3$ and $Ru(NH_3)_6Cl_3$.

Precursor	Weight % Ru			
$Ru(NO)(NO_3)_3$	10.1	5.7	3.8	1.9
$Ru(NH_3)_6Cl_3$	6	4	2.4	1.1

Ru/Alumina

A 5 wt.% Ru/Alumina catalyst was obtained from Sigma-Aldrich in powdered form which was in a reduced state.

5.1.2 Catalyst Characterisation Techniques and Procedures

The following techniques were used to obtain certain characteristics of the catalysts used.

5.1.2.1 Determination of Ru Content

In order to determine the Ru content in the various prepared catalysts, Inductively Coupled Plasma-Optical Emission Spectrometry (ICP-OES) using a Varian ICP 730-ES spectrophotometer was used. The samples were digested and calibration curves were produced in order to calculate the weight percentage of Ru in the samples provided.

5.2 Selective Methanation Test Unit

The Process and Instrument Drawing (P&ID) found in figure 20 is explained as follows:

The gasses, N_2, Ar, CO, and H_2, were fed through in-house manifolds while CO_2 and He were fed via gas tanks situated in reactor hoods. All gasses passed through a filter in order to remove any particles that could potentially damage equipment downstream. Pressure reducing regulators (**PRR 1-5**) lowered the inlet pressure from 60 bar to 20 bar before entering the mass flow controllers (**MFC 1-5**) which then control the flow rate of gas. In order to feed He when needed, the N_2 MFC was used. The gasses were then fed into a blend pot which was set at a pressure of 6 bar_g using a back pressure regulator (**BPR 1**).

The overflow of feed gas coming into the blend pot was taken directly to the selection valve where it can be analysed on the Micro GC. The flow rate into each reactor (**Reactor 1-3**) was controlled by a second set of MFC's (**MFC 6-8**). The pressure in each reactor was controlled by three BPR (**BPR 2-4**). The HPLC pump fed water to reactor 1-3 by means of a micro-volume T-piece which houses 4 capillaries. The capillaries allowed the water to be split equally into each reactor where it is converted to steam at high temperatures. The gasses passed through the reactors and any water vapour present was removed via a condenser and the gas was sampled by the Micro GC using the selection valve. This allowed the bypass or one of three reactors to be sampled. The specific details of water delivery is further explained in section 5.2.6.

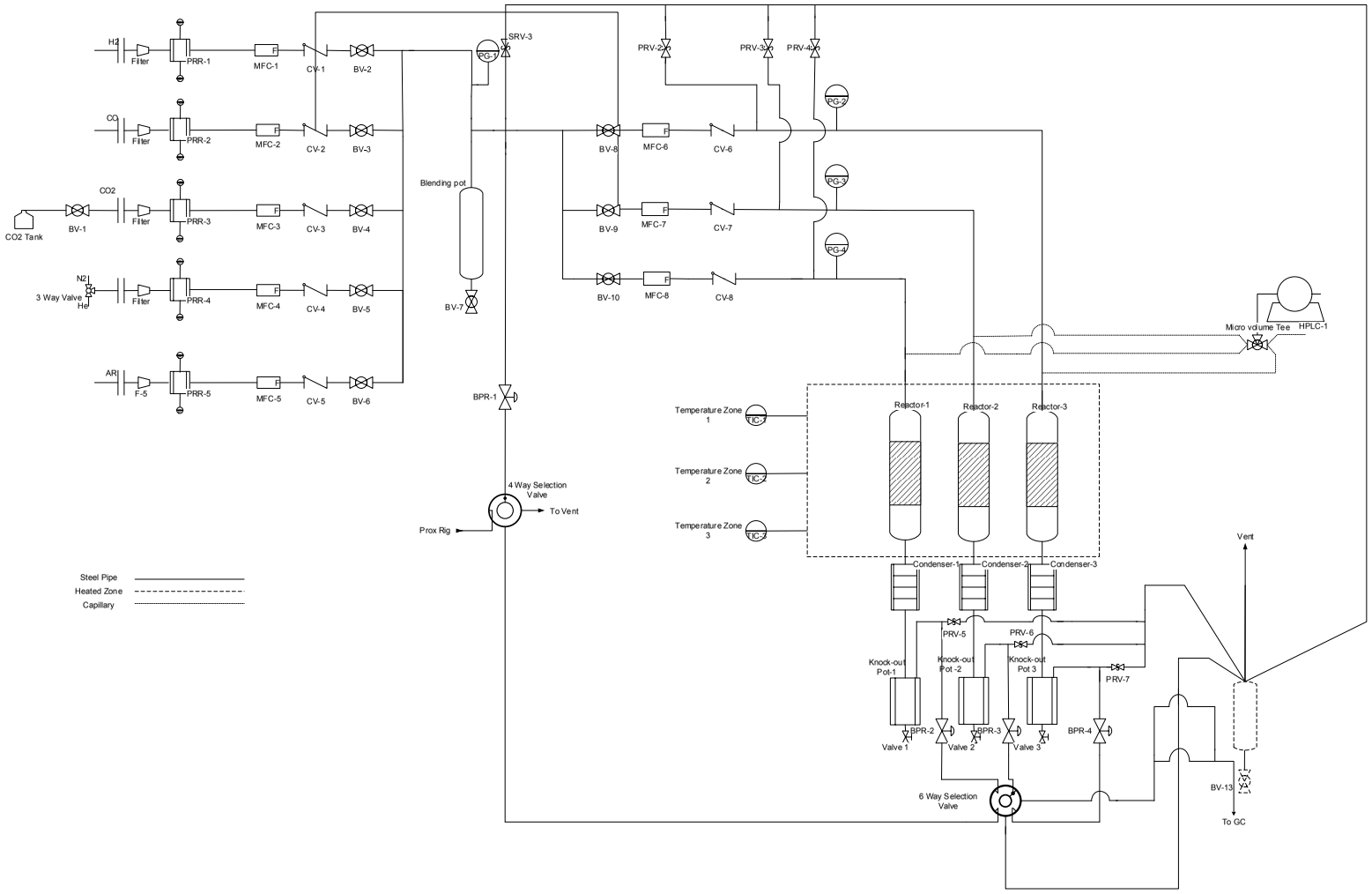

Figure 20 : Process and Instrument Drawing (P&ID).

5.2.1 Temperature Profiling

Temperature profiling of the reactors were performed for temperatures between 180°C and 220°C in order to determine the isothermal zone. The various temperatures were set using three Gefron 800P temperature controllers which controlled the temperature for three heating bands. Once the temperature was set, it was allowed to equilibrate before the measurements were taken using thermocouples inserted inside the thermowell. The position of the thermowell can be seen in Section 5.2.7 figure 22. The thermocouples were marked every 1 cm and placed in the thermowell where the temperature at each interval was recorded. Graph 1 below displays the temperature profiles observed for temperatures 180°-220°C. The graphs for temperature profiles of reactor 2 can be found in Appendix B.

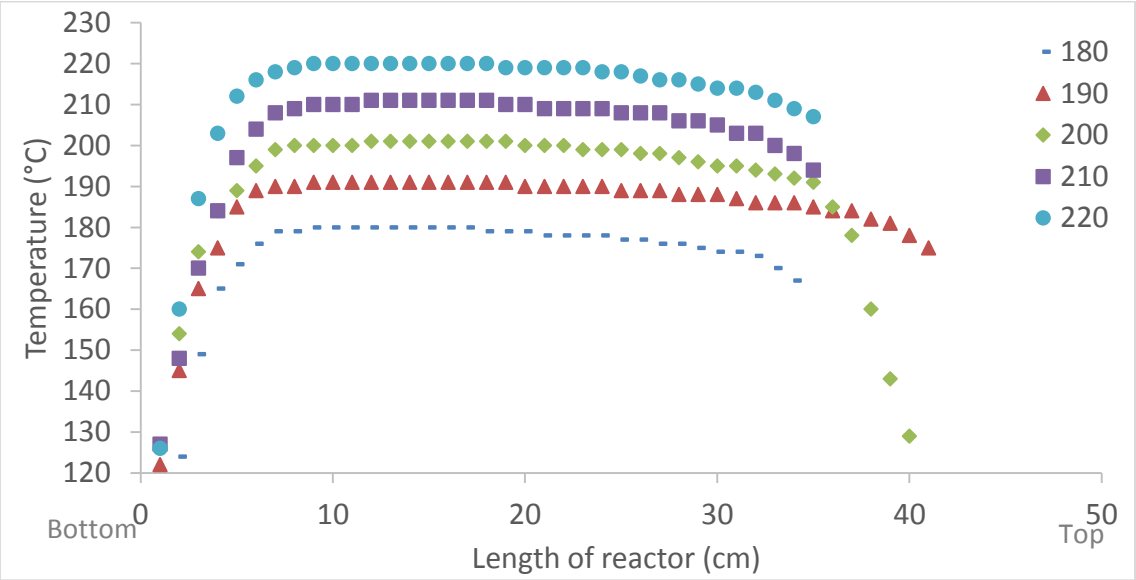

Graph 1 : Temperature profile of reactor 1 for temperature range 180°C-220°C.

Table 10 : Set points used on the Gefron 800P temperature controllers to reach desired temperatures.

Temperature	Set points		
	Heating Band 1	Heating Band 2	Heating Band 3
160	150	150	150
170	159	159	159
180	167	167	167
190	176	176	176
200	184	184	184
210	198	198	198
220	204	204	204

5.2.2 Pressure and Leak Testing

Pressure tests were performed on all three reactor systems in order to assess whether the system was able to maintain a set pressure. This was carried out by filling the reactor with nitrogen and allowing the reactors to pressurise to 5 bar. All fittings were tested for leaks by applying Snoop®, a liquid leak detector, which causes bubbles to form indicating the presence of gas leaks.

5.2.3 Pressure Relief Valves

The pressure relief valves (**PRV 5- PRV 7**) were each set at 9 bar. This was done by closing the relief valves then pressurising the rig to 10 bar using nitrogen gas. The relief valves were slowly opened and the pressure drop was observed until 9 bar. The rig was pressurised once again to 10 bar to ensure a 1 bar pressure drop would be observed.

5.2.4 MFC Calibration

In order to determine the difference in flow rate set points and the observed flow rate of gasses through the MFC's, calibration curves were produced for specific gasses. The Brookes Mass Flow Controllers were calibrated using a bubble flow meter for a specific gas. Calibration curves were obtained by setting a range of flow rates and measuring the flow rate observed by the bubble flow meter. All flow rates were converted to standard temperature and pressure. The calibration curve for H_2 can be found in graph 2 and calibration curves for all other gasses can be found in Appendix C.

In order to calibrate for CH_4, the CO MFC was temporarily fed with CH_4 and calibrated using the same procedure for all gasses. This is due to the expected flow rate of CO and CH_4 being different at the same set point.

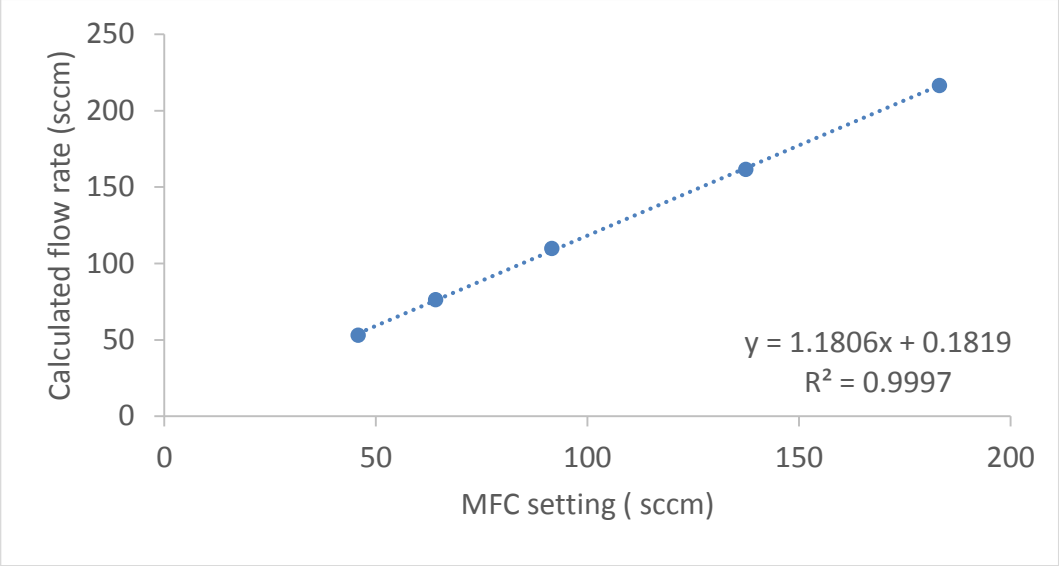

Graph 2 : MFC Calibration curve obtained for H_2.

5.2.5 Feed Compositions

The gasses were all supplied by Air Liquide and delivery is explained in section 5.2. Table 11 summarise the percentage of each gas used in the feed. Feed composition A was used in the preliminary experiment whereas feed B was used in all other experiments performed. The feed composition was altered as N_2 and Ar exhibit the same retention time on the COX column, which did not allow for the peak areas to be distinguished from one another.

Table 11 : Feed composition A and B used in the experimental setup.

Feed	**A**	**B**
Species	Percentage (%)	Percentage (%)
H_2	50	59
N_2	14	0
CO	1	1
CO_2	20	20
H_2O	10	10
Ar	5	10

5.2.6 Water Delivery

In order to feed 10% water to the reactor, the volume of water required for each space velocity needed to be calculated. This was done by calculating the number of moles using the molar volume of liquid. Using the molecular mass of water, the volume of water required can be calculated using the equations below:

Table 12 : Example of calculation for volume of water required to feed 10% water in a total flow of 100ml/min.

Total volume required (ml/min)	10
Molar Volume (Vm=L/mol)	22.41
Moles (n)	0.0004
Volume (ml/min)	0.008

$$V_m = \frac{nRT}{P} \qquad n = \frac{V}{V_m}$$

Due to the low flow rates of water required in the feed and the limitations of the HPLC pump (SSI Series I; range: 0.1-10 ml/min.), the water was introduced into the reactor via a capillary. The dimensions of the capillaries used are given in table 13 below. Figure 21 illustrates the Vici micro-volume T-piece which was attached to the HPLC pump in order to connect the (1/16 inch) steel tubing to the capillary. Graphite ferrules which were able to house two capillaries were used in order to split the flow of water to four different outlets.

Table 13 : Lengths of capillaries fitted into micro-volume T-piece.

	Length (cm)	Diameter(mm)
Waste	37	0.05
Reactor 1	119	0.05
Reactor 2	119	0.05
Reactor 3	119	0.05

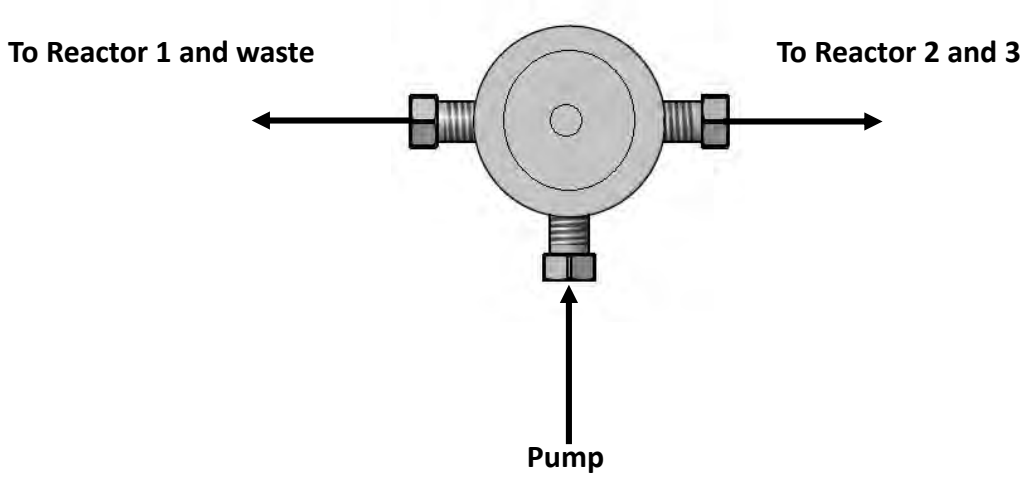

Figure 21: Vici Microvolume T-piece.

The ratio of the waste and reactor capillary lengths are proportional to the ratio of the flow rate of water through them. Therefore the lengths of all capillaries needed to be carefully selected in order to deliver the required volume of water to the reactors. The capillaries were calibrated to determine the total flow rate of water through all reactors, compared to the setting on the HPLC pump. The graph below is the calibration curve obtained for various pump settings.

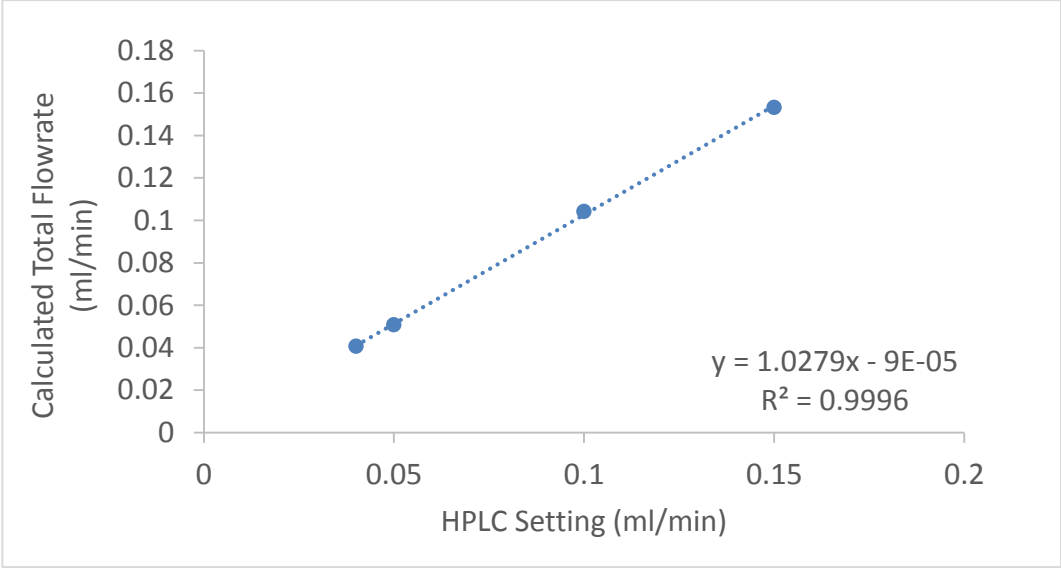

Graph 3 : The calibration curve obtained for the HPLC pump.

The linear nature of the curve indicates that the flow rate on the HPLC pump correlates well with the total flow rate calculated from all capillaries. The tables 20 to 23 in Appendix D presents the results for the split flow in the three reactor capillaries and the waste capillary. The split between the three reactor capillaries were very similar. This ensures that the same amount of H_2O is fed into the three reactors.

5.2.7 Reactor Assembly

The reactor design used throughout the experiments can be found in figure 22. The three fixed bed reactors were made from German grade 1.4401 stainless steel. The reactors have an internal diameter of 16mm. The reactors are inserted into three cores where they are housed along with three heating bands. The three heating bands operate individually in order to create an isothermal zone wherein the catalyst bed will be situated. The temperature profile of the three reactors for the temperatures between 180°C and 220°C can be found in section 5.2.1.

The reactors were packed with glass wool inserted at the bottom of the reactor to prevent silicon carbide from entering the rest of the pipes. The reactor was then filled with 35 ml of silicon carbide up until the base of the catalyst bed. The catalyst was then inserted followed by silicon carbide to fill the remainder of the reactor volume. The reactor was then sealed to prevent any gas leaks from occurring.

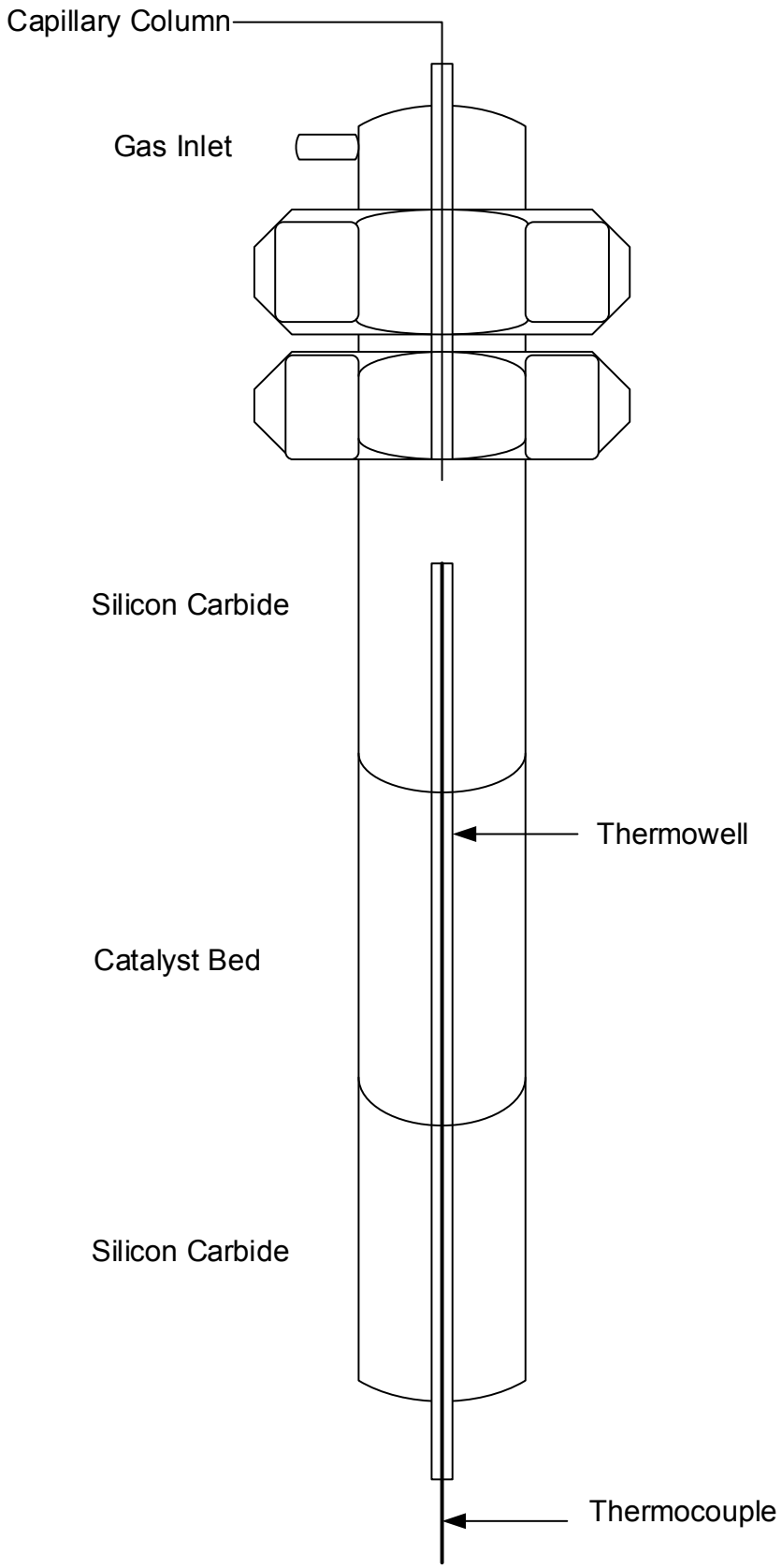

Figure 22 : Fixed bed reactor design.

5.2.8 Water Knock Out

The water was fed to the reactor in liquid state and once it came into contact with the silicon carbide at high temperatures, it vaporised. In order to prevent water vapour from entering the Micro GC, a condenser was placed below the reactor to allow the water vapour to condense into the knockout pot where the water is collected and removed. The condenser consists of coils where a mixture of antifreeze and water flows through. The mixture was fed to the system via a Lauda Alpha cooling bath set at 4°C.

The condensed water collected in the knockout pots were measured after every experimental run before the HPLC pump setting was changed. The volume from each reactor and the waste stream was calculated by measuring the mass of water that was collected.

The total volume of water measured at all outlets correlated well with the change in volume obtained from the scale measurements. The theoretical flow rate of water calculated from the HPLC pump corresponded to the calculated flow rates obtained from the volume of water collected over the time period of an experimental run.

Heating lines were wrapped around and along piping and regulators to prevent condensation of remaining water vapour from occurring before entering the Micro GC. The heating lines were set at 60°C and were well insulated. The temperature of the heating lines were monitored by a thermocouple inserted between the heating line and insulation.

5.2.9 Sampling Procedure

The sampling of product from the different reactors and the by-pass was done using a 6-way selection valve. A schematic of the valve is shown in figure 23. There are essentially 4 different inlets which include three reactor streams and the bypass, where the outlets are either the GC or the vent. In the figure 23 position A, the sample loop is filled whereas in position B, the sample contained in the sample loop is sent to the GC for analysis. By manually switching the valve, using a Vici valve controller, four outlets can be sampled to analyse the desired streams.

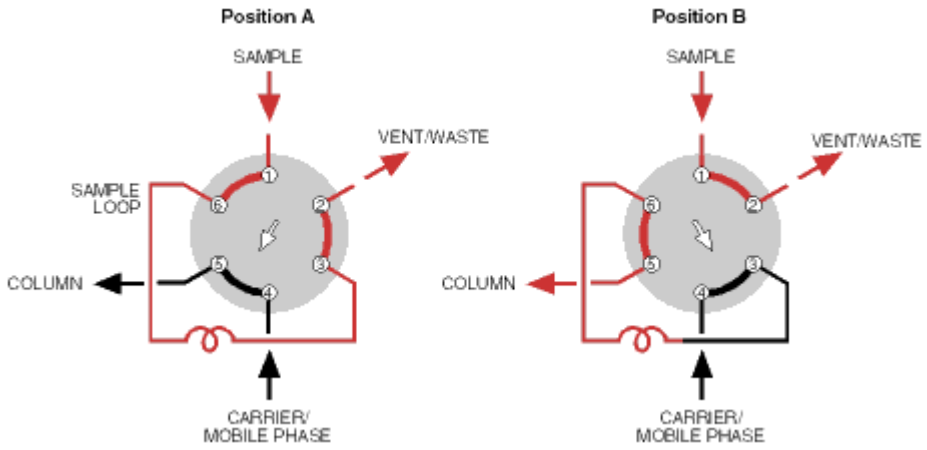

Figure 23 : Schematic of the VIci valve used to sample the different product streams.

5.3 Test Procedure

The following procedure was performed after the catalysts were placed in the reactors and leak and pressure tests were completed. Experimental runs were performed between 160°C and 220°C and space velocities ranging from 800 ml/g_{cat}.h to 25000 ml/g_{cat}.h.

5.3.1 Reduction Procedure

In order to obtain the Ru in its metallic state, a decomposition and reduction procedure was performed. The decomposition step allowed for the complex's ligands to slowly decompose whereas the reduction step allowed for the uptake of H_2 to change the oxidation state of Ru from Ru^{3+} to Ru^0. A stepwise heating rate was achieved using Gefron 800P temperature controllers where the desired heating rate and hold time was set.

Ru/Zeolite

The prepared catalysts (1.1 wt.%, 2.4 wt.%, 4 wt.% and 6 wt.%) were reduced using the following reduction treatment:

- Catalysts were decomposed in flowing He at a heating rate of 0.4°C/min until 350°C.
- Catalysts were held at 350°C for 1 hour.
- Catalysts were purged with H_2 and reduced for 1 hour.

The reduction procedure for the 1.9 wt.% Ru/Y zeolite was performed in the same manner with the exception of the heating rate of 0.8°C/min used.

Ru/Al_2O_3

The same procedure was used prior to testing the commercial Ru/Al_2O_3 catalyst.

5.3.2 Start-Up Procedure

The start-up procedure which followed the reduction of the catalyst in the reactor was as follows:

- MFC 1-5 were set to the desired flow rates and the gas mixture was allowed to mix for 30 minutes in the blend pot.
- The heating lines were set to 60°C.
- A thermocouple was placed inside the reactor in the same positon of the catalyst bed in order to monitor the temperature throughout the reaction.

- The feed was sampled by the Micro GC in order to determine the composition before it was allowed to pass through the reactor.
- The HPLC pump was set to the flow rate required and switched on to allow water to enter the reactor.

5.3.3 Online Procedure

In order to sample the products under different reaction conditions and monitor the reaction, the following procedure was carried out:

Changing space velocity: When changing the space velocity, the reaction would re-establish steady state after 4 hours. Space velocity was calculated using equation 1.

$$Space\ Velocity = \frac{flowrate*60}{mass\ of\ catalyts} = \frac{ml}{g_{cat}.h} \qquad \textbf{Equation 1}$$

Changing temperature: When changing the temperature, the set points were changed and the temperature was allowed to equilibrate for 5 hours to allow the reaction to reach steady state. When the temperature was decreased, the reactor was allowed to cool naturally.

5.3.4 Shut Down Procedure

The shutdown procedure carried out once the reaction is complete is as follows:

- Sampling of the product was stopped on the Micro GC.
- All gasses were switched off by switching off the MFC. Nitrogen was left to flow through the reactors to flush the system.
- The HPLC pump was switched off to terminate the flow of water to the reactor.
- The temperature was set to room temperature and the reactor was allowed to cool in nitrogen.

5.4 Product Analysis

To distinguish between the various species in the product stream and calculate their concentrations, an online Varian CP 4900 Micro GC was used whereby the details of the modules used, calibration and data work up will be discussed in further detail.

5.4.1 The Micro GC

In order to analyse the gas composition in both the dry feed gas and product stream, the online Micro GC coupled with a TCD detector was used. The Micro GC consists of four modules in order to separate the different constituents present in the product and feed streams. Each module comprises of its own injector, column and TCD detector. The table 14 below summarises the details of each module and settings used.

Table 14: Settings used for the four modules present in the Micro GC.

Channel	1	2	3	4
Column type	Molsieve 5A ^{BF}	Molsieve 5A ^{BF}	5 CB	COX
Column length(m)	10	20	10	1
Injector Temperature(°C)	110	110	40	109
Sampling line temperature(°C)	60	60	60	60
Column temperature (°C)	110	100	50	80
Column head pressure (kPa)	200	200	70	110
Carrier gas	Ar	H_2	H_2	H_2
Species analysed	H_2	Ar,CO,CH_4,N_2	CO_2	Ar, CO, CH_4 , CO_2

5.4.2 CO Detection Limit

Catalysts prepared using $Ru(NO_3)_3NO$ were used in the initial testing phase of this study. These tests were performed in order to determine whether the rig setup and all equipment were functioning properly, and that accurate results could be measured.

From initial testing, the GC modules were found to be insufficient in determining the concentration of CO at extremely low levels. The lowest concentration of CO detectable on the $MS5^{BF}$ (20m) column was equivalent to 88% conversion of CO. The gap between 88% and 100% conversion, where no peak for CO was observed, was insufficient in calculating accurate conversion and selectivities.

For all further testing, a COX column was installed which allowed for lower concentrations of CO to be detected, as the retention time for CO on this column was much shorter, compared to that of the $MS5^{BF}$ column. This produced a narrower peak on the chromatograms obtained via the micro GC. The highest conversion that can be measured on the COX column is >99%. To further quantify the CO concentration in the low ppm range, an ABB AO2040 gas analyser was used when 100% CO conversion was achieved. The analyser is capable of detecting 0-400 ppm of CO.

5.4.3 Micro GC Calibration

To identify the gas species on the chromatogram, the retention time of each species needed to be determined. This was done by flowing each individual gas with a known concentration of Ar, to be used as the internal standard. The different retention times for each gas on the various columns is summarised in table 15. Prior to these runs, channel 1 and 2 were baked at 180°C overnight in order to remove any contaminants trapped on the columns which alter the retention times of some species.

Table 15: Retention times for various species on respective columns.

Gas	Retention Times (min)			
	Column 1	Column 2	Column 3	Column 4
Ar		0.57		0.4
H_2	0.36			
CO		1.03		0.5
CO_2			0.65	2.6
CH_4		0.98		1.2

Calibration of the micro GC was performed by allowing the feed gas to be sampled every 4 minutes for 4-5 hours. The concentrations of each gas were altered to produce 5 different mixtures while keeping the concentration of Ar and the total volume constant. The chromatograms in figure 24 to 27 (Appendix E) were obtained whereby the areas of the peak were used to produce calibration curves for each gas. The calibration curve for CO on the $MS5^{BF}$ 20m column can be seen in graph 4. Calibration curves for all other species can be found in Appendix E.

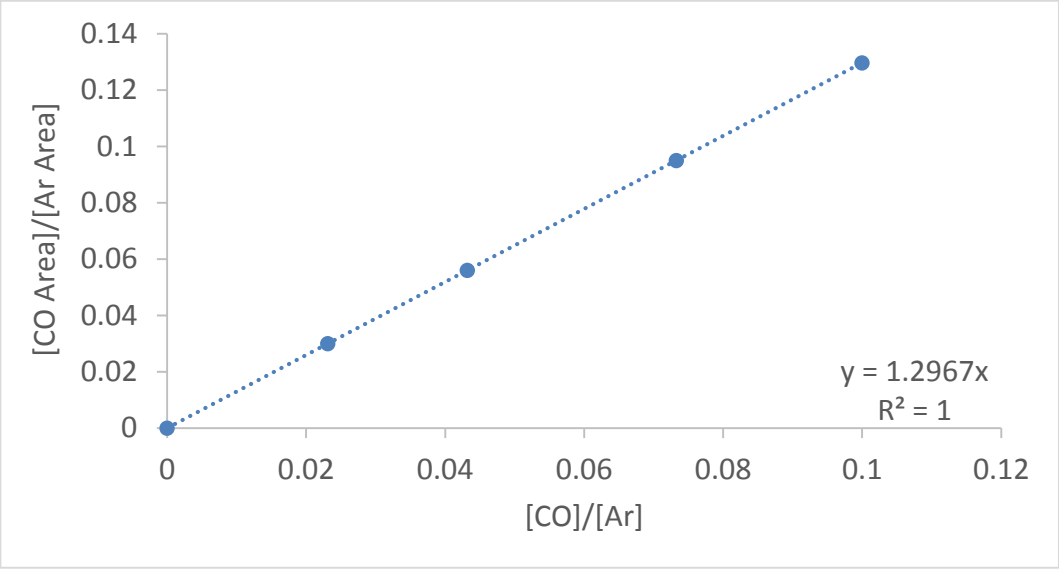

Graph 4 : Calibration curve obtained for CO in the COX column.

5.4.4 The Effect of Water Vapour on GC Calibration

In order to test whether the presence of water vapour affected the calibration curves obtained on the GC, the same feed mixture was sampled through the by-pass where no water vapour was present, and through a reactor filled with SiC fed with H_2O.

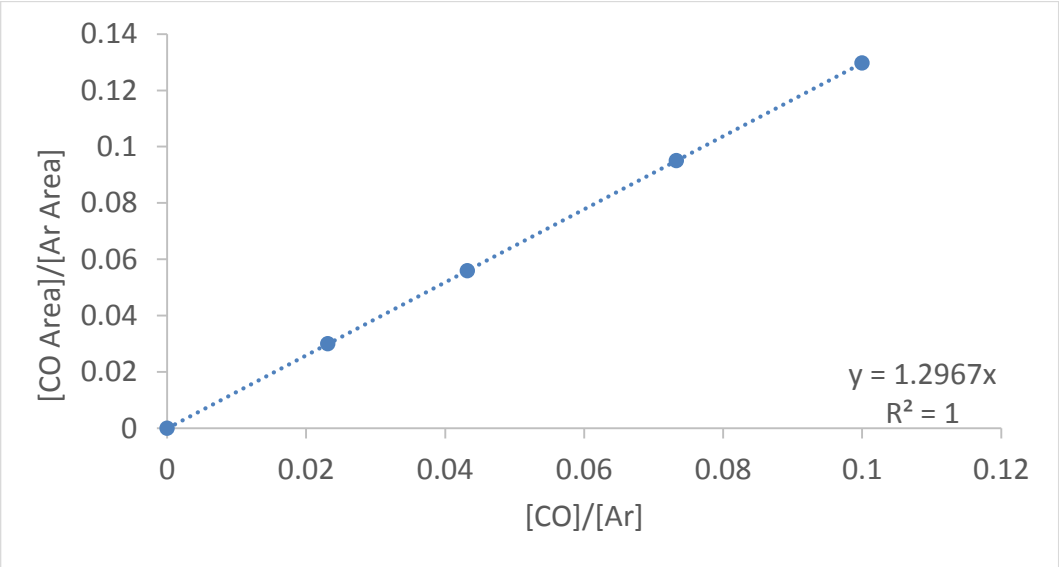

Graph 5 : The calibration curve obtained for CO on the Micro GC in the absence of H_2O.

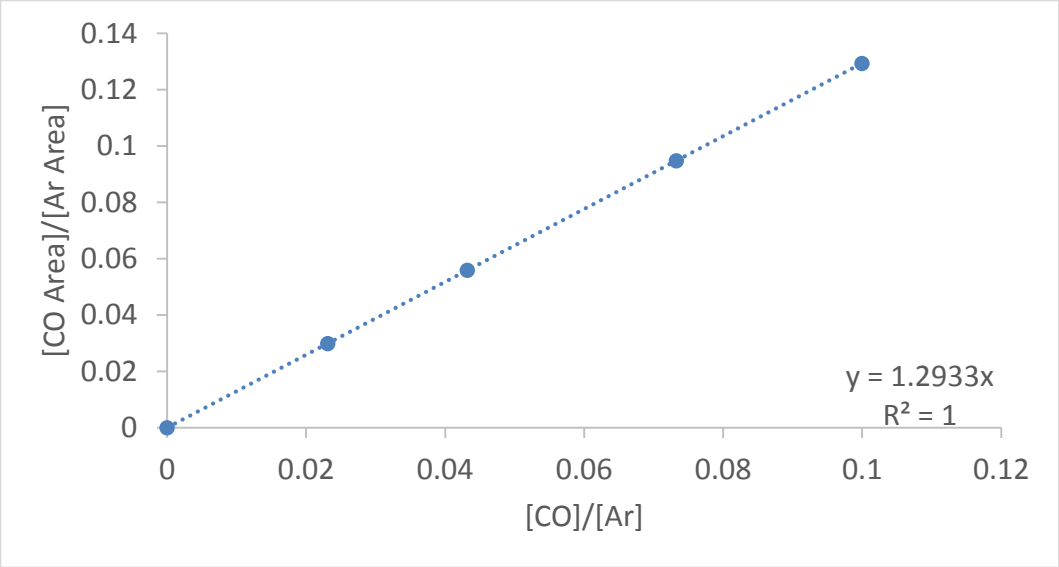

Graph 6 : The calibration curve obtained for CO on the Micro GC in the presence of H_2O.

The variation between the gradients of the two curves were found to be 0.2% which indicates that there is no significant difference between them. There is no effect of the water vapour being present as most of the water vapour is knocked out of the feed when passing through the condenser. Therefore it is acceptable to use the calibration curves obtained via the by-pass. This also allows for the GC to be recalibrated at any time if need be.

5.4.5 Micro GC Data Workup

The molar flow rates of each species in the feed as well as the product stream were calculated by means of the calibration graphs obtained from the Micro GC calibration displayed in table 16, where the equation 2 is the equation of the curves. The graphs for each species in the feed can be found in Appendix E.

Table 16 : Equations for gasses obtained from calibration curves for different GC modules.

Column	Species	Equation
MS5	H_2	y = 5.0512
COX	CO	y= 1.2967
	CH_4	y = 1.2539
	CO_2	y = 1.6202

$$\frac{Area_A}{Area_{Ar}} = RRF_A \frac{Moles_A}{Moles_{Ar}} + C_A \qquad \textbf{Equation 2}$$

$$Molar\ Flow\ rate_A = \left(\frac{\left(\frac{Area_A}{Area_{Ar}}\right) - C_A}{RFF_A} \right) \times Molar\ Flow\ rate_{Ar} \qquad \textbf{Equation 3}$$

The area of species A relative to the area of Ar are plotted on the y axis where the moles of species A relative to the moles of Ar are plotted on the x axis. The gradient of the linear curve that is produced is equivalent to the relative response factor (RRF) of the specific gas. This value is then used to calculate the molar flow rates of species using equation 3.

The area of species A and that of Ar , obtained from the integration of the chromatogram peaks, are used along with the RRF and the molar flow rate of Ar to determine the molar flow rate of species A. This is done for all gas species relative to Ar where these molar flow rates are used to calculate conversion, selectivity and carbon balances. To calculate the molar flow rates of species entering the reactor, the chromatograms obtained from analysing the feed were used. The conversion of CO was calculated using equation 4. The selectivity towards CO was calculated using equation 5 whereas the selectivity towards CO_2 was calculated using equation 6. The carbon balance for each reaction was calculated using equation 8.

$$X_{CO} = \frac{\dot{n}_{CO,feed} - \dot{n}_{CO,product}}{\dot{n}_{CO,feed}} \times 100\% \qquad \textbf{Equation 4}$$

$$S_{CO} = \frac{\dot{n}_{CO\ converted}}{\dot{n}_{CH_4 Produced}} \times 100\% \qquad \textbf{Equation 5}$$

$$S_{CO_2} = \frac{\dot{n}_{CO_2\ converted}}{\dot{n}_{CH_4 Produced}} \qquad \textbf{Equation 6}$$

$$S_{CO} + S_{CO_2\ Converted} = 1 \qquad \textbf{Equation 7}$$

$$C_{Balance} = \left(\frac{\dot{n}_{CO\ In} + \dot{n}_{CO_2\ In}}{\dot{n}_{CO\ Out} + \dot{n}_{CO_2\ Out} + \dot{n}_{CH_4\ Out}}\right) \times 100\% \qquad \textbf{Equation 8}$$

The carbon balance for all experiments were found to be in the range of 100±2%. The carbon balances for all reactions are within an acceptable range for all conversions and selectivities to be considered correct. All carbon balances for reactions can be found in Appendix F.

6. Results and Discussion

6.1 Catalyst Synthesis

In order to determine the weight percentage of Ru present on the catalyst, characterisation procedures were performed after the catalysts were prepared.

6.1.1 ICP-OES Results

The catalysts were synthesised as explained in section 5.1.1 where the intended loadings of Ru were given. To determine the Ru content in the prepared catalysts, ICP-OES was performed on all samples. The results of the analysis are given in table 17 below.

Table 17 : The loadings of Ru obtained from ICP-OES analysis.

Calculated (wt.% Ru)	ICP-OES (wt.% Ru)
$Ru(NO_3)_3(NO)$	
1.9	1.39
3.8	1.87
5.7	2.15
10	2.41
$Ru(NH_3)_6Cl_3$	
1.1	1
2.4	2.2
4	3.68
6	5.4

It is clear from the ICP-OES results that the intended loading of Ru was not achieved in catalysts prepared using the $Ru(NO_3)_3NO$ complex. The maximum loading that was achieved was 2.41 wt.% when a 10 wt.% Ru loading was intended. Less variation in the intended and observed loadings of Ru were achieved when using the $Ru(NH_3)_6Cl_3$ precursor.

6.2 Preliminary Results

A 1.4 wt.% Ru/Y zeolite prepared using $Ru(NO_3)_3(NO)$ was tested between 190°C and 210°C over a range of space velocities between 1700 ml/g_{cat}.h and 17000 ml/g_{cat}.h for SMET. The catalyst was reduced as explained in section 5.3.1. As the temperature is increased from 190°C to 210°C, the CO conversion increased from 81% to 95% at a SV of 8500 ml/g_{cat}.h as seen in graph 7. The effect of temperature cannot be seen at low SV because the catalyst is capable of achieving 99% to 100% conversion over the temperature range. With increasing SV the conversion decreases for all recorded temperatures.

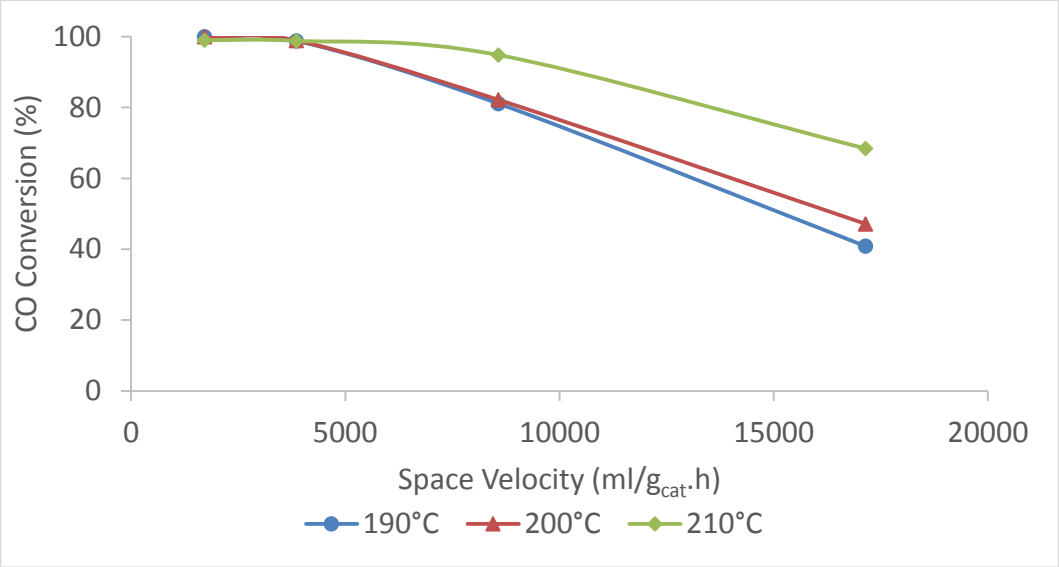

Graph 7 : The CO conversion curve for 1.4 wt. Ru/Y zeolite between 190°C and 210°C.

The effect of temperature on selectivity is more evident over the range of SV. At conversions close to 100% at 1700 ml/g_{cat}.h, the corresponding selectivities differed for all temperatures. Higher selectivities for CO methanation are obtained at lower temperatures. This means that less methanation of CO_2 occurs at 190°C.

Selectivities exceeding 100% are also observed in graph 8. One recalls from section 5.4.5 that CO selectivity is defined as the ratio of CO consumed from the feed over CH_4 produced. Selectivity for CO in excess of 100% then means that more CO is being converted than CH_4 is being produced. This is balanced by a proportional and negative selectivity for CO_2 because all carbon is accounted for in the carbon balance. A negative selectivity for CO_2 is nothing other than formation of CO_2, from CO. This is simply the WGS reaction occurring over the catalyst. Selectivity values in excess of 100% are a reflection of CO being converted to CH_4 and to CO_2, the contribution of either is easily estimated by looking at the CH_4 formation in graph 9. All selectivity values and CH_4 formation data can be found in Appendix F.

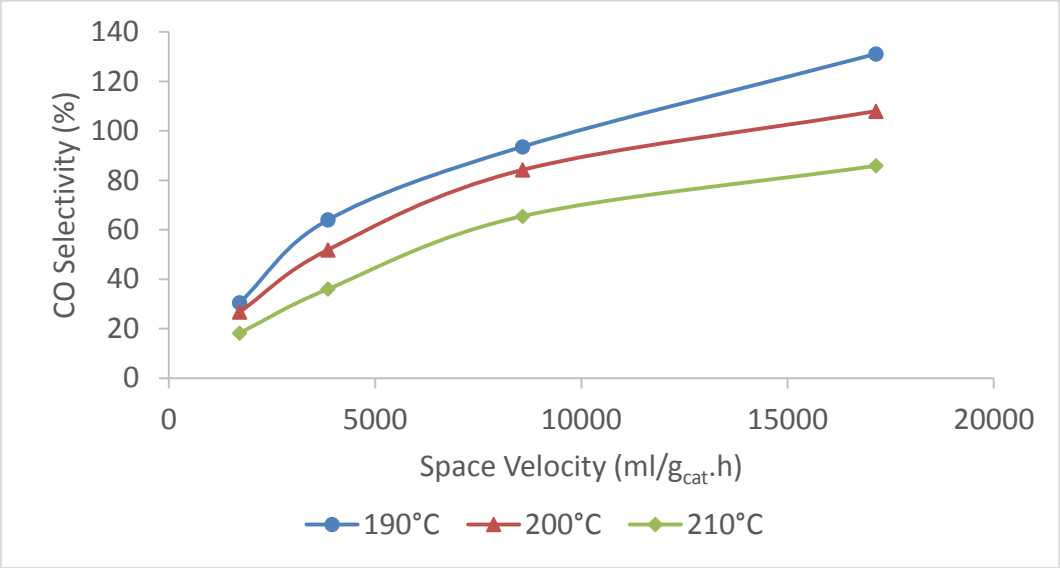

Graph 8 : The CO selectivty curve for 1.4 wt.% Ru/Y zeolite between 190°C and 210°C.

An example can make this clear. Comparing graph 8 and 9 one observes that for example at the highest tested SV, selectivities exceed 100% at 190°C (131%) and 200°C (108%) but not at 210°C (85%). On the other hand, the formation of CH_4 is lowest at 190°C (0.31%) and highest at 210 °C (0.79%). The contribution of the WGS reaction to converting CO becomes smaller at higher temperature because the WGS is an exothermic reaction.

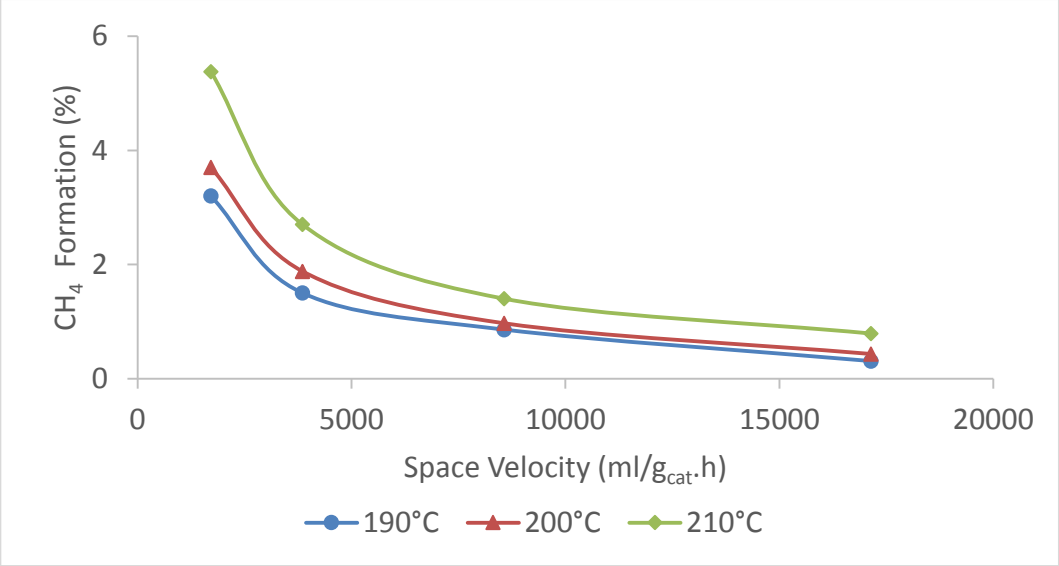

Graph 9 : The CH_4 formation for 1.4 wt.% Ru/Y zeolite between 190°C and 210°C.

Selectivities for CO that are lower than 100% demonstrate that CO_2 methanation also takes place. A viewing of the CH_4 formation in graph 9 also demonstrates that especially at low SV more CH_4 is formed from CO_2 than from CO. We are interested in high selectivities for CO at high conversions of CO. It is apparent from graph 7 and 8 that high selectivities for CO are typically obtained at low CO conversions, unfortunately. In summary then, the salient numbers from this test are a 64 % CO selectivity at ≈99% CO conversion at 190°C. This result should be kept in mind for comparison to further tests.

The remaining catalysts prepared using $Ru(NO_3)_3(NO)$ showed low activity for CO methanation as complete CO conversion was rarely achieved at 190°C. Temperatures above 190°C were needed in order for CO methanation to occur. These catalysts seem to be less active for CO methanation at temperatures reported in literature. For further experiments, catalysts prepared using the $Ru(NH_3)_6Cl_3$ precursor was used as the improved results are expected.

6.3 The Ruthenium/ Y Zeolite Catalyst

Catalysts prepared from $Ru(NH_3)_6Cl_3$ with loadings of 1 wt.%, 2.2 wt.%, 3.6 wt.% and 5.4 wt.% Ru were tested after undergoing decomposition (0.4°C/min) in He until 350°C where the catalysts were reduced in H_2. The slow heating rate was used to ensure that all moisture was removed from the catalyst prior to reduction. In work done by Verdonck *et al*., 1980, a faster heating rate (≈ 4°C/min) was used as the reduction was performed under vacuum. The removal of water is important to prevent hydrolysis of the zeolite framework and sintering of the Ru metal. The slow heating also ensures that the bulk of Ru is contained within the zeolite pores and does not migrate to the outer framework. The catalysts were tested in the range of 160°C to 210°C at SV between 850 ml/g_{cat}.h and 25000 ml/g_{cat}.h.

6.4 The Effect of Loading

The effect of loading on the CO conversion, CO selectivity and CH_4 formation was investigated by testing catalysts prepared with different Ru loadings under the same reaction conditions.

The percentage of CH_4 produced for all catalysts at 190°C over the range of SV can be seen in graph 10. The 5.4 wt.% catalyst was found to be the most active towards the methanation reaction as the highest percentage of CH_4 was produced. According to Eckle *et al*., 2012, the higher loaded catalysts such as the 5.6 wt.% in their study, contained larger particles of Ru, in addition to small nano-particles, compared to lower loaded catalysts. These large particles are more active for methanation of both CO and CO_2. The lower loaded catalysts consist of smaller Ru particles, which are less active for the methanation of CO_2, prevent excessive amounts of CH_4 from being formed.

As the loading is decreased, the percentage of CH_4 formed for a given set of conditions (SV and temperature) decreases. The 1 wt.% Ru/Y zeolite forms significantly less CH_4 compared to the other three catalysts. This could be due to the Ru loading being insufficient for the methanation reaction as the expected particle size of the 1 wt.% and 2.2 wt.% catalyst are assumed to similar according to the study performed by Eckle, S *et al*. 2012.

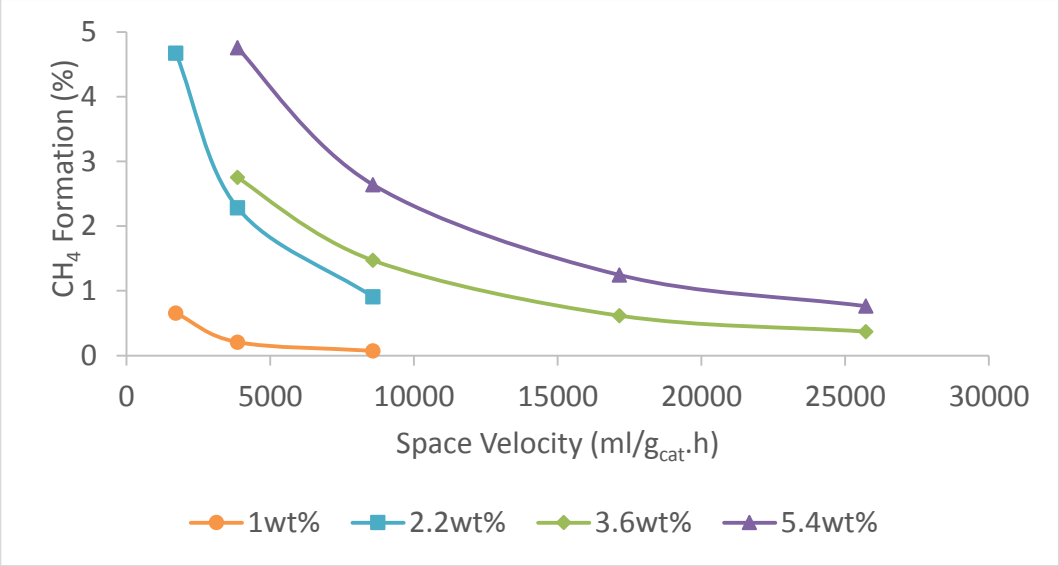

Graph 10 : The effect of loading on the formation of CH_4 at 190°C between 1700 ml/g_{cat}.h and 25000 ml/g_{cat}.h.

Graph 11 shows the conversion of CO at 190°C for all four catalysts over the range of SV. The effect of loading on the conversion of CO can only be seen at high SV where 100% CO conversion is no longer achieved. This is due to all catalysts, with the exception of 1 wt.%, being able to convert 100% CO at 190°C at low SV. As the loading is increased from 1 wt.% to 5.4 wt.%, the conversion of CO increases over the range of SV. The 1 wt.% catalyst shows very little activity for CO methanation which is evident from the low CO conversions and the low percentage of CH_4 produced, compared to the 2.2 wt.% Ru/Y zeolite. This indicates that there is exists a minimum loading of Ru needed for the reaction to take place.

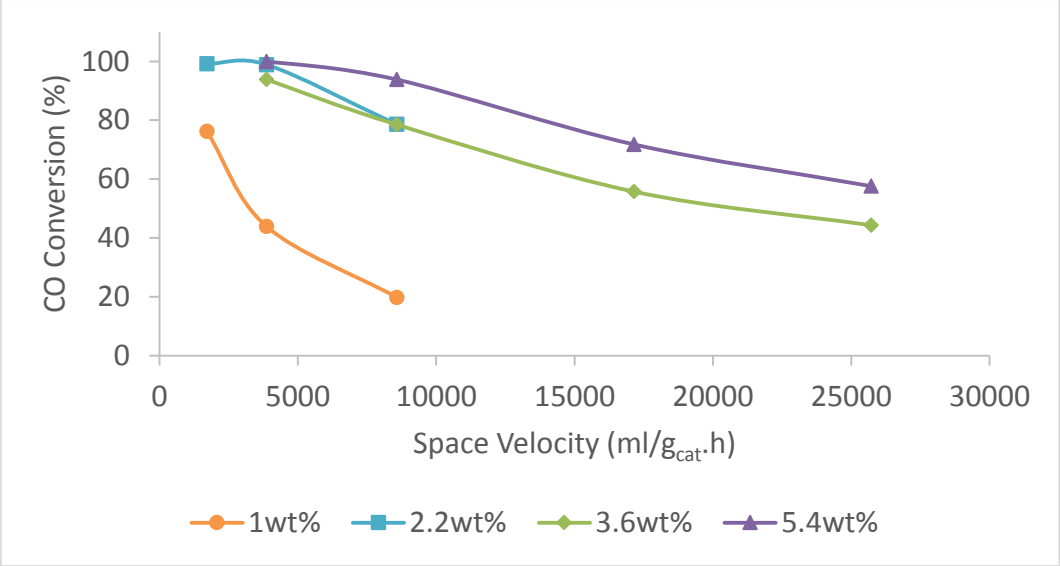

Graph 11 : The effect of loading on the CO conversion at 190°C between 1700 ml/g_{cat}.h and 25000 ml/g_{cat}.h.

Obtaining 100% CO conversion is crucial as the target is <10 ppm of CO remaining in the feed. However, this needs to be achieved by consuming the least amount of H_2 gas. The selectivity of the catalyst is what differs among these catalysts as the loading is changed. Graph 12 shows the selectivity of these catalyst at 190°C over the range of SV.

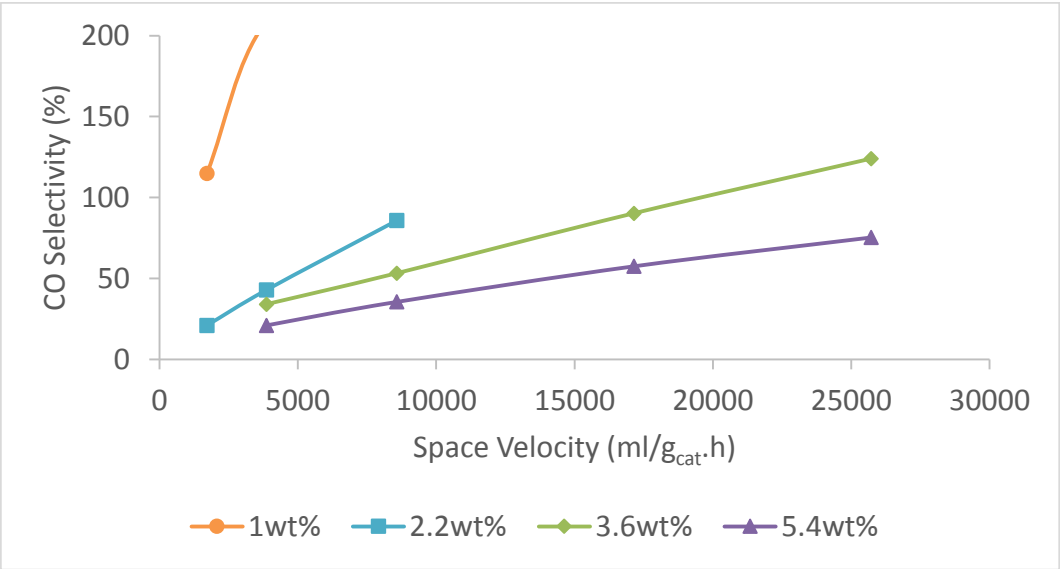

Graph 12 : The effect of loading on the CO selectivity at 190°C between 1700 ml/g_{cat}.h and 25000 ml/g_{cat}.h.

It is clear that as the loading is decreased, the selectivity of catalysts toward CO methanation increases. It should be noted that the selectivity of the 1 wt.% catalyst exceeds 100% due to the catalyst not being active for methanation but rather active for the WGS reaction. The 2.2

wt.% catalyst is seen to display the highest CO selectivity with high CO conversions. According to Eckle *et al*., 2012, the selectivity of the Ru/zeolite is affected by the size of the Ru nano-particles.

The high selectivity displayed by this catalyst is due to the Ru nano-particles being less active for the dissociation of CO_2 and subsequent methanation, compared to the larger particles found in catalysts with higher metal loadings. In characterisation studies performed by Eckle *et al*., 2012, lower loaded catalysts were found to have most of the metal present in the zeolite pores and only a few large particles on the outer surface of the zeolite framework.

The same explanation can be used on the catalysts tested in this study as we assume the catalyst used by Eckle *et al*., 2010 to be Ru/Y zeolite. According to graph 12, the selectivity is negatively affected by an increase in Ru loading. This is due to the difference in the rate at which CO is converted and the rate at which CH_4 is formed for the different catalysts. For the 5.6 wt.% catalyst in their study, the rate of CO conversion was slower than the rate at which CH_4 formed, which caused the selectivity to drop below 100% in low concentrations of CO. This indicates that CO_2 methanation is taking place. As the loading is decreased, the difference between the CO conversion and CH_4 formation rate decreased until the rates for these two reactions become similar. This was observed for the 2.2 wt.% Ru/zeolite as a selectivity of 100% toward CO was observed under all reaction conditions.

6.5 The Effect of Reaction Temperature

From the investigation into the effect of Ru loading, the 2.2 wt.% Ru/Y zeolite displayed the highest selectivity towards CO at 190°C. Therefore the 2.2 wt.% Ru/Y zeolite will be used to explain the effect of reaction temperature. All catalysts were however tested under all these conditions. The results obtained for the remaining catalysts can be found in Appendix F.

The effect of temperature on the CH_4 formation can be seen in graph 13 for a 2.2 wt.% Ru/Y over the temperatures between 160°C and 190°C. CH_4 formation is seen to increase with temperature and decrease with SV. CH_4 formation exceeding 1% comes from CO_2 methanation as there is only 1% CO in the feed.

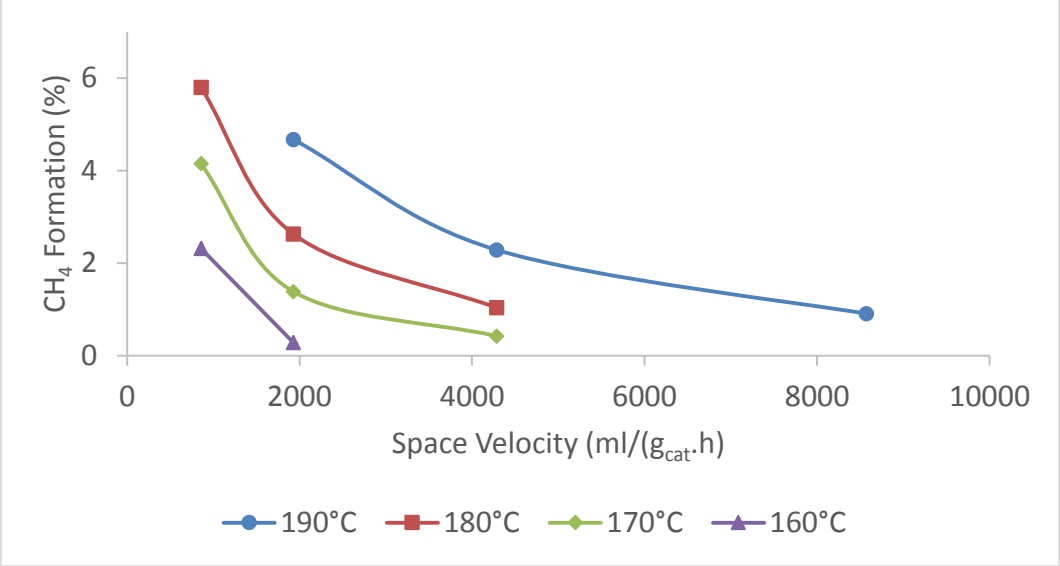

Graph 13 : The effect of temperature on CH_4 formation between 800 ml/g_{cat}.h and 8500 ml/g_{cat}.h for the 2.2 wt.% Ru/Y zeolite.

The effect of temperature is not noticeable at low SV in graph 14 where 100% conversion across the temperature range is achieved. As the temperature is increased from 160°C to 190°C, at a SV of 4000 ml/g_{cat}.h, the CO conversion increases from 72% to 98%.

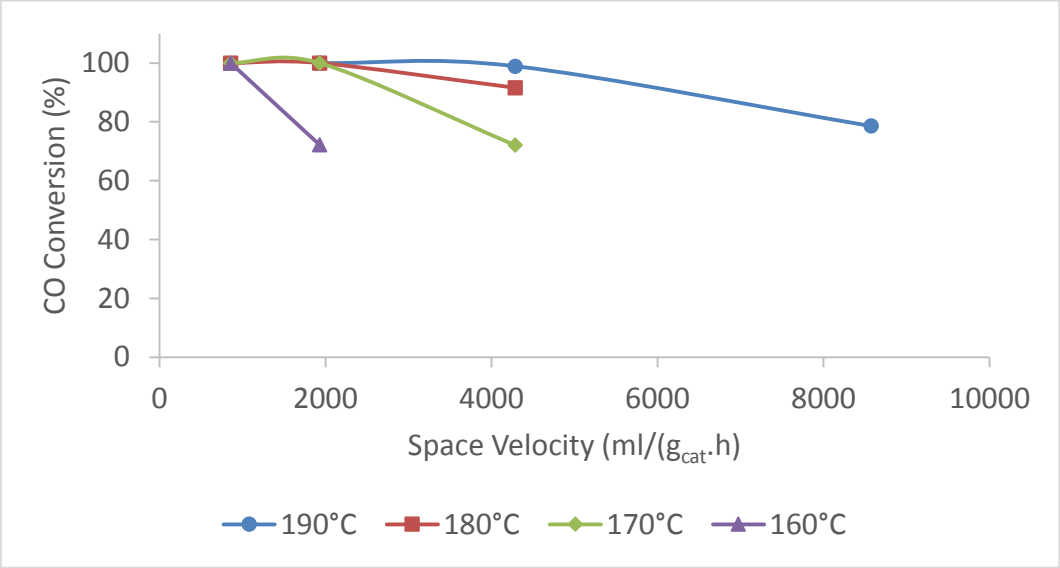

Graph 14 : The effect of temperature on CO conversion between 800 ml/g_{cat}.h and 8500 ml/g_{cat}.h for the 2.2 wt.% Ru/Y zeolite.

The selectivity for the 2.2 wt.% Ru/Y zeolite is seen in graph 15 below. The effect of temperature on selectivity can be observed at a SV of 2000ml/g_{cat}.h as the selectivity of the catalyst increases from 21% at 190°C to 72% at 170°C. The same effect of temperature on selectivity is observed for catalysts with different loadings

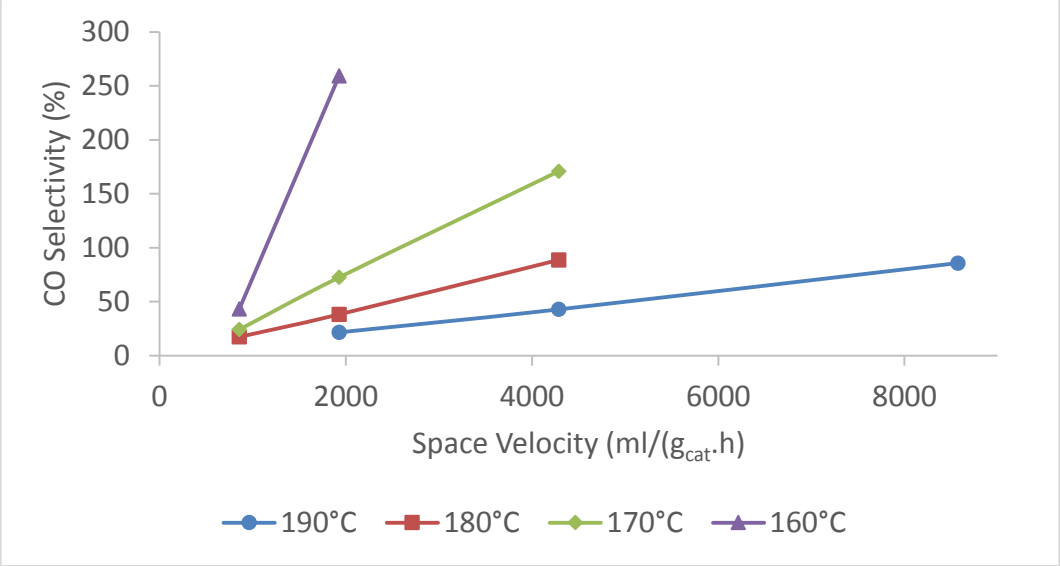

Graph 15 : The effect of temperature on CO selectivity between 800 ml/g_{cat}.h and 8500 ml/g_{cat}.h for the 2.2 wt.% Ru/Y zeolite.

Selectivities exceeded 100% at 160°C and 170°C which points to the production of CO_2 via the WGS reaction. The highest selectivity of 72% was obtained at 100% conversion at 170°C. The H_2 consumption for this catalyst for all temperatures can be seen in graph 16. High H_2 consumption such as 25% corresponds to high CH_4 formation where CO and CO_2 methanation took place. The ideal H_2 consumption is 3% with 100% CO conversion, as this rules out the presence of CO_2 methanation.

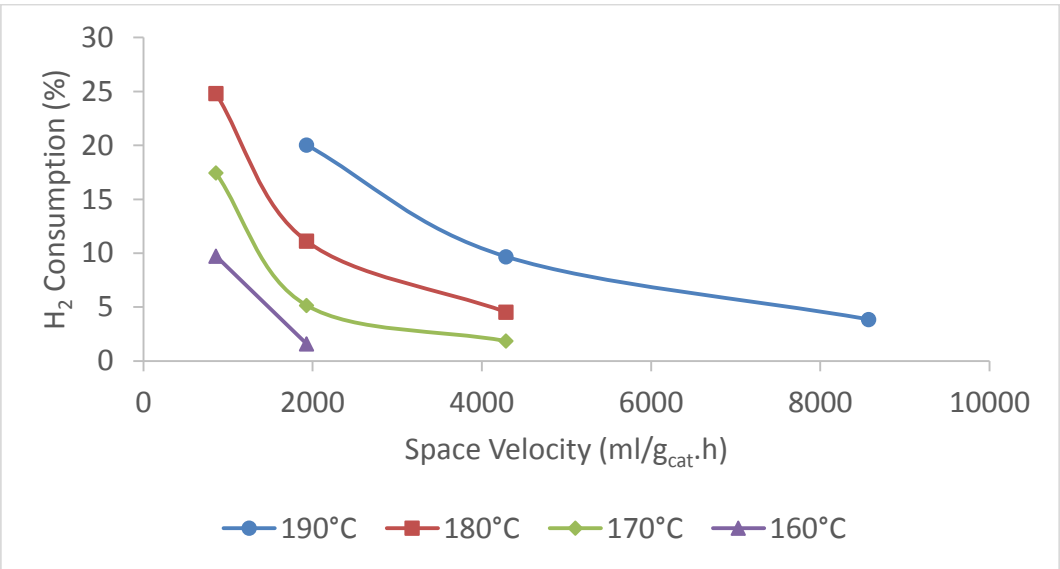

Graph 16 : The effect of temperature on H_2 consumption between 850 ml/g_{cat}.h and 8500 ml/g_{cat}.h for the 2.2 wt.% Ru/Y zeolite.

6.6 Water Gas Shift Activity

It is important to always take into account whether the CO converted is equal to or less than the CH_4 produced when calculating the selectivity towards CO as values approaching 100% could not be true values. At certain reaction conditions, catalysts displayed selectivities exceeding 100% as the amount of CO converted is greater than the amount of CH_4 produced. Therefore, CO is converted to something other than CH_4. There is no evidence of paraffin or olefin formation, nor is there any evidence of carbon deposition on the catalyst – as demonstrated by the lack of catalyst deactivation and a carbon balance that adds up to 100% within reasonable experimental error. We conclude that CO is converted to CO_2 via the WGS reaction.

If WGS contributes to CO being converted, difficulties arise in estimating the selectivity for CO and the selectivity for CO_2 methanation. Potentially, CO is first converted to CO_2 through the WGS whereupon CO_2 is methanated. Thus the apparent, measured selectivity for CO methanation is an overestimate for the actual selectivity for CO methanation and the apparent, measured selectivity for CO_2 methanation is an underestimate of the actual CO_2 methanation selectivity. Therefore, in order to be able to claim with any degree of accuracy that the reported, measured selectivities reflect the real selecitivities, the contribution of the WGS reaction needs to be determined under reaction conditions where both CO and CO_2 methanation take place.

In order to determine the activity of the catalyst toward the WGS reaction, the 2.2 wt.% Ru/Y zeolite was tested at 4600 ml/g_{cat}.h under the same reaction conditions, with the exception of CO_2 being absent in the feed. An inert gas was used to replace CO_2 in order to maintain the same partial pressure of the remaining gas species. The detection of any CO_2 present would indicate the presence of the WGS reaction as the CO is converted into CO_2 instead of CH_4.

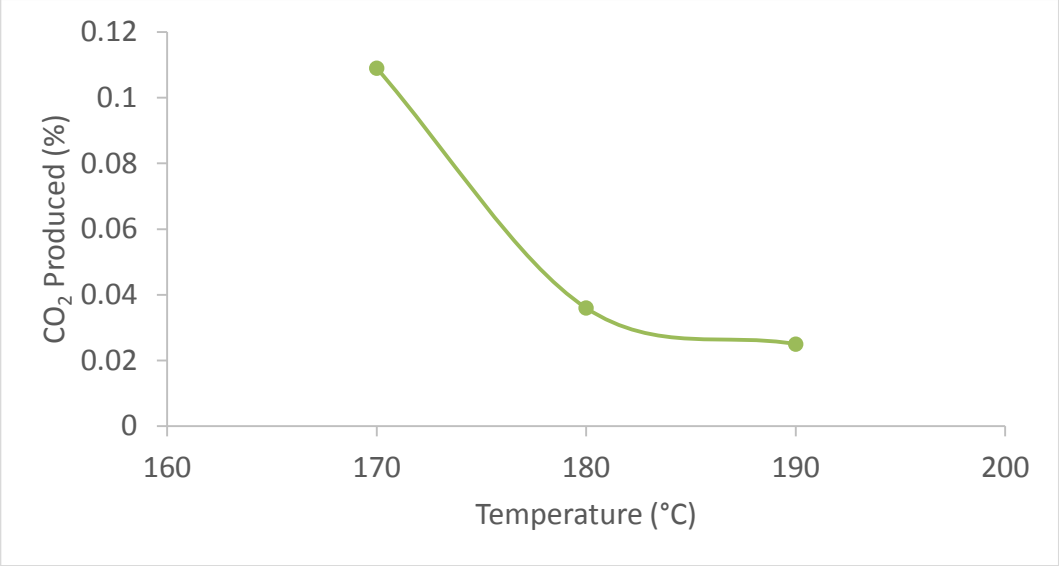

Graph 17 : The effect of temperature on CO_2 production between 170°C and 190°C at 4600 ml/g_{cat}.h for the 2.2 wt.% Ru/Y zeolite; Feed compostion: 1% CO, 59% H_2, 10% Ar, 10% H_2O and 20% He.

The results for this experiment shown in graph 17 confirm that the WGS reaction is taking place, as trace amounts of CO_2 were being detected in both the COX and 5CB GC columns. As the temperature increased, the amount of CO_2 formed decreased. This is due to the WGS reaction being exothermic. At high temperatures around 230°C, the RWGS reaction becomes dominant.

Although the percentage of CO_2 in this experiment is small, in comparison to only 1% CO being present in the feed, the results are not as insignificant. During the experiment at 170°C, under the same conditions with the exception of CO_2 present, the catalyst produced >0.1 % CO_2. The values observed in graph 17 are net CO_2 formation values. The exact amount of CO_2 formed from CO cannot be directly calculated as the methanation of CO_2 cannot be ruled out. Therefore CO and CO_2 methanation along with the WGS reaction are taking place. The formation of CO_2 in this experiment only confirms that the CO_2 present was formed from CO via the WGS reaction.

6.7 The Effect of CO Concentration on Selectivity

The results obtained for the 2.2 wt.% Ru/Y zeolite did not fully agree with those published by Eckle *et al*., 2011. Although 100% conversion was achieved, the highest selectivity was 72% at 170°C whereas the catalyst used in their study displayed 100% selectivity toward CO at 190°C. At higher temperatures in the present study, the selectivity decreased below 72%. The table below summarises the differences in the feed composition used in this study and in the work done by Eckle *et al*., 2011.

Table 18 : The feed compositions used in the present study compared to work done by Eckle *et al*., 2011.

Composition (%)	Present Study	Eckle *et al*., 2011
CO	1	0.6
H_2	59	81.8
H_2O	10	0
CO_2	20	15.5
N_2	0	2.8

The variations in the feed compositions suggest that the difference in selectivities obtained could be due to the difference in CO concentration present in the feed. The feed in this study was then changed to 0.5% CO while increasing the H_2% to 59.5% in order to maintain the partial pressures of the remaining gas species. The graph 18 and 19 below shows the CO conversion and exit CO concentration, respectively.

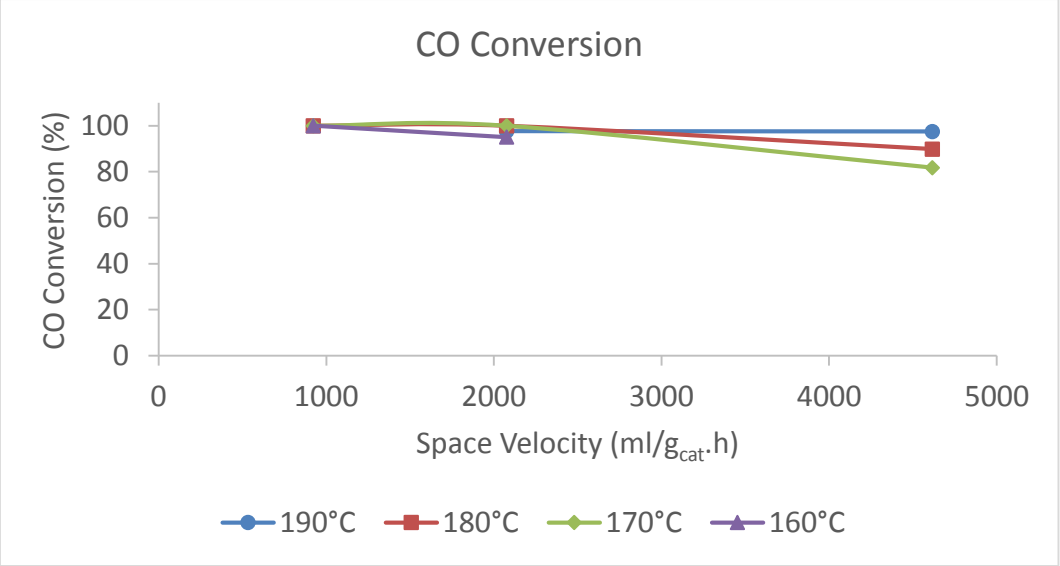

Graph 18 : The effect of temperature on CO converrsion between 900 ml/g_{cat}.h and 4600 ml/g_{cat}.h for the 2.2 wt.% Ru/Y zeolite containing 0.5% CO in the feed.

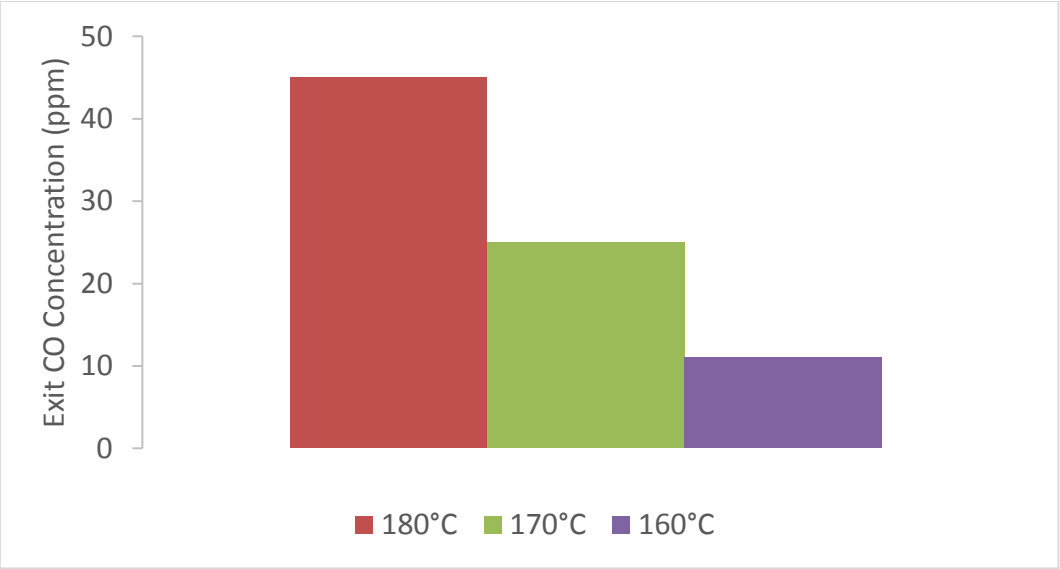

Graph 19 : The effect of temperature on the exit CO concentration of 2.2 wt.% Ru/Y zeolite.

Higher CO conversions were achieved over the temperature range when the concentration of CO was lowered from 1% to 0.5%. This is attributed to a lower concentration of CO that the catalyst needs to convert. The exit CO concentration was measured using the ABB AO2040 analyser when 100% conversion was achieved at a SV of 900 ml/g_{cat}.h at the different reaction temperatures. This was to quantify the low levels of CO that remained that was not detectable by the COX column. From the measurements, it is clear that the

catalyst is able to lower the CO concentration between 10 ppm and 25 ppm. However, these low concentration correspond to percentages of CH_4 which exceed 2%, which is four times the amount of CO present. The formation of CH_4 can be seen in graph 20.

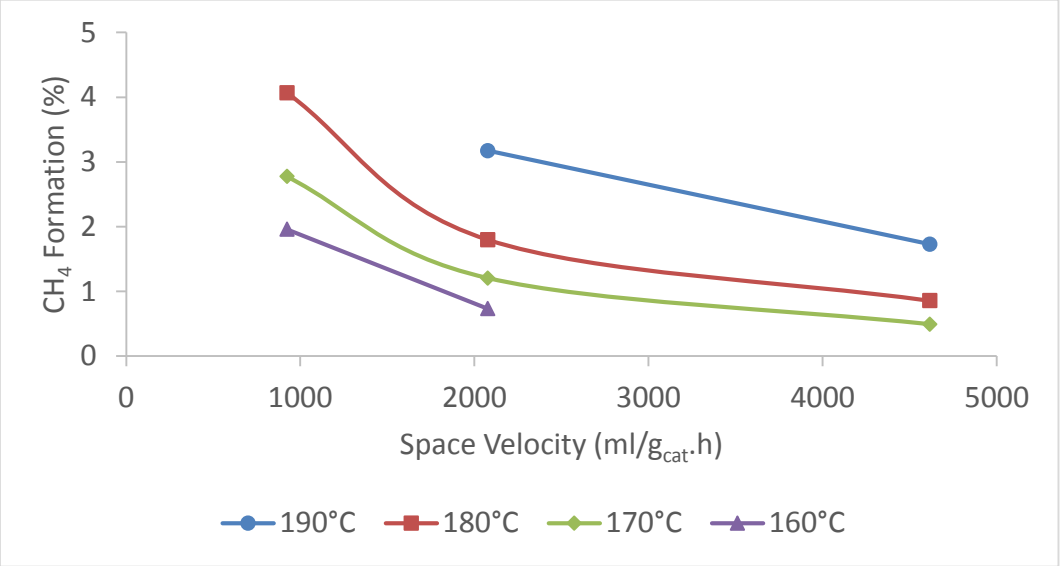

Graph 20 : The effect of temperature on CH_4 formation between 900 ml/g_{cat}.h and 4600 ml/g_{cat}.h for the 2.2 wt.% Ru/Y zeolite containing 0.5% CO in the feed.

The effect of CO concentration on selectivity can be seen in graph 21. The selectivities for both 1% (solid) and 0.5% (dotted) CO present in the feed are observed over the temperature range. At a SV of 2000 ml/g_{cat}.h at 180°C, a selectivity of 38% is observed when 1% CO is present in the feed. When compared to 0.5% CO present in the feed at the same conditions, a CO selectivity of only 27% is observed. In this case, when the temperature is lowered to 170°C at the same SV, a CO selectivity of 41% is observed. Similar selectivities can be achieved when 0.5% CO is present at lower temperatures compared to conditions when 1% CO is present in the feed.

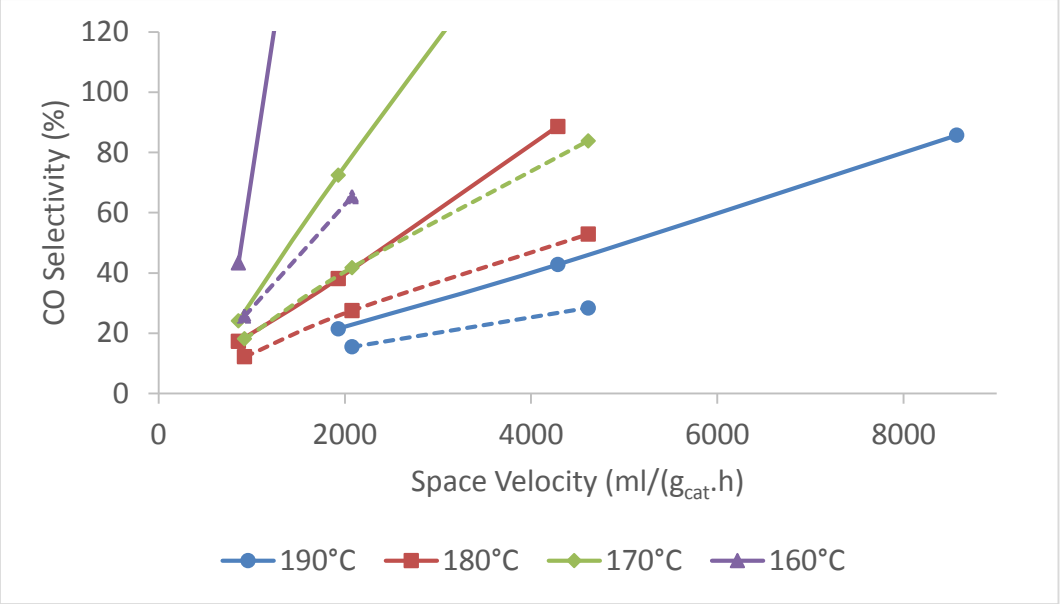

Graph 21 : The effect of temperature on CO selectivity between 1700 ml/g_{cat}.h and 2500 ml/g_{cat}.h for the 2.2 wt.% Ru/Y zeolite containing 0.5% CO (dotted) and 1% CO (solid) in the feed.

Changing the concentration of CO did not result in 100% CO selectivity as stated in work done by Eckle *et al*., 2011 as it was reported that the 2.2 wt.% Ru/zeolite displayed 100% CO selectivity over the range of CO concentrations. Other factors such as catalyst preparation techniques could have an effect on the results obtained.

6.8 The Effect of Water Vapour Content

The effect of the water vapour content on CO conversion and CO selectivity was investigated by changing the concentration of water vapour in the feed from 10% to 20% at a temperature of 190°C and at 4300ml/g_{cat}.h. As the water content was increased, the concentration of H_2 was decreased in order to keep the concentration of the remaining gas species constant.

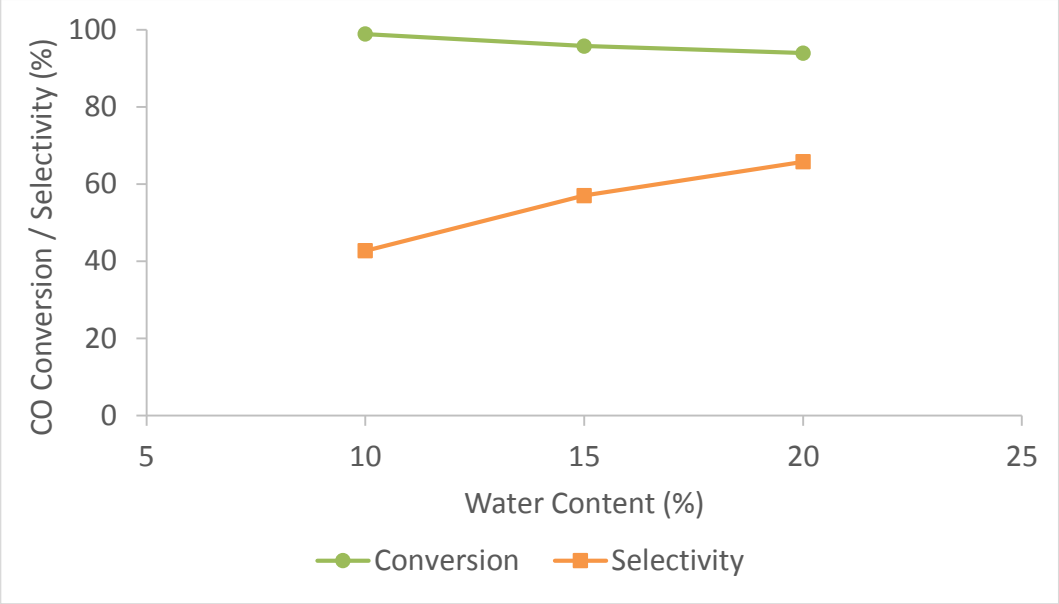

Graph 22: The effect of water content on CO conversion and selectivity for the 2.2 wt.% Ru/Y zeolite; Reaction temperature: 190°C, SV =4300 ml/g_{cat}.h.

An increase in water vapour decreased the CO conversion slightly from 99% at 10% H_2O, to 94% at 20% H_2O. The effect on CO selectivity was more significant. An increase from 43% to 66% was observed when the H_2O content was doubled. In work done by Panagiotopoulou *et al*., 2008, the effect of H_2O content on CO conversion and selectivity was investigated using Ru/Al_2O_3. It was reported that an increase in H_2O content from 0% to 30% suppressed the methanation of CO_2, thereby increasing selectivity, whereas the conversion of CO was not significantly affected. The temperature at which CO_2 methanation was initiated, had increased which caused the selectivity to increase. The same explanation could be true for the Ru/Y zeolite as similar results were observed.

The effect could be attributed to the proposed mechanisms of CH_4 formation from CO and CO_2. It was suggested by Twigg, 1989 that when CH_4 forms from CO, CO dissociates into C and O whereupon both species are hydrogenated to form CH_4 and H_2O. CO_2 methanation proceeds via the dissociation to CO following the RWGS and then a subsequent hydrogenation step to form CH_4. An increase in H_2O would hinder the RWGS thereby suppressing the methanation of CO_2.

6.9 The Ru/Al_2O_3 Catalyst

To compare the Ru/Y zeolites to commonly used catalysts for SMET, the 5 wt.% Ru/Al_2O_3 obtained from Sigma Aldrich was tested. The catalyst was tested at temperatures between 170°C and 210°C using the feed composition B in table 11 section 5.2.5. According to studies performed by Panagiotopoulou *et al.*, 2009, Djinovic *et al.*, 2011, and Dagle *et al.*, 2007, the 5 wt.% is the optimum loading of Ru/Al_2O_3 for SMET.

In graph 23 below, the effect of temperature on the CH_4 formation over the range of SV can be seen. At increasing SV, the CH_4 formation decreases due to the reduced contact time between the reactant and the catalyst. This catalyst responds to changes in temperature in a similar manner to the Ru/Y zeolite. An increase in temperature from 170°C to 200°C causes an increase in CH_4 formation from 0.13% to 2.58% at a SV of 4000 ml/g_{cat}.h.

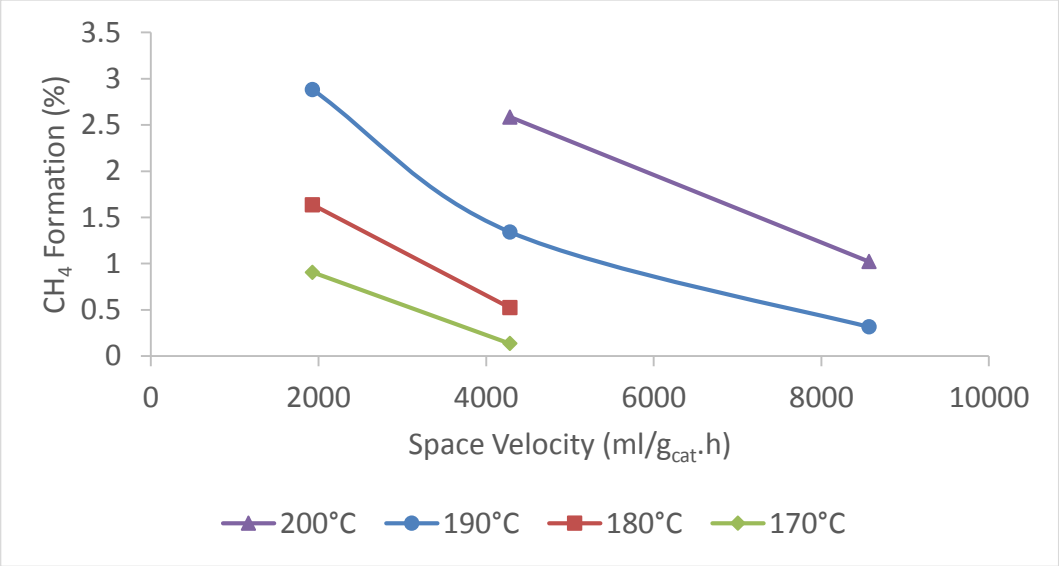

Graph 23 : The effect of temperature on CH_4 formation between 1900 ml/g_{cat}.h and 8500 ml/g_{cat}.h.

The effect of temperature on conversion is seen in graph 24. At higher temperatures, the conversion decreases gradually as SV is increased, whereas at lower temperatures, the decrease in conversion is steeper. Higher temperatures favour the CO methanation reaction which allows for complete conversion to take place.

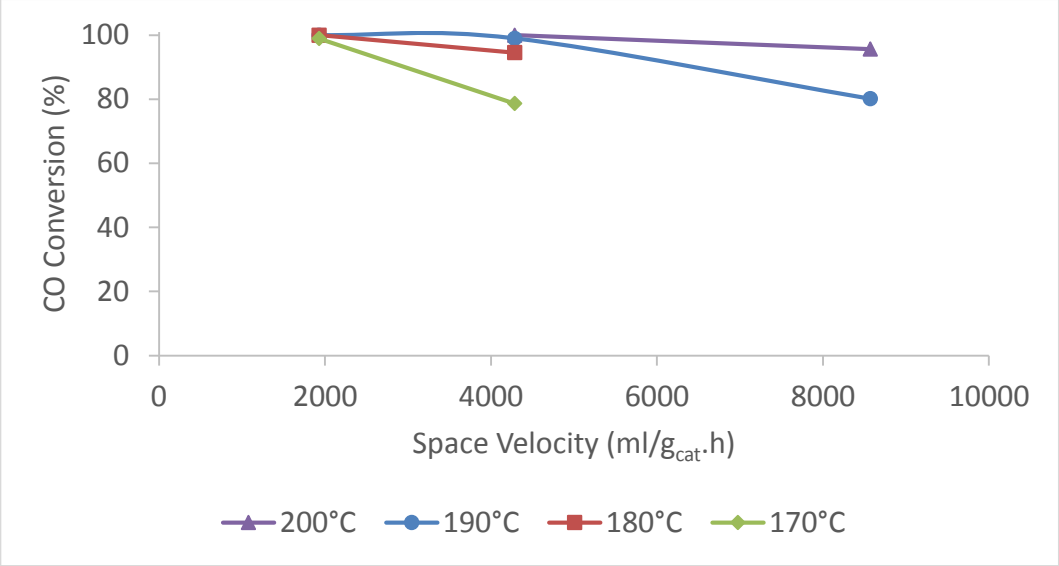

Graph 24 : The effect of temperature on CO converrsion between 1900 ml/g_{cat}.h and 8500 ml/g_{cat}.h.

The selectivities observed for this catalyst are shown in graph 25 for the different reaction temperatures. At 200°C and 8500ml/g_{cat}.h, 95% CO conversion and 92% selectivity was observed. As the temperature is decreased along with SV, the selectivity toward CO increases. Selectivities are once again seen to exceed 100% which indicates the presence of WGS reaction converting CO to CO_2. The highest selectivity observed for this catalyst was 60% while achieving 100% conversion of CO at 180°C. At 170 °C, 98.9% CO conversion and 109 % selectivity combine to give the highest yield of CH_4 from CO reported anywhere in this study. It would have been interesting to see if at an even lower temperature and lower SV, complete CO conversion with > 100% selectivity could be obtained.

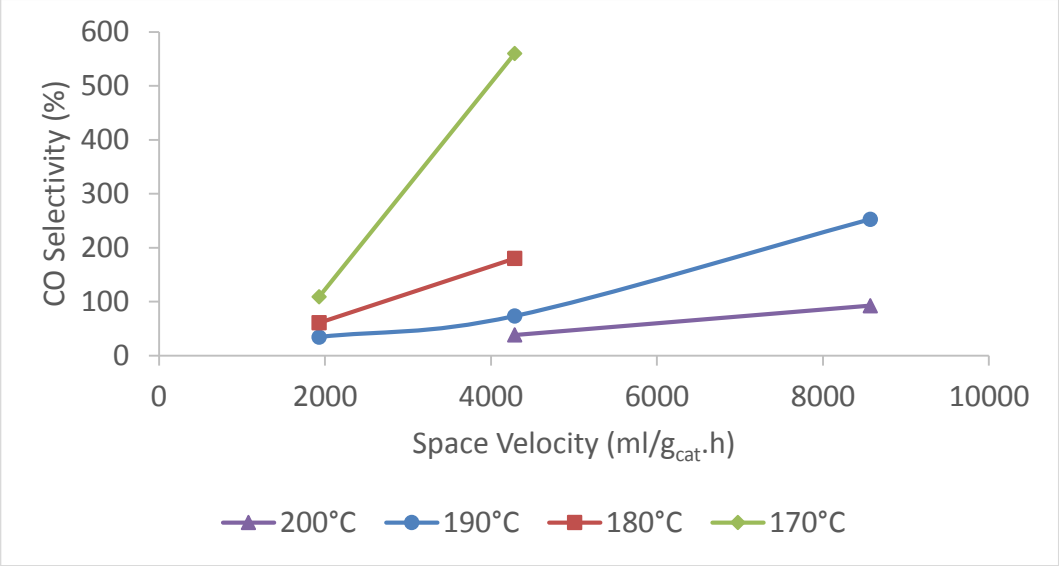

Graph 25 : The effect of temperature on CO selectivity between 1900 ml/g_{cat}.h and 8500 ml/g_{cat}.h.

The 2.2 wt.% Ru/Y zeolite and 5 wt.% Ru/Al_2O_3 are the two most promising catalysts for CO methanation. Table 19 below summarises the conditions under which the best results were obtained for each of the catalysts at 100% conversion.

Table 19 : The reaction conditions whereby the highest CO selectivities were obtained.

	5 wt.% Ru/Alumina	2.2 wt.% Ru/Zeolite
CO Conversion (%)	100	100
CO Selectivity (%)	60	72
H_2 consumption (%)	≈6	≈5
Temperature (°C)	180	170
SV (ml/g_{cat}.h)	2000	2000

The 2.2 wt.% Ru/Y is capable of removing CO at lower temperatures compared to the Ru/Al_2O_3 while displaying higher selectivities toward CO. Both 2.2 wt.% Ru/Y and 5 wt.% Ru/Al_2O_3 could have displayed 100% CO conversions and higher selectivities to those seen in table 19 had the catalysts been tested at lower temperatures and SV.

6.10 Catalyst Deactivation Test

To determine the stability of the catalyst, the deactivation with regards to CO conversion was calculated for the 2.2 wt.% Ru/Y zeolite. The catalyst was exposed to the different reactions conditions and was returned to the original conditions of 190°C and a SV of 4300 ml/g_{cat}.h after 160 hours on stream.

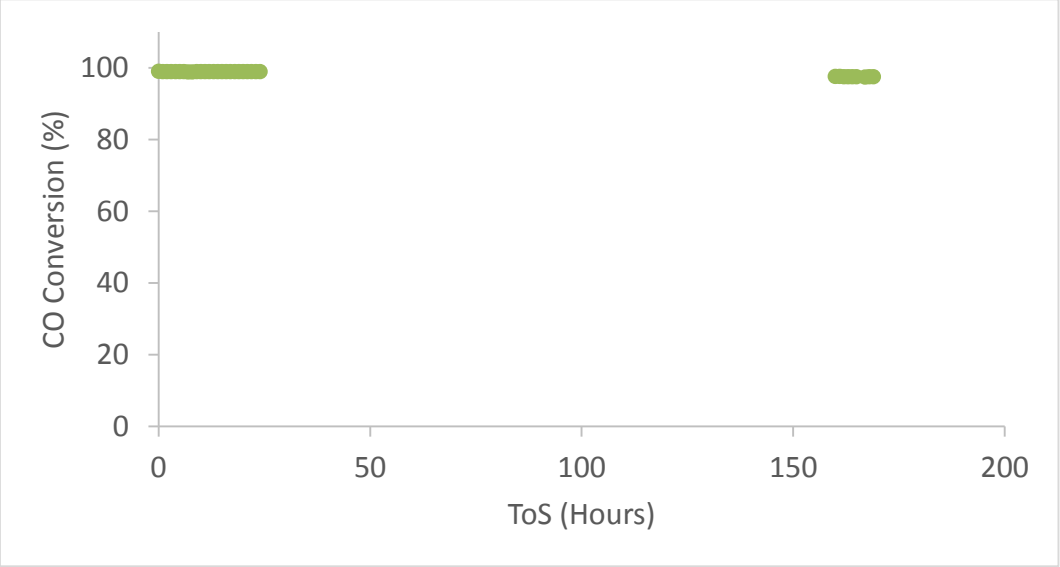

Graph 26 : The deactivation of the CO conversion for the 2.2 wt.% Ru/Y zeolite over 160 hours of stream.

Graph 26 above displays the CO conversion that was obtained at the beginning of the experiment and after 160 hours on stream where the conversion decreased from 99% to 97%. The catalyst can be considered stable over the time period as only a 2% decrease in CO conversion was obtained.

7. Conclusions and Recommendations

From the investigation into the Ru/Y zeolite and Ru/Al_2O_3 for SMET, the following conclusions have been made.

Based on the calculations used to determine the CEC capacity of the Y zeolite, we can confidently state that the zeolite used in studies performed by Eckle *et al*., 2010 is zeolite Y. Zeolites with higher Si/Al ratios would need a greater CEC in order to exchange 5.6 wt.% Ru into the zeolite framework.

From the investigation into the effect of Ru loading and reaction temperature, the 2.2 wt.% Ru/Y zeolite performed best at 170°C with an observed selectivity of 72% at 100% CO conversion. Large percentages of CH_4 were produced by catalysts with higher loadings causing lower CO selectivities to be observed. The 1 wt.% Ru/Y catalyst was less active for SMET compared to all loadings as it was not capable of converting 100% CO under any of the conditions tested.

Higher temperatures were more favourable for both CO and CO_2 methanation. The temperature as well as SV needed to be lowered for high selectivity and complete conversion of CO to be achieved. Catalysts were also found to be active for the WGS reaction which resulted in selectivities exceeding 100%. This was also confirmed by testing for WGS activity in the absence of CO_2. Selectivities that exceed 100% with 100% CO conversion are advantageous as it would result in the removal of CO with a lower consumption of H_2. H_2 would both be consumed during methanation, and produced via WGS reaction, lowering the net consumption of H_2.

The effect of CO concentration on CO selectivity was investigated by decreasing the concentration from 1% to 0.5% as Eckle *et al*.,2011 reported that Ru/zeolite was 100% selective under various CO concentrations. Decreasing the CO concentration from 1% to 0.5% allowed for similar selectivities to be obtained at the same SV but at lower temperatures. With 1% CO, a selectivity of 38% at 180°C was observed whereas at 170°C, a selectivity of 41% was observed when the feed contained 0.5% CO.

The 2.2 wt.% catalyst was also found to be stable over a time period of 160 hours on stream where a 2% decrease in CO conversion was observed at 190°C. The water vapour content also affected the catalyst where an increase in water vapour from 10% to 20% increased selectivity significantly from 43% to 66%, a slight decrease in CO conversion from 99% to 94% was observed at 190°C. This was due to the increase in H_2O content hindering the RWGS reaction which is the mechanism by which CO is produced from CO_2 before methanation occurs.

The 5 wt.% Ru/Al_2O_3 displayed 100% CO conversion and 60% selectivity at 180°C. It was also observed that Ru/Al_2O_3 is capable of ≈100% CO conversions and >100% selectivity at temperatures well below 200°C, as 98.9 % CO conversion and 109% selectivity was obtained at 170°C.

Both the 2.2 wt.% Ru/Y zeolite and Ru/Al_2O_3 are capable of completely removing CO while displaying high CO selectivities at lower temperatures than reported in any of the literature cited and under realistic feed compositions containing CO,H_2,CO_2 and H_2O. A further decrease in both temperature and SV simultaneously could result in improved CO selectivities while maintaining 100% conversion for both catalysts.

The lower SV would allow for enough contact time between reactants and the catalyst for complete conversion to be obtained, while the low temperature would prevent CO_2 methanation from occurring. This combination would give rise to high CO selectivities with low H_2 consumption. Loadings between 1 wt.% and 2.2 wt.% could be synthesised and tested at low temperatures and SV in order to determine whether the CO selectivity could be further improved.

Complete removal of CO and higher CO selectivities can be achieved at lower temperatures using the 2.2 wt.% Ru/Y zeolite compared to the Ru/Al_2O_3. This will produce a CO-free, H_2 rich gas suitable for PEMFC use.

8. References

Amphlett, J.C., Mann, R.F. & Peppley, B.A. 1996. “On board hydrogen purification for steam reformation/ PEM fuel cell vehicle power plants” *International Journal of Hydrogen Energy,* vol.21, no. 8, pp. 673-678.

Ashraf, M.A., Ercolino, G., Specchia, S. & Specchia, V. 2014, "Final step for CO syngas clean-up: Comparison between CO-PROX and CO-SMET processes", *International Journal of Hydrogen Energy,* vol. 39, no. 31, pp. 18109-18119.

Ball, M. & Weeda, M. 2015, "The hydrogen economy – Vision or reality?", *International Journal of Hydrogen Energy,* vol. 40, no. 25, pp. 7903-7919.

Ch. Baerlocher, C., and McCusker, L.B., Database of Zeolite Structures, Available: http://www.iza-structure.org/databases/ [2014, May]

Chen, Y.W., Wang, H.T. & Goodwin Jr., J.G. 1984, "Support effects on CO hydrogenation over Ru/Zeolite catalysts", *Journal of Catalysis,* vol. 85, no. 2, pp. 499-508.

Csicsery, S.M. 1986, "Catalysis by shape-selective zeolites-science and technology", Pure and Applied Chemistry, vol. 58, no. 6, pp. 841-856.

Dagle, R.A., Wang, Y., Xia, G., Strohm, J.J., Holladay, J. & Palo, D.R. 2007, "Selective CO methanation catalysts for fuel processing applications", *Applied Catalysis A: General,* vol. 326, no. 2, pp. 213-218.

Davis, R.J. 2003, "New perspectives on basic zeolites as catalysts and catalyst supports", Journal of Catalysis, vol. 216, no. 1–2, pp. 396-405.

Devrim, Y., Devrim, H. & Eroglu, I., 2015, "Development of 500 W PEM fuel cell stack for portable power generators", *International Journal of Hydrogen Energy, vol. 40*, no. 24, pp.7707-7719

Djinović, P., Galletti, C., Specchia, S. & Specchia, V. 2011, "Ru-based catalysts for CO selective methanation reaction in H_2-rich gases", *Catalysis Today,* vol. 164, no. 1, pp. 282-287.

Eckle, S., Anfang, H. & Behm, R.J. 2011, "What drives the selectivity for CO methanation in the methanation of CO_2-rich reformate gases on supported Ru catalysts?", *Applied Catalysis A: General,* vol. 391, no. 1–2, pp. 325-333.

Eckle, S., Augustin, M., Anfang, H. & Behm, R.J. 2012, "Influence of the catalyst loading on the activity and the CO selectivity of supported Ru catalysts in the selective methanation of CO in CO_2 containing feed gases", *Catalysis Today,* vol. 181, no. 1, pp. 40-51.

Eckle, S., Denkwitz, Y. & Behm, R.J. 2010, "Activity, selectivity, and adsorbed reaction intermediates/reaction side products in the selective methanation of CO in reformate gases on supported Ru catalysts", *Journal of Catalysis,* vol. 269, no. 2, pp. 255-268.

Fuel Cell Today, 2012, Fuel Cell basics- Technology types, Available at: http://www.fuelcelltoday.com/about-fuel-cells/case-studies/technology-types [2015, August]

Galletti, C., Specchia, S. & Specchia, V. 2011, "CO selective methanation in H_2-rich gas for fuel cell application: Microchannel reactor performance with Ru-based catalysts", *Chemical Engineering Journal,* vol. 167, no. 2–3, pp. 616-621.

Icardi, U.A., Specchia, S., Fontana, G.J.R., Saracco, G. & Specchia, V. 2008, "Compact direct methanol fuel cells for portable application", *Journal of Power Sources,* vol. 176, no. 2, pp. 460-467.

Jacobs, P.A., Verdonck, J., Nijs, R. & Uytterhoeven, J.B. 1979, "Carbon Monoxide Hydrogenation over Ruthenium Zeolites" in AMERICAN CHEMICAL SOCIETY, pp. 15-23.

Kalmula, B. & Kondapuram, V.R. 2015, "Fuel processor – fuel cell integration: Systemic issues and challenges", *Renewable and Sustainable Energy Reviews,* vol. 45, no. 0, pp. 409-418.

Kolb, G. 2008, Fuel Processing for Fuel Cells, Wiley-VCH, Weinheim.

Kuehl, G.H, In Catalysis and Zeolites, J. Weitkamp, L. Puppe (Eds.), Springer 1999

Lower, S. 2013, *Hard water and water softening*.
Available: http://www.chem1.com/CQ/hardwater.html [2014, May].

Marchenko, O.V. & Solomin, S.V. 2015, "The future energy: Hydrogen versus electricity", *International Journal of Hydrogen Energy,* vol. 40, no. 10, pp. 3801-3805.

Meier, W.M. 1986, "Zeolites and the zeolite-like materials", Pure and Applied Chemistry, vol. 58, no. 10, pp. 1323-1328.

Naccache, C. & Taarit, Y.B. 1980, "Recent developments in catalysis by zeolites", Pure and Applied Chemistry, vol. 52, pp. 2175-2189.

Oukaci, R., Sayari, A. & Goodwin Jr., J.G. 1987, "Preparation effects in zeolite-supported metal catalysts: Influence of decomposition/reduction on Ru particle size", *Journal of Catalysis,* vol. 106, no. 1, pp. 318-322.

Panagiotopoulou, P., Kondarides, D.I. & Verykios, X.E. 2008, "Selective methanation of CO over supported noble metal catalysts: Effects of the nature of the metallic phase on catalytic performance", *Applied Catalysis A: General,* vol. 344, no. 1–2, pp. 45-54.

Panagiotopoulou, P., Kondarides, D.I. & Verykios, X.E. 2009, "Selective methanation of CO over supported Ru catalysts", *Applied Catalysis B: Environmental,* vol. 88, no. 3–4, pp. 470-478.

Pearce, J.R., Mortier, W.J. & Uytterhoeven, J.B. 1979, "Oxidation-reduction behaviour of highly dispersed ruthenium in RuNaY zeolite", *Journal of the Chemical Society, Faraday Transactions 1: Physical Chemistry in Condensed Phases,* vol. 75, no. 0, pp. 1395-1402.

Ren, J., Gao, S., Tan, S. & Dong, L. 2015, "Hydrogen economy in China: Strengths–weaknesses–opportunities–threats analysis and strategies prioritization", *Renewable and Sustainable Energy Reviews,* vol. 41, pp. 1230-1243.

Schwarz, J.A., Contescu, C. & Contescu, A. 1995, "Methods for Preparation of Catalytic Materials", *Chemical Reviews,* vol. 95, no. 3, pp. 477-510.

Shekhawat, D., Spivey, J. & Berry, D. 2011. Fuel Cells: Technologies for fuel processing. 1st ed. Oxford: Elsevier

Shi, Y., Cioffi, C., Gao, S., Thompson, C., Chintawar, P. & Cross, J. 2002, "Catalytic reforming of hydrocarbons for fuel cell applications", *Fuel Cell Chemistry Division Reprints,* vol. 47, no. 2, pp. 545.

Smirniotis, P. & Gunugunuri, K. 2015, *Water Gas Shift Reaction: Research Developments and Applications,* Elsevier Science.

Smith, J.V. 1984, "Definition of a zeolite", Zeolites, vol. 4, no. 4, pp. 309-310.

Twigg, M.V. 1989, *Catalyst Handbook,* 2nd ed, Wolfe Publishing, London.

Verdonck, J.J., Jacobs, P.A. & Uytterhoeven, J.B. 1979, "Catalysis by a ruthenium complex heterogenized in faujasite-type zeolites: the water gas-shift reaction", *Journal of the Chemical Society, Chemical Communications,* no. 4, pp. 181-182.

Verdonck, J.J., Jacobs, P.A., Genet, M. & Poncelet, G. 1980, "Redox behaviour of transition metal ions in zeolites. Part 8.-Characterization of a ruthenium metal phase in NaY zeolite", *Journal of the Chemical Society, Faraday Transactions 1: Physical Chemistry in Condensed Phases,* vol. 76, pp. 403.

VICI sample injection- 6 port valve, Available: http://www.vici.com/support/app/app11j.php, [2015, August]

Appendix A

CEC Capacity of Zeolite Y

Element	Molecular Mass	
H	**1**	**g/mol**
Si	**28.09**	**g/mol**
Al	**26.98**	**g/mol**
O	**16**	**g/mol**
Ru	**101.07**	**g/mol**

In 1g zeolite with 5.6 wt.% Ru :

Based on $n = \frac{m}{M}$

There exists: 0.056 g Ru^{3+} and 5.54 x10^{-4} mol Ru^{3+}

Molecular Formula: $(SiO_2)n\text{-}x(AlO_2)x(M^+)x$ Where x =Si/Al

Si/Al	**3**	
Si+Al	192	
Al	48	
Si	144	
$(SiO_2)144(AlO_2)48(H^+)48$		
$M_{zeolite}$	11532	g/mol
$m_{zeolite}$	1	g
$n_{zeolite}$	8.67152 x10^{-5}	mol
Acid sites	4.16 x10^{-3}	mol
Al sites	4.16 x10^{-3}	mol
Capacity for Ru^{3+}	1.39 x10^{-3}	mol
% of CEC used	39.93	%

Acid Sites = $n_{zeolite}$ x Al = Al Sites

Capacity for Ru^{3+} = Al/3

CEC % = Capacity for Ru^{3+} x 100

Appendix B

Temperature Profiles of Reactor 2

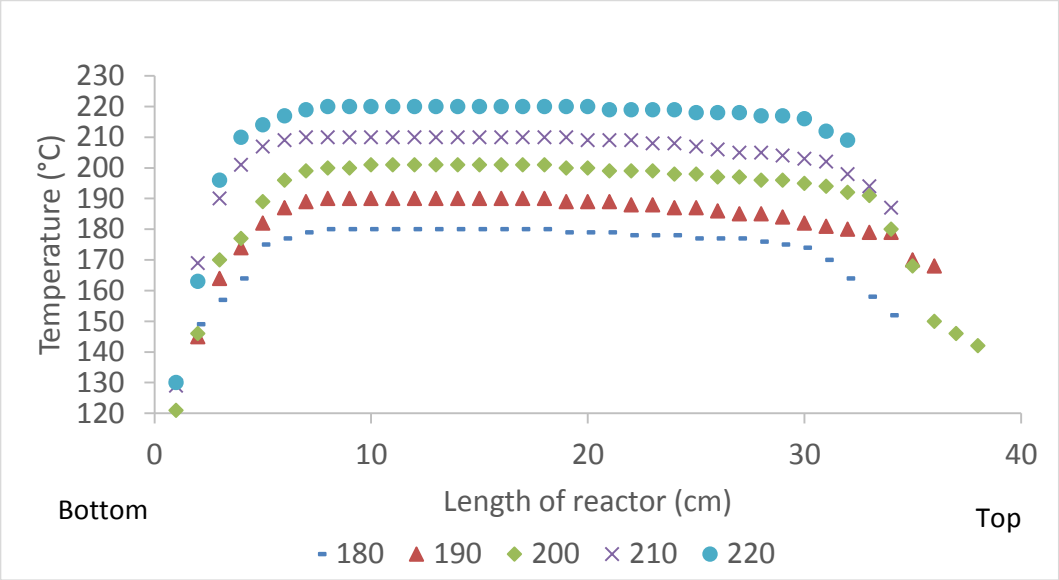

Graph 27 : Temperature profile for reactor 2 over the range 180°C-220°C

Appendix C

MFC Calibration Curves

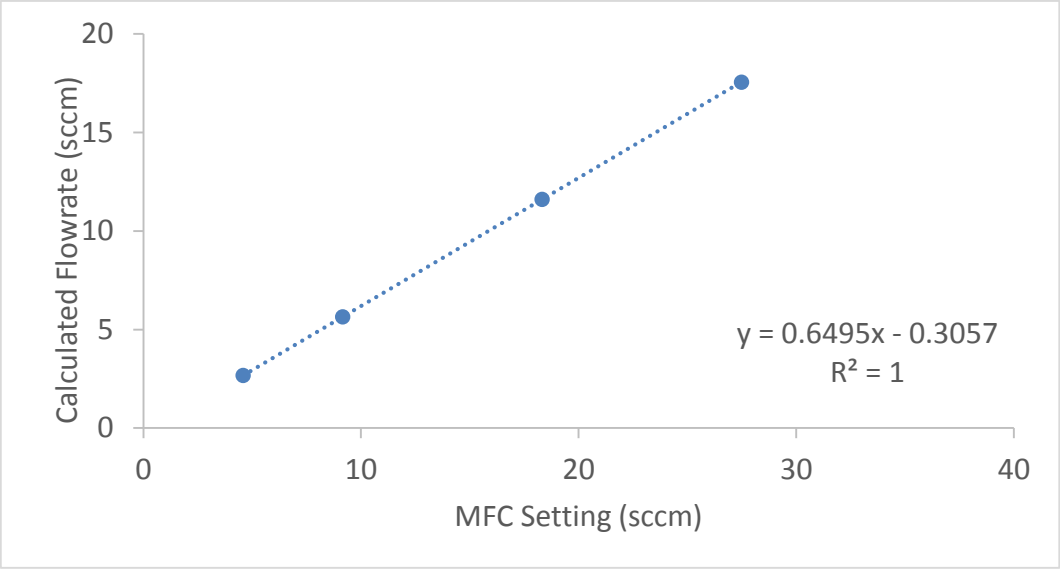

Graph 28 : MFC Calibration curve for CH_4.

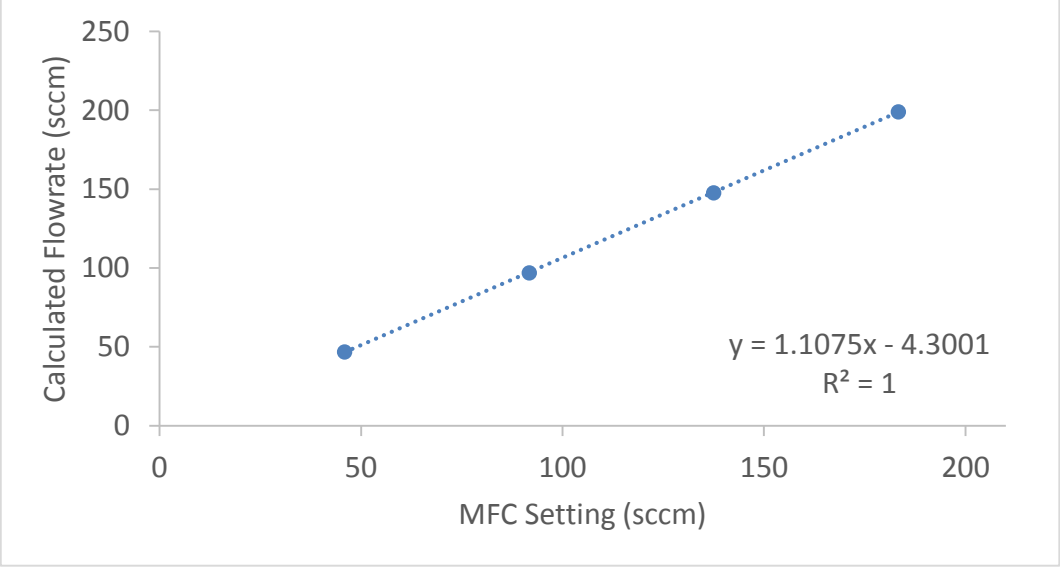

Graph 29: MFC Calibration curve for CO_2.

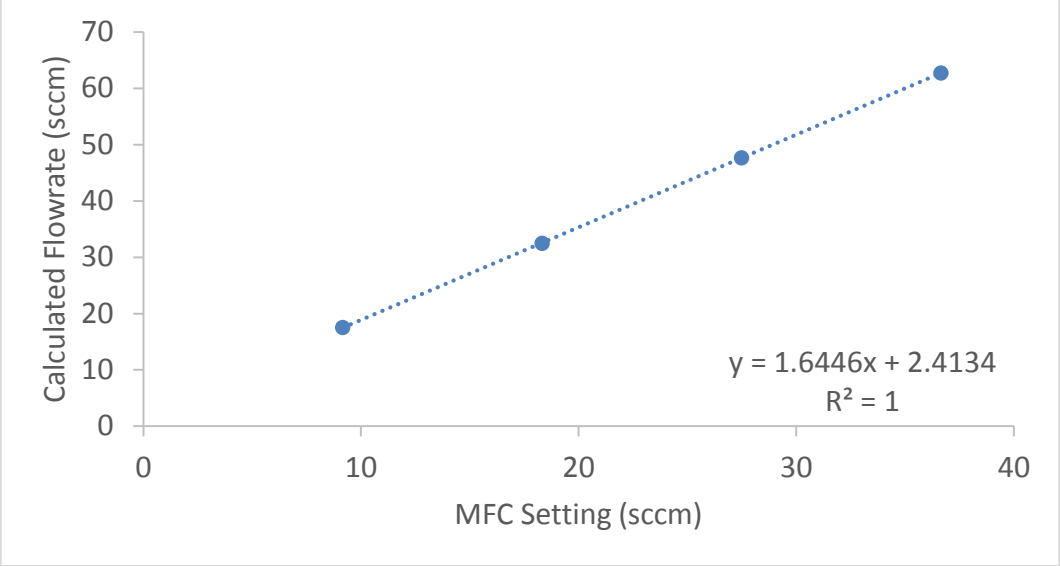

Graph 30 : MFC Calibration curve for Ar.

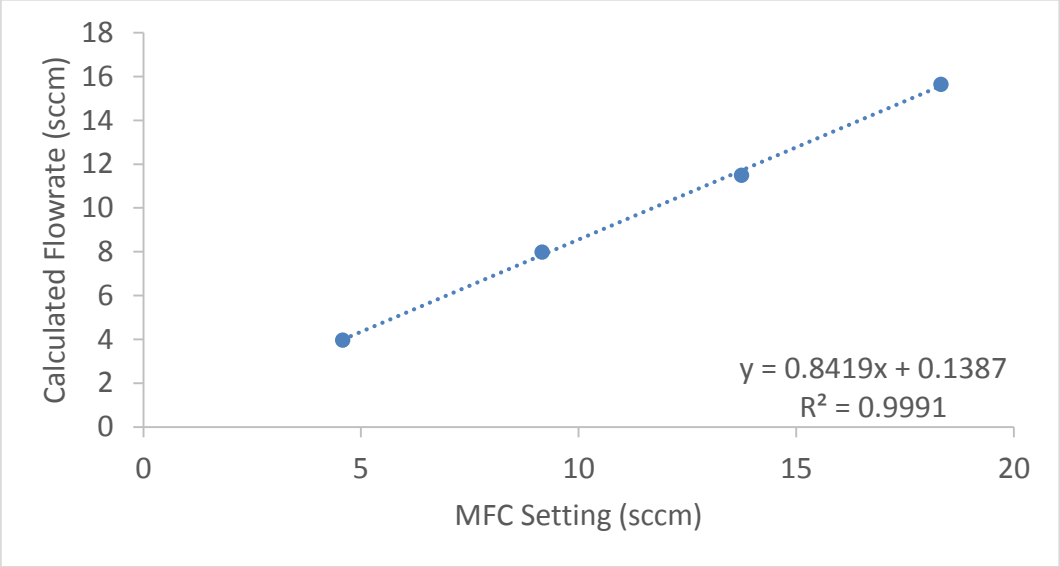

Graph 31 : MFC Calibration curve for CO.

Appendix D

Capillary Calibration

The formula used to calculate the lengths of capillaries needed based on flow rate are given along with the calibration tables for different flow rates are given below:

$$\Delta P_{viscous} = \frac{8 \cdot Q \cdot \eta \cdot L}{\pi \cdot r^4}$$

Q ∝ c/L

Q	**Flow rate (m^3/s)**
$L_{capillary}$	**Length (m)**
$r_{capillary}$	**Radius (mm)**
$\Delta P_{capillary}$	**Pressure Drop (Pa)**
C	**Constant**

Table 20 : Split flow rate in capillaries with an HLPC setting of 0.15 ml/min over a 30 minute period.

	Mass Before (g)	Mass After (g)	Volume (ml)	Flow rate (ml/min)
R 1	**66.94**	**67.64**	**0.7**	**0.0233**
R 2	**63.97**	**64.74**	**0.77**	**0.0257**
R 3	**65.02**	**65.79**	**0.77**	**0.0257**
W	**63.3**	**65.72**	**2.42**	**0.0807**
Total				**0.1553**

Table 21 : Split flow rate in capillaries with an HLPC setting of 0.10 ml/min over a 60 minute period.

	Mass Before (g)	Mass After (g)	Volume (ml)	Flow rate (ml/min)
R 1	**67.64**	**68.58**	**0.94**	**0.0157**
R 2	**64.74**	**65.79**	**1.05**	**0.0175**
R 3	**65.79**	**66.85**	**1.06**	**0.0177**
W	**65.72**	**68.92**	**3.2**	**0.0533**
Total				**0.1042**

Table 22 : Split flow rate in capillaries with an HLPC setting of 0.05 ml/min over a 90 minute period.

	Mass Before (g)	Mass After (g)	Volume (ml)	Flow rate (ml/min)
R 1	**68.58**	**69.23**	**0.648**	**0.0072**
R 2	**65.79**	**66.57**	**0.78**	**0.0087**
R 3	**66.85**	**67.61**	**0.76**	**0.0084**
W	**68.92**	**71.31**	**2.39**	**0.0266**
Total				**0.0509**

Table 23 : Split flow rate in capillaries with an HLPC setting of 0.04 ml/min over a 120 minute period.

	Mass Before (g)	Mass After (g)	Volume (ml)	Flow rate (ml/min)
R 1	**69.23**	**69.9**	**0.67**	**0.0056**
R 2	**66.57**	**67.37**	**0.8**	**0.0067**
R 3	**67.61**	**68.44**	**0.83**	**0.0069**
W	**71.31**	**73.9**	**2.59**	**0.0216**
Total				**0.04075**

Appendix E

GC Calibration Curves

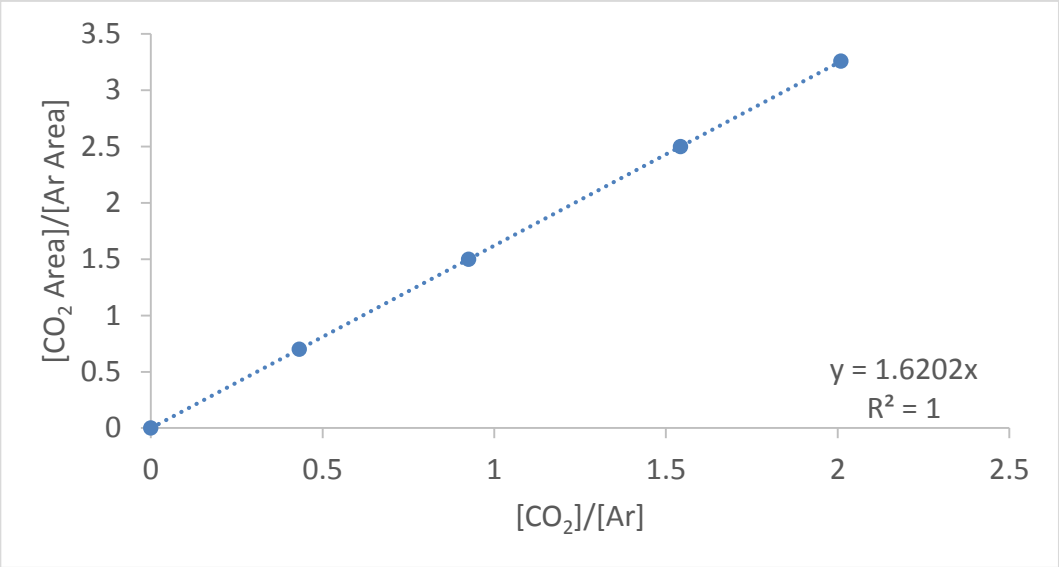

Graph 32 : Calibration curve obtained for CO_2 on the COX column.

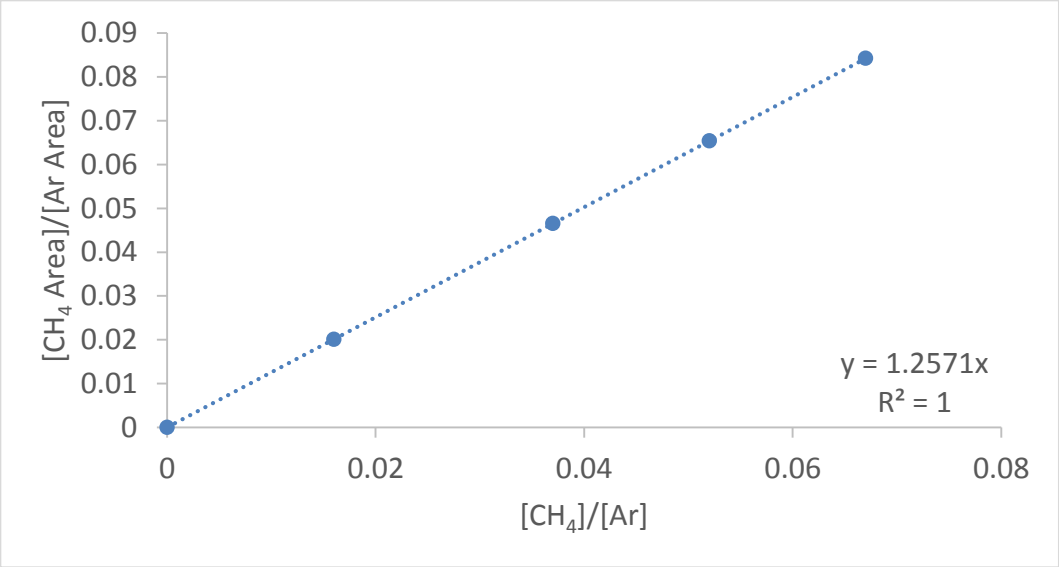

Graph 33 : Calibration Curve obtained for CH_4 on the COX column

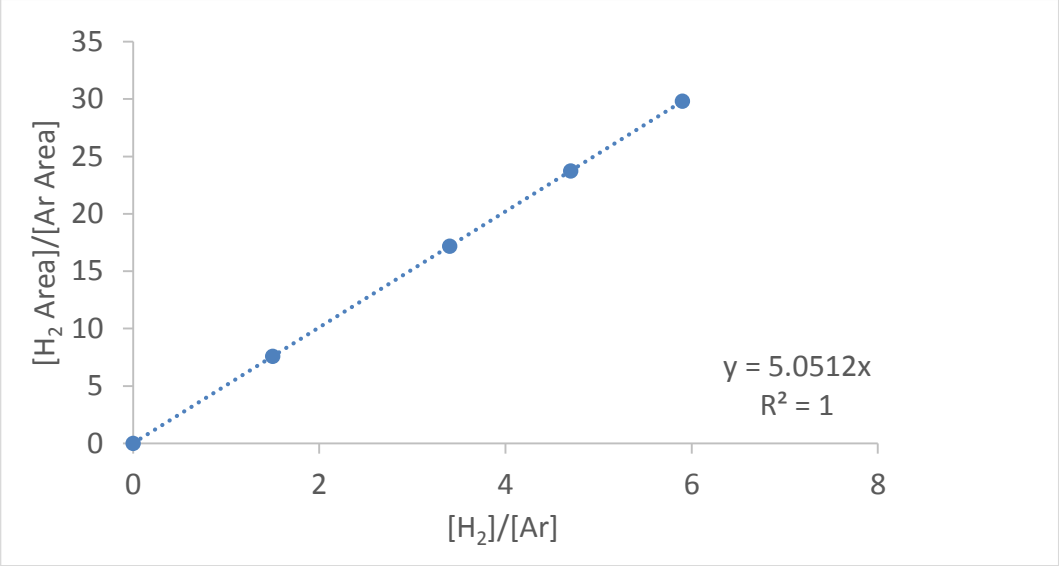

Graph 34: Calibration curve obtained for H_2 on the COX column.

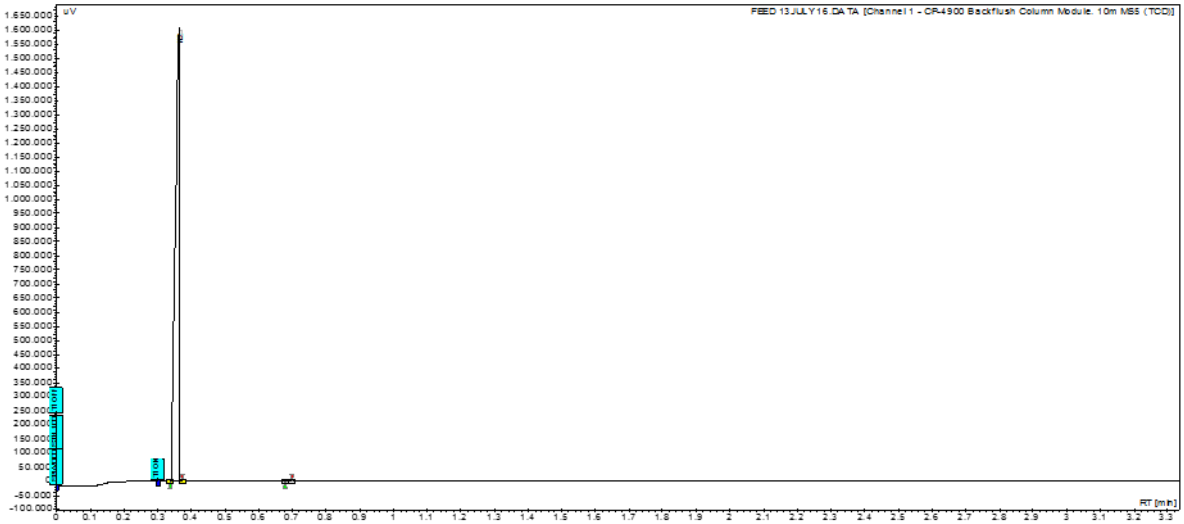

Figure 24: Chromatogram obtained from the 10m $MS5^{BF}$ column during the analysis of the feed stream.

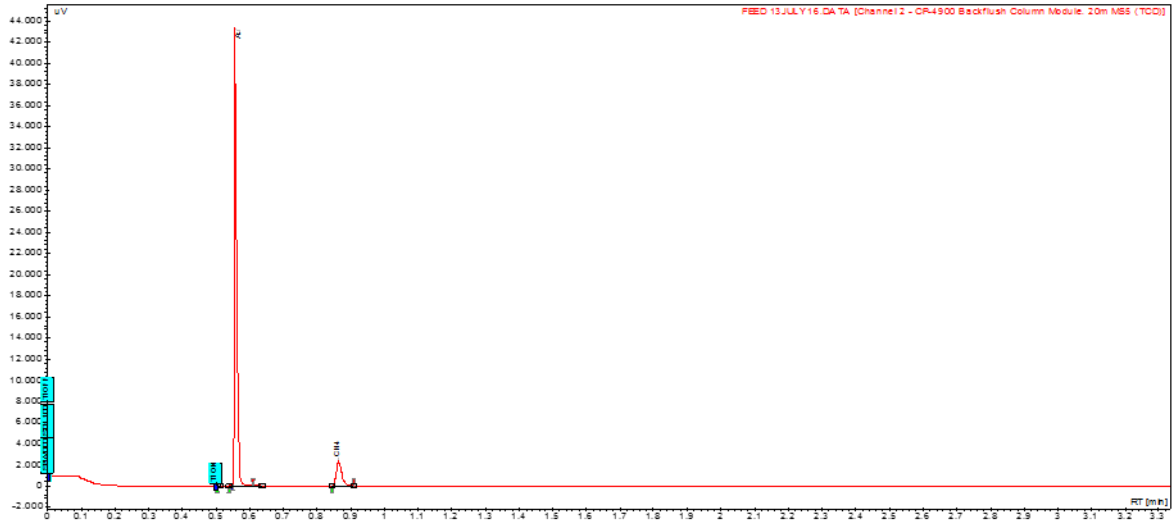

Figure 25: Chromatogram obtained from the 20m MS5^{BF} column during the analysis of the feed stream.

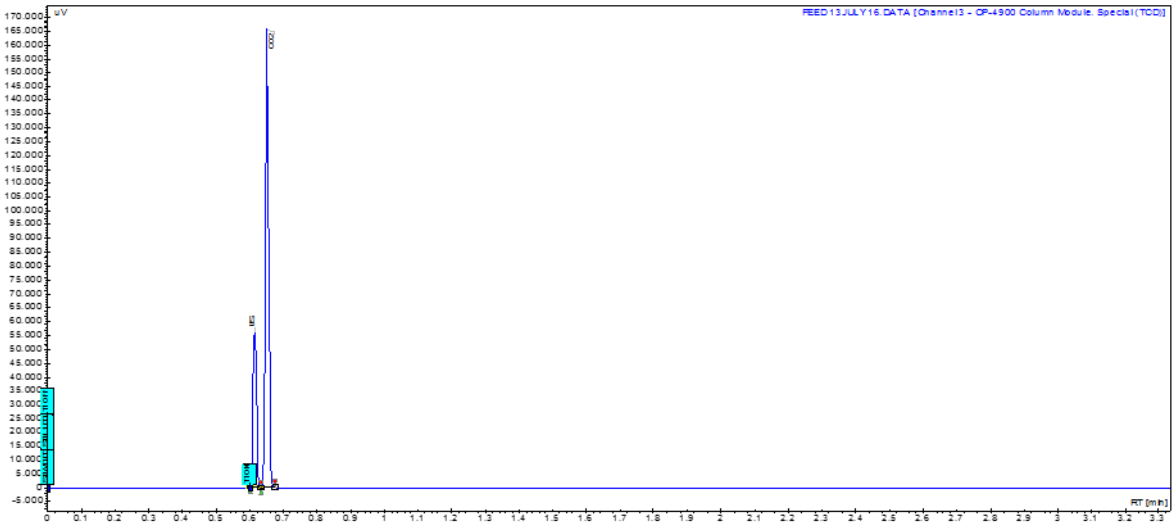

Figure 26: Chromatogram obtained from the 10m 5CB column during the analysis of the feed stream.

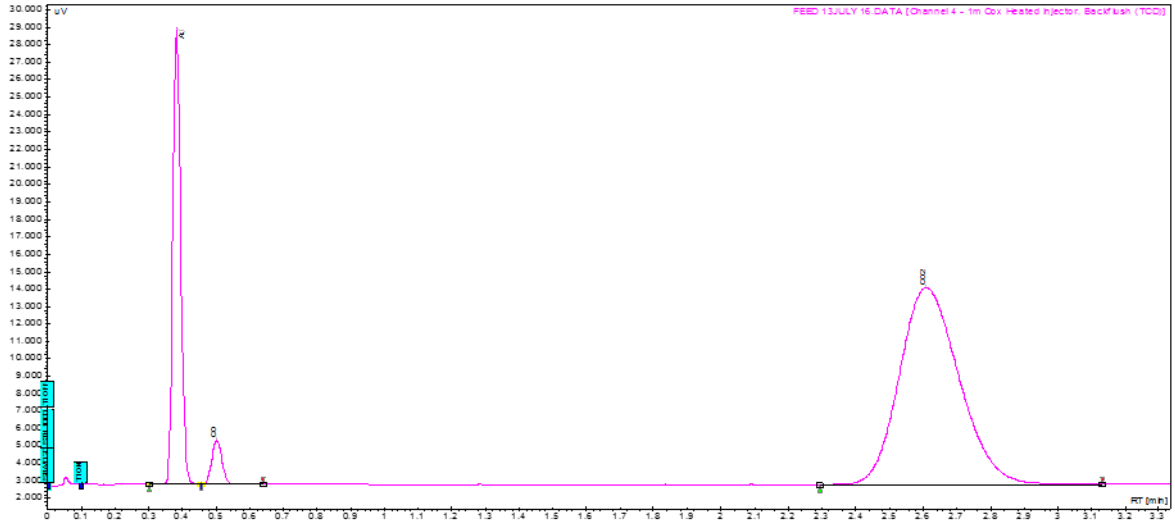

Figure 27: Chromatogram obtained from the 1m COX column during the analysis of the feed stream.

Appendix F

Experimental Data

The data tables for all catalysts tested along with graphs of conversion, CO selectivity and CH_4 formation are given below:

Table 24 : Experimental data for 1.4 wt.% Ru/Y zeolite tested between 190°C and 210°C.

Temp (°C)	SV ($ml/g_{cat}.h$)	CO Conversion (%)	CO Selectivity (%)	Carbon Balance	% CH_4	H_2 Consumed (%)
190	1714	100	30.5	99.97	3.2	13
	3857	98.84	63.99	100.97	1.5	5.82
	8571	81.14	93.6	101.36	0.859	3.30
	17143	40.86	131.1	100.8	0.308	1.13
200	1714	100	26.73	101.01	3.7	15.2
	3857	98.93	51.89	100.79	1.88	7.22
	8571	82.2	84.2	100.29	0.97	3.53
	17143	47.16	108	100.16	0.432	1.74
210	1714	99.02	18.24	101.2	5.38	22.4
	3857	98.84	36.03	99.24	2.7	10.82
	8571	94.84	65.52	100.46	1.4	5.28
	17143	68.43	85.87	99.82	0.79	2.92

Table 25 : Experimental data for 2.2 wt.% Ru/Y zeolite tested between 160°C and 190°C.

Temp (°C)	SV ($ml/g_{cat}.h$)	CO Conversion (%)	CO Selectivity (%)	Carbon Balance	% CH_4	H_2 Consumed (%)
190	1929	100.00	21.50	101.1	4.67	20.04
	4286	98.92	42.78	101.5	2.28	9.69
	8571	78.59	85.72	101.4	0.91	3.87
180	857	100.00	17.29	102	5.80	24.82
	1929	100.00	38.14	102.1	2.63	11.12
	4286	91.59	88.65	100.48	1.04	3.83
170	857	100.00	24.15	102.7	4.15	17.45
	1929	100.00	72.49	100.69	1.38	5.16
	4286	72.06	170.80	100.47	0.42	1.86
160	857	100.00	43.30	102	2.31	9.74
	1929	72.17	259.27	101.7	0.28	1.60

Table 26 : Experimental data for 1 wt.% Ru/Y zeolite tested between 160°C and 190°C.

Temp (°C)	SV ($ml/g_{cat}.h$)	CO Conversion (%)	CO Selectivity (%)	Carbon Balance	% CH_4	H_2 Consumed (%)
190	857	76.19	114.95	101.3	0.65	2.62
	1928	43.96	208.94	100.59	0.21	0.78
	4285	19.81	270.50	100.13	0.07	0.24
180	857	90.27	118.22	101.6	0.77	2.94
	1928	41.77	327.52	101.1	0.13	0.53
	4285	21.76	374.45	100.62	0.06	0.21
170	857	55.48	352.33	100.6	0.16	0.79
	1928	26.87	475.09	100.7	0.06	0.02
	4285	15.3	538.1	101.8	0.028	-0.16
160	857	31.98	513.92	101.7	0.06	0.20
	1928	16.78	639.72	100.1	0.03	-0.01

Table 27 : Experimental data for 3.6 wt.% Ru/Y zeolite tested between 160°C and 190°C.

Temp (°C)	SV ($ml/g_{cat}.h$)	CO Conversion (%)	CO Selectivity (%)	Carbon Balance	% CH_4	H_2 Consumed (%)
190	3857	93.89	34.04	101.4	2.75	11.47
	8571	78.51	53.20	101.7	1.47	6.32
	17142	55.73	90.23	100.8	0.62	2.77
	25714	44.30	124.00	100.7	0.37	1.78
180	1714	100.00	22.67	100.21	4.40	17.38
	3857	91.22	52.98	100.51	1.72	6.37
	8571	70.22	95.98	101.7	0.73	3.00
170	1714	100.00	33.00	100.48	2.95	12.11
	3857	85.11	79.27	101.8	1.07	4.34
	8571	53.51	206.50	101.7	0.26	1.01
160	1714	88.53	117.10	99.42	0.75	0.98
	3857	53.50	281.20	100.65	0.19	0.15

Table 28 : Experimental data for 5.4 wt.% Ru/Y zeolite tested between 160°C and 190°C.

Temp (°C)	SV ($ml/g_{cat}.h$)	CO Conversion (%)	CO Selectivity (%)	Carbon Balance	% CH_4	H_2 Consumed (%)
190	3857	100.00	20.92	101.7	4.76	20.07
	8571	93.83	35.44	101.7	2.64	11.18
	17142	71.77	57.45	100.9	1.25	5.22
	25714	57.60	75.25	100.83	0.76	3.25
180	1714	100.00	15.86	101.9	6.30	26.54
	3857	100.00	31.52	101.8	3.16	12.98
	8571	86.91	61.61	100.98	1.41	5.58
170	1714	100.00	23.14	100.34	4.30	16.90
	3857	97.78	51.60	99.5	1.89	6.25
	8571	72.50	103.00	101.5	0.70	2.85
160	1714	98.52	52.29	99.09	1.87	5.70
	3857	76.93	116.30	101.92	0.66	2.80

Table 29 : Experimental data for 5 wt.% Ru/Al_2O_3 tested between 170°C and 200°C.

Temp (°C)	SV ($ml/g_{cat}.h$)	CO Conversion (%)	CO Selectivity (%)	Carbon Balance	% CH_4	H_2 Consumed (%)
190	1929	100.00	34.44	101.70	2.88	12.9
	4286	98.98	73.23	102.00	1.34	5.78
	8571	80.16	252.79	102.00	0.31	1.99
180	1929	100.00	60.77	100.79	1.64	5.70
	4286	94.56	179.90	101.89	0.52	2.65
170	1929	98.93	108.75	100.17	0.90	2.5
	4286	78.69	560.00	100.66	0.14	0.03
200	4286	100.00	38.14	99.90	2.58	9.79
	8571	95.64	92.38	100.00	1.02	3.35

Table 30 : Experimental data for 2.2 wt.% Ru/Y zeolite tested between 160°C and 190°C with 0.5 % CO.

Temp (°C)	SV ($ml/g_{cat}.h$)	CO Conversion (%)	CO Selectivity (%)	Carbon Balance	% CH_4	H_2 Consumed (%)
190	2077	97.64	15.50	100.86	3.17	13.36
	4615	97.53	28.41	100.4	1.73	6.84
180	923	100.00	12.20	101.22	4.07	17.5
	2077	100.00	27.52	100.46	1.80	7.36
	4615	89.88	52.88	99.84	0.86	3.49
170	923	100.00	18.15	100.71	2.77	11.49
	2077	100.00	41.81	100.58	1.20	4.95
	4615	81.77	83.88	99.81	0.49	1.89
160	923	100.00	25.70	100.48	1.96	8.15
	2077	95.05	65.39	100.32	0.73	2.97

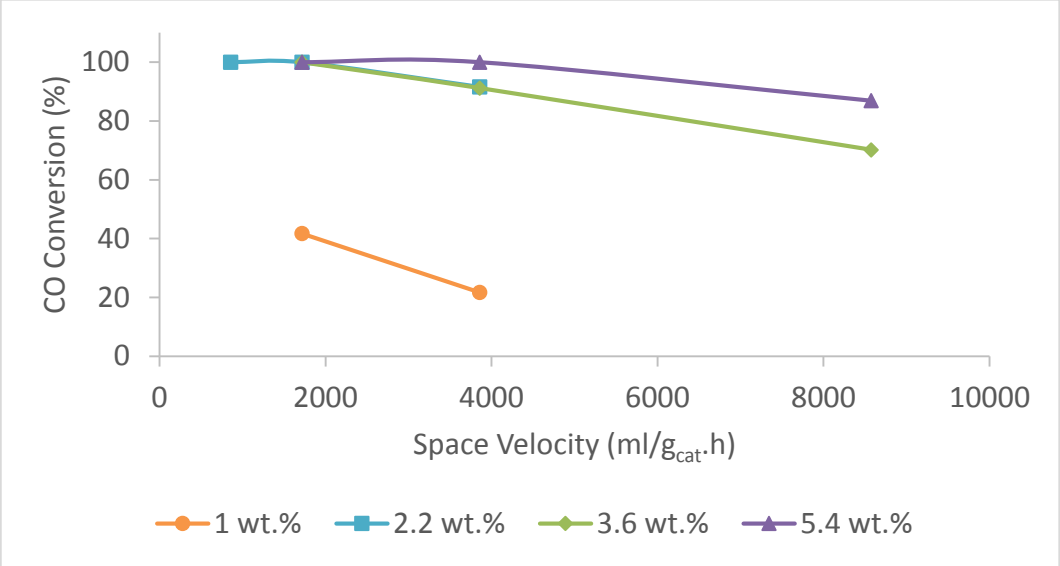

Graph 35: The effect of loading on CO conversion at 180°C between 800 ml/g_{cat}.h and 8500 ml/g_{cat}.h.

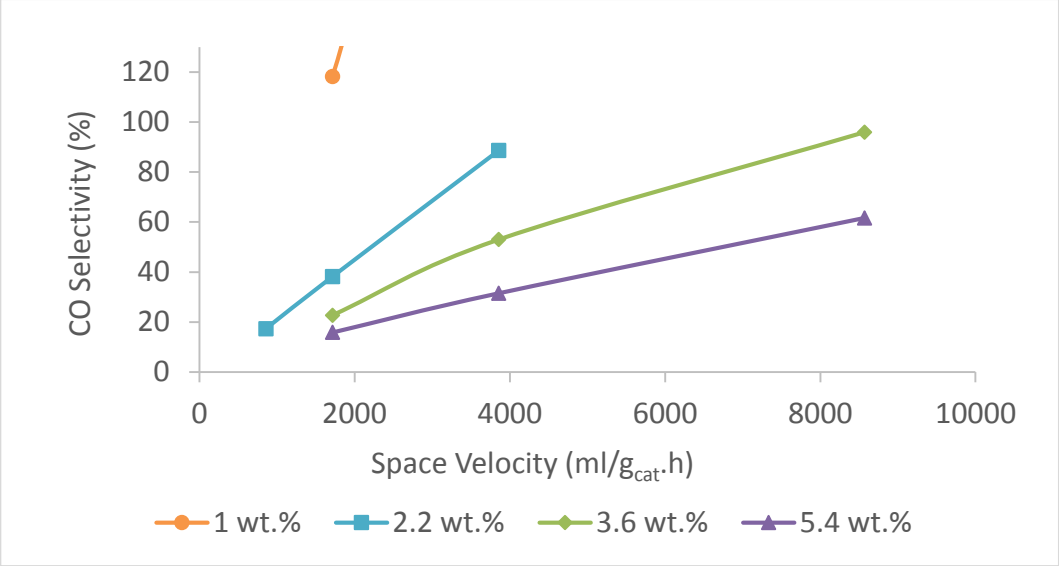

Graph 36: The effect of loading on CO selectivity at 180°C between 800 ml/g_{cat}.h and 8500 ml/g_{cat}.h.

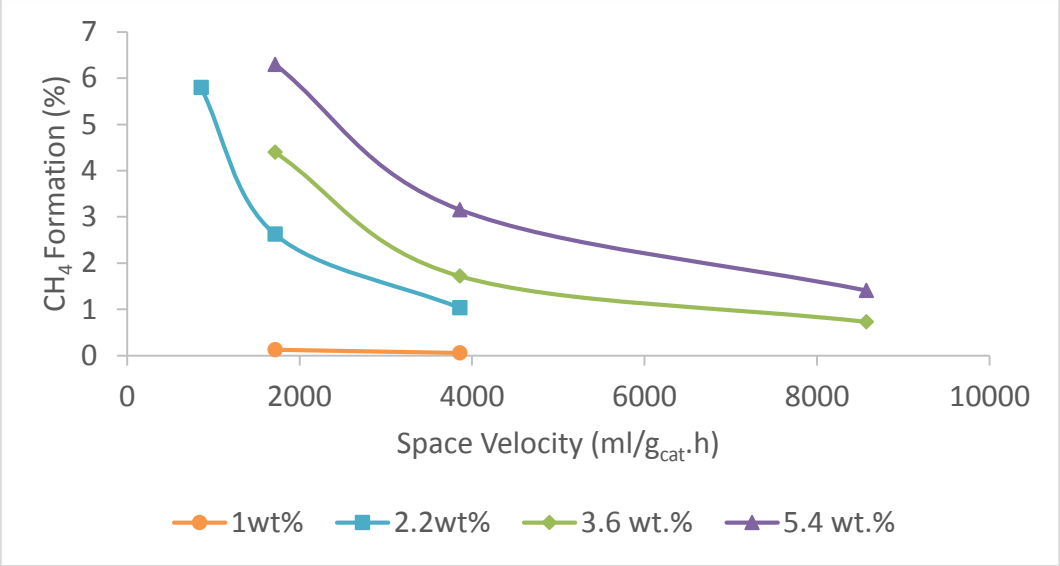

Graph 37: The effect of loading on the formation of CH_4 at 180°C between 800 ml/g_{cat}.h and 8500 ml/g_{cat}.h.

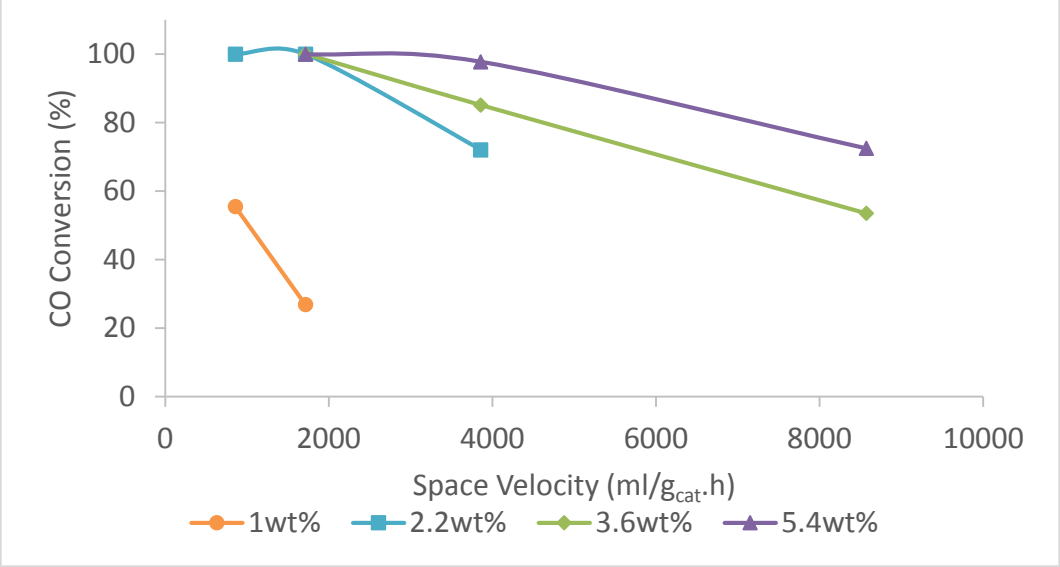

Graph 38: The effect of loading on CO conversion at 170°C between 800 ml/g_{cat}.h and 8500 ml/g_{cat}.h.

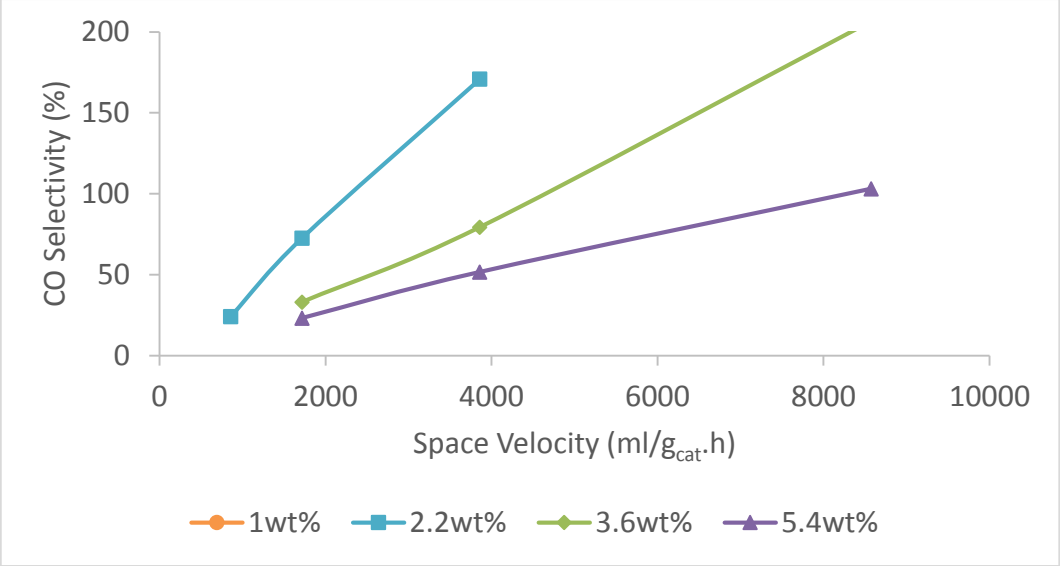

Graph 39: The effect of loading on CO selectivity at 170°C between 800 ml/g_{cat}.h and 8500 ml/g_{cat}.h.

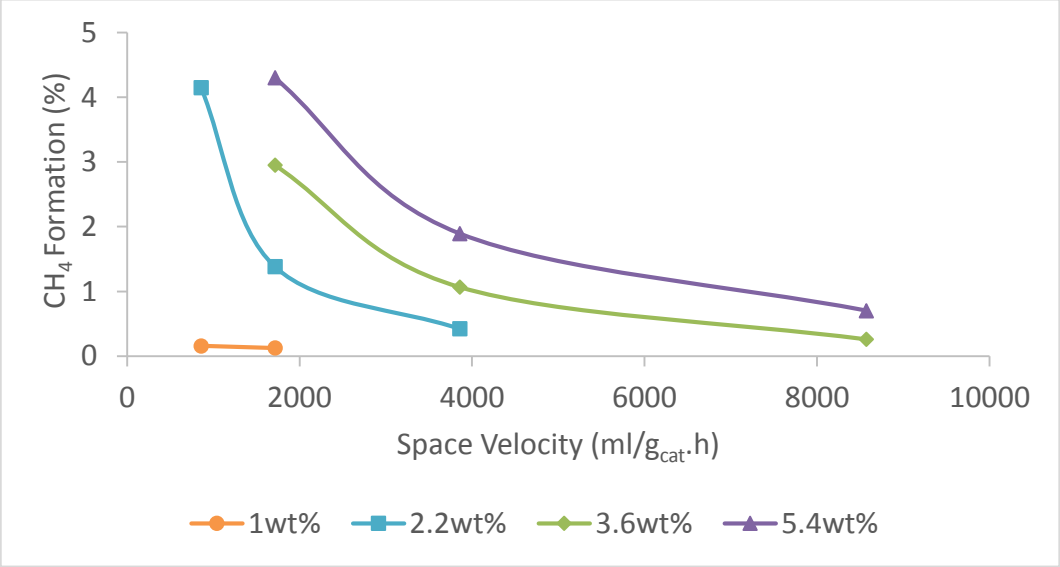

Graph 40: The effect of loading on the formation of CH_4 at 170°C between 800 ml/g_{cat}.h and 8500 ml/g_{cat}.h.

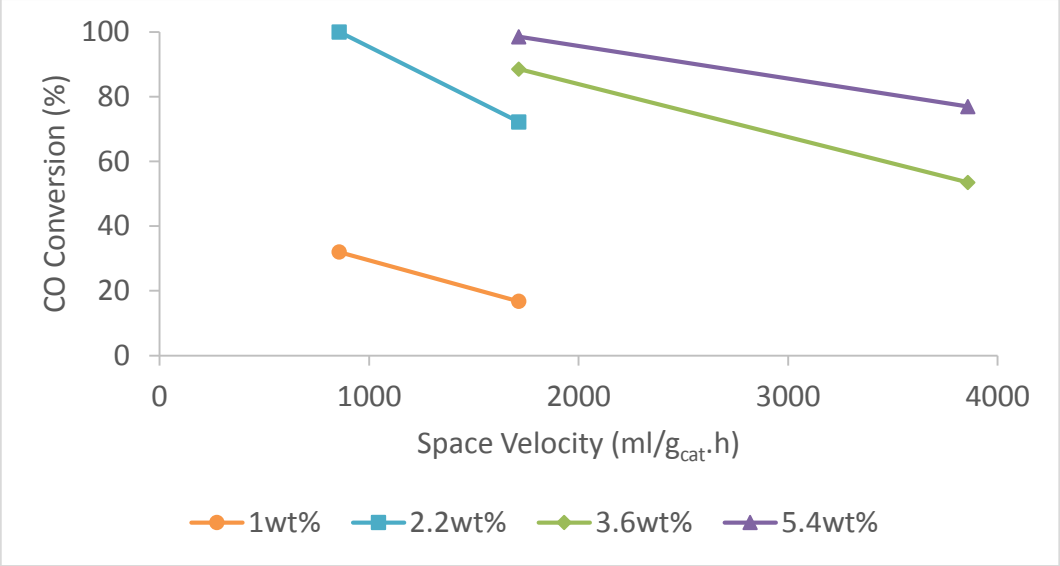

Graph 41: The effect of loading on CO conversion at 160°C between 800 ml/g_{cat}.h and 4000 ml/g_{cat}.h.

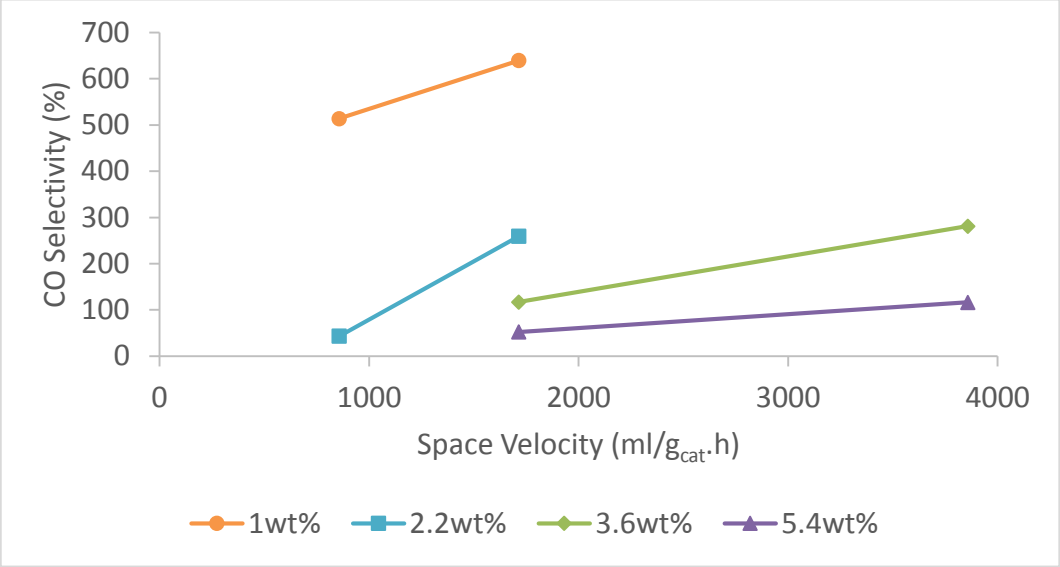

Graph 42: The effect of loading on CO selectivity at 160°C between 800 ml/g_{cat}.h and 4000 ml/g_{cat}.h.

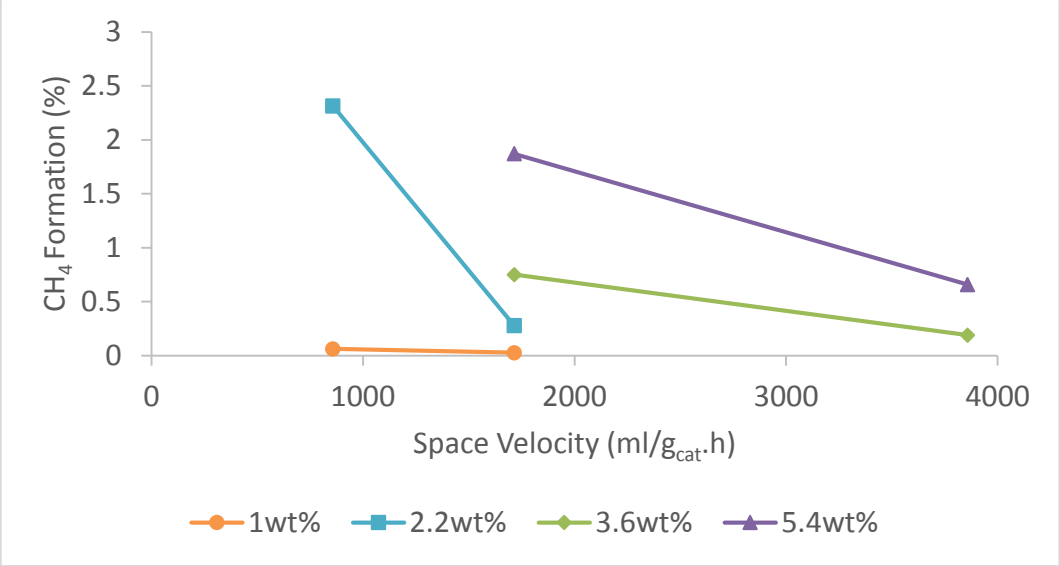

Graph 43: The effect of loading on the formation of CH_4 at 160°C between 800 ml/g_{cat}.h and 4000 ml/g_{cat}.h.